Continental Magmatism: The Surface Manifestation of Dynamic Interactions Between Cratonic Lithosphere, Mantle Plumes and Edge-Driven Convection

Thomas Duvernay[1], D. Rhodri Davies[1], Christopher Mathews[1], Angus H. Gibson[1], and Stephan C Kramer[2]

[1]Australian National University
[2]Imperial College London

November 22, 2022

Abstract

Several of Earth's intra-plate volcanic provinces occur within or adjacent to continental lithosphere, with many believed to mark the surface expression of upwelling mantle plumes. Nonetheless, studies of plume-derived magmatism have generally focussed on ocean-island volcanism, where the overlying rigid lithosphere is of uniform thickness. Here, we investigate the interaction between mantle plumes and heterogeneous continental lithosphere using a series of geodynamical models. Our results demonstrate that the spatio-temporal magmatic expression of plumes in these continental settings is complex and strongly depends on the location of plume impingement, differing substantially from that expected beneath oceanic lithosphere. Where plumes ascend beneath thick continental cratons, the overlying lid locally limits decompression melting. However, gradients in lithospheric thickness channel plume material towards regions of thinner lithosphere, activating magmatism away from the plume conduit, sometimes simultaneously at locations more than a thousand kilometres apart. This magmatism regularly concentrates at lithospheric steps, where it may be difficult to distinguish from that arising through edge-driven convection, especially if differentiating geochemical signatures are absent, as implied by some of our results. If plumes impinge in regions of thinner lithosphere, the resulting asthenospheric flow regime can force material downwards at lithospheric steps, shutting off pre-existing edge-related magmatism. In addition, under certain conditions, the interaction between plume material and lithospheric structure can induce internal destabilisation of the plume pancake, driving complex time-dependent magmatic patterns at the surface. Our study highlights the challenges associated with linking continental magmatism to underlying mantle dynamics and motivates an inter-disciplinary approach in future studies.

Continental Magmatism: The Surface Manifestation of Dynamic Interactions Between Cratonic Lithosphere, Mantle Plumes and Edge-Driven Convection

Thomas Duvernay[1], D. Rhodri Davies[1], Christopher R. Mathews[1], Angus H. Gibson[1], Stephan C. Kramer[2]

[1]Research School of Earth Sciences, Australian National University, Canberra, ACT, Australia
[2]Department of Earth Science and Engineering, Imperial College London, London, UK

Key Points:

- The interaction between mantle plumes and continental lithosphere produces complex spatial and temporal magmatic trends at the surface.
- Lithospheric thickness gradients channel plume material towards areas of thin lithosphere, facilitating melting far from the plume conduit.
- Magmatic contributions from edge-driven convection and mantle plumes can be challenging to distinguish in continental settings.

Corresponding author: Thomas Duvernay, `thomas.duvernay@anu.edu.au`

Abstract

Several of Earth's intra-plate volcanic provinces occur within or adjacent to continental lithosphere, with many believed to mark the surface expression of upwelling mantle plumes. Nonetheless, studies of plume-derived magmatism have generally focussed on ocean-island volcanism, where the overlying rigid lithosphere is of uniform thickness. Here, we investigate the interaction between mantle plumes and heterogeneous continental lithosphere using a series of geodynamical models. Our results demonstrate that the spatio-temporal magmatic expression of plumes in these continental settings is complex and strongly depends on the location of plume impingement, differing substantially from that expected beneath oceanic lithosphere. Where plumes ascend beneath thick continental cratons, the overlying lid locally limits decompression melting. However, gradients in lithospheric thickness channel plume material towards regions of thinner lithosphere, activating magmatism away from the plume conduit, sometimes simultaneously at locations more than a thousand kilometres apart. This magmatism regularly concentrates at lithospheric steps, where it may be difficult to distinguish from that arising through edge-driven convection, especially if differentiating geochemical signatures are absent, as implied by some of our results. If plumes impinge in regions of thinner lithosphere, the resulting asthenospheric flow regime can force material downwards at lithospheric steps, shutting off pre-existing edge-related magmatism. In addition, under certain conditions, the interaction between plume material and lithospheric structure can induce internal destabilisation of the plume pancake, driving complex time-dependent magmatic patterns at the surface. Our study highlights the challenges associated with linking continental magmatism to underlying mantle dynamics and motivates an inter-disciplinary approach in future studies.

Plain Language Summary

As explained by the theory of plate tectonics, most of Earth's volcanism concentrates on the boundaries between lithospheric plates. However, a significant class of volcanism occurs within plate interiors. This volcanism is usually associated with the ascent of mantle plumes — buoyant upwellings of hot rock that rise through the mantle towards Earth's surface. Yet, the exact link between mantle plumes and surface volcanism is not fully understood, particularly in continental regions where Earth's outermost shell — the lithosphere — exhibits substantial variations in thickness and composition, owing to a complex and protracted evolutionary history. In the present study, we use multi-resolution 3-D computational models to simulate the interaction between mantle plumes and heterogeneous continental lithosphere to demonstrate how the structure and geometry of this overlying lithospheric 'lid' shape the volcanic response at Earth's surface. Our results provide new pathways towards understanding the link between surface volcanism and underlying dynamical processes within Earth's interior.

1 Introduction

Volcanism on Earth is conceptualised within the framework of plate tectonics, which describes the planet's outermost shell — the lithosphere — as a collection of mobile, rigid plates separated by discrete tectonic boundaries. Relative motion between these surface plates induces melting in the sub-lithospheric mantle, either through passive decompression at a mid-ocean ridge (e.g. Sengör & Burke, 1978) or enrichment in volatile elements at a subduction zone (e.g. Tatsumi et al., 1986). Such plate boundary settings host most of Earth's magmatic activity (e.g. Crisp, 1984), although a significant class of volcanism occurs within plate interiors (Figure 1). This so-called intra-plate volcanism is difficult to reconcile with plate tectonic theory (e.g. Turcotte & Oxburgh, 1978). Our current understanding of its origins relies on the notion of upwelling convective currents within Earth's mantle, both at small and large scales, which lead to decompression melting in

Figures/LAB_Plume_Volc.pdf

Figure 1. Intra-plate volcanism in the context of lithospheric structure. Background colours show a seismically-derived estimate of lithospheric thickness from Davies et al. (2019). White segments, sourced from Bird (2003), delimit tectonic plate boundaries. Purple diamonds indicate the location of primary and clearly resolved plumes, based upon full-waveform seismic tomography (French & Romanowicz, 2015); additional magenta triangles denote intra-plate volcanic regions from the catalogue of Steinberger (2000) that display a clear, long-lived age progression for over 15 Myr, which strongly supports generation by deep-rooted mantle plumes (e.g. Courtillot et al., 2003). Red dots mark Neogene volcanic occurrences on continents, as compiled by Ball et al. (2021), which are generally restricted to thinner regions of lithosphere. The figure highlights several areas where upwelling mantle plumes rise in close proximity to cratonic lithosphere, for example, within and adjacent to the African, North American and Australian continents.

the shallow asthenosphere that is largely independent of surface plate motions (e.g. Ito et al., 1996; King & Anderson, 1998; Ribe & Christensen, 1999; King & Ritsema, 2000; Jellinek & Manga, 2004; Farrington et al., 2010; Conrad et al., 2011; Kaislaniemi & van Hunen, 2014; Duvernay et al., 2021).

Large-scale upwelling flow takes the form of mantle plumes — buoyant parcels of hot rock that rise from a thermal boundary layer at the core-mantle boundary towards Earth's surface (e.g. Morgan, 1971). The vigorous ascent of plumes through the upper mantle, as well as their rooting in the higher-viscosity lower mantle, ensures that their location remains stable relative to overlying lithosphere, providing a straightforward explanation for age-progressive volcanism both in the oceans and on continents (e.g. Morgan, 1971; Duncan & Richards, 1991; Davies, Rawlinson, et al., 2015). Smaller-scale convective motions occur shallower and manifest, for example, as edge-driven flows that develop adjacent to lithospheric steps (e.g. King & Anderson, 1998). More precisely, in the context of passive margins, denser oceanic lithosphere destabilises and sinks through the underlying asthenosphere, driving an upwelling return flow in the form of a convective cell that facilitates modest decompression melting (e.g. Duvernay et al., 2021). Alternatively, the presence of favourably oriented asthenospheric shear can stimulate similar ascending currents and associated magmatism where the lithosphere rapidly thins (e.g. Conrad et al., 2010; Duvernay et al., 2021). In combination, these shallow mechanisms are postulated to explain intra-continental and continental margin volcanism at a number of locations (e.g. King & Ritsema, 2000; Demidjuk et al., 2007; King, 2007; Conrad et al., 2011; Missenard & Cadoux, 2012; Davies & Rawlinson, 2014; Klöcking et al., 2018).

The role of mantle plumes in generating ocean island volcanism is becoming increasingly well understood (e.g. Davies & Davies, 2009; Ballmer et al., 2011; Ballmer, Ito, & Cheng, 2015; Gassmöller et al., 2016; Bredow et al., 2017; T. Jones et al., 2017). However, their contribution towards continental volcanism remains unclear, given difficulties in separating plume-related magmatism from that produced by the shallower mechanisms described above (e.g. King, 2007). Figure 1 illustrates that most Neogene continental volcanic provinces (Ball et al., 2021) are located in regions of comparatively thin lithosphere (generally less than ~ 90 km thick), adjacent to step-changes in lithospheric thickness. Whilst such settings are favourable for edge- and shear-driven mechanisms (e.g. Conrad et al., 2011; Duvernay et al., 2021), Figure 1 also illustrates that many of these volcanic regions lie in close proximity to mantle plumes. Decompression melting is unlikely at the high pressures underlying continental cratons (e.g. Davies, Rawlinson, et al., 2015; Niu, 2021), and, thus, it has been argued that the preferential occurrence of volcanism in areas of thinner continental lithosphere is due to the channelling of plume material into these regions (e.g. Ebinger & Sleep, 1998; Sleep et al., 2002; Nyblade & Sleep, 2003; Manglik & Christensen, 2006). Accordingly, the relative contributions of edge-related mechanisms and mantle plumes remain unclear and are likely variable across different volcanic provinces. Pulling apart these contributions is challenging, particularly since they may interact, as is hinted by the observational record in several places (e.g. Ebinger & Sleep, 1998; Nyblade & Sleep, 2003; Davies, Rawlinson, et al., 2015; Kennett & Davies, 2020).

Among the intra-plate volcanic provinces highlighted in Figure 1, several show evidence of an interplay between edge-related convective instabilities and mantle plumes. In eastern Australia, the combination of age-progressive and non-age-progressive volcanism, onshore and offshore of a continent with a step-like lithospheric architecture (e.g. Fishwick et al., 2008; Fishwick & Rawlinson, 2012; Rawlinson et al., 2017), makes it challenging to identify and isolate the dynamical mechanisms controlling Cenozoic volcanism (e.g. Wellman & McDougall, 1974; Johnson et al., 1989; Davies & Rawlinson, 2014; Davies, Rawlinson, et al., 2015; Kennett & Davies, 2020; Ball et al., 2021). To add further complexity, even the age-progressive volcanic chains, postulated to be the surface expression of mantle plumes, display volcanic gaps in regions of thick lithosphere, indicating that lithospheric thickness variations control where plume-related melting can occur and where the resulting melts can rise to the surface (e.g. Davies, Rawlinson, et al., 2015; Niu, 2021; Ball et al., 2021). The African continent hosts several volcanic provinces adjacent to ancient cratonic terrains and is underlain by one of the two deep-mantle, large low seismic velocity provinces that spawn several of Earth's mantle plumes (e.g. Ashwal & Burke, 1989; Ritsema et al., 2011; Austermann et al., 2014; Davies, Goes, & Sambridge, 2015). Africa, therefore, constitutes a setting in which multiple mechanisms, both shallow and deep-rooted, likely combine to dictate the nature and characteristics of surface volcanism (e.g. Ebinger & Sleep, 1998; Nyblade & Sleep, 2003; Ball et al., 2019). In western North America, the presence of the Yellowstone caldera and its associated 15 Myr age-progressive volcanic track (e.g. Smith et al., 2009) contrasts with the occurrence of many smaller non-age-progressive volcanic fields, including those surrounding the Colorado Plateau (e.g. Afonso et al., 2016; Klöcking et al., 2018). The extensive Abrolhos Volcanic Complex on the South American continent, where volcanism was locked to the moving plate from 70 Myr to 35 Myr, prior to its emergence at the age-progressive Vitória-Trindade Ridge (dos Santos et al., 2021), hints at a complex dynamical regime modulated by cratonic lithosphere, edge-related processes and upwelling mantle flow. Finally, in Anatolia, another continental region with significant variations in lithospheric thickness, the origin of recent Neogene volcanism is debated, with studies advocating an interaction between ascending plume-like flow and lithospheric instabilities (e.g. Özdemir & Güleç, 2014; McNab et al., 2018; Nikogosian et al., 2018).

The intricacies that characterise many volcanic provinces at Earth's surface illustrate that additional efforts are required to obtain a deeper understanding of how plumes interact with continental lithosphere and the associated shallow convective processes to control the generation of intra-plate volcanism within Earth's highly heterogeneous continents. However, despite recent modelling and observational efforts to constrain the nature and dynamics of shallow convective flows (e.g. Kaislaniemi & van Hunen, 2014; van den Hove et al., 2017; Duvernay et al., 2021), few studies have systematically analysed their interaction with upwelling mantle plumes, particularly in a highly heterogeneous continental setting (e.g. Farrington et al., 2010; Koptev et al., 2015). The examples described above suggest that such interactions could be critical to controlling the distribution and intensity of intra-plate volcanism in these settings.

In this study, through a series of numerical simulations, we analyse the interaction between mantle plumes and continental lithospheric structure and the resulting impact on shallow convective processes. Our study builds on Duvernay et al. (2021), where edge-driven convection and shear-driven upwelling were examined in isolation, allowing us to illustrate how the incorporation of plumes can explain complex magmatic patterns observed within and adjacent to Earth's continents, as described above. Our simulations incorporate continents of different geometries and include variations in the depth and architecture of the continental lithosphere-asthenosphere boundary (LAB) consistent with those imaged on Earth (e.g. Afonso et al., 2016; Rawlinson et al., 2017). For each simulation, the plume's location relative to the continent is varied, allowing us to examine plume-lithosphere interaction across a wide range of configurations.

Our results demonstrate that even when plumes impinge beneath regions of thicker lithosphere, magmatism concentrates beneath thinner lithosphere, consistent with the volcanic record displayed in Figure 1: lithospheric structure channels the spread of plume material towards regions of thinner lithosphere, where it melts. Importantly, this highlights how the locus of plume arrival, relative to the continent, determines the magmatic response. Moreover, we emphasise that plumes impinging beneath continental interior can trigger melting simultaneously in distinct regions, sometimes located several hundreds of kilometres away from the conduit and over a thousand kilometres apart. Plumes can also shut off pre-existing decompression melting zones at lithospheric steps by driving lateral flow towards the steps, impeding previous ascending currents. Our findings provide fundamental new insight into the generation of intra-plate volcanism within Earth's continents and shed light on the critical processes and interactions that shape the magmatic response to underlying dynamics.

2 Methods

The simulations presented here build on those of Duvernay et al. (2021). They utilise Fluidity — a finite element, control-volume computational modelling framework (e.g. Davies et al., 2011; Kramer et al., 2012, 2021) — to solve the equations governing incompressible (Boussinesq) mantle dynamics. Simulations are run within a 3-D Cartesian box of dimensions 4000:4000:660 km (x:y:z) and take advantage of Fluidity's anisotropic, unstructured, adaptive meshing capabilities. Furthermore, they exploit Fluidity's multi-material (Wilson, 2009) and particle-in-cell (Mathews, 2021) functionalities to track, respectively, individual materials — continental crust, continental lithosphere and oceanic lithosphere/mantle, which can have distinct material properties — and melt production across the computational domain. Melt productivity is calculated using the parameterisation of Katz et al. (2003), which is coupled to a modified version of the framework of McKenzie (1984), as described in Duvernay et al. (2021).

In all simulations, deformation is accommodated through diffusion creep, and the associated viscosity is defined using a classical Arrhenius law that is both pressure- and temperature-dependent,

$$\mu = A \times \exp\left(\frac{E^* + \rho_0 g \overline{z}\, V^*}{R(T + \psi \overline{z})}\right). \tag{1}$$

Table 1. *Model parameters common to all simulations*

Name	Symbol	Value	Units
Reference Density	$\rho_0^{Mant} \mid \rho_0^{Cont} \mid \rho_0^{Crust}$	3370 | 3300 | 2900[a]	$\mathrm{kg\,m^{-3}}$
Gravity	g	9.8	$\mathrm{m\,s^{-2}}$
Gas Constant	R	8.3145	$\mathrm{J\,K^{-1}\,mol^{-1}}$
Thermal Expansion	α	3×10^{-5}[b]	$\mathrm{K^{-1}}$
Surface Temperature	T_S	290	K
Mantle Temperature	T_M	1650[c,d]	K
Plume Temperature	T_P	1800	K
Plume Injection Velocity	v_P	10	$\mathrm{cm\,yr^{-1}}$
Plume Disc Radius	R_P	200	km
Adiabatic Gradient	ψ	4×10^{-4}[e]	$\mathrm{K\,m^{-1}}$
Thermal Diffusion	κ	6×10^{-7}[f]	$\mathrm{m^2\,s^{-1}}$
Internal Heating (Crust)	ϕ	2.6×10^{-13}[g]	$\mathrm{K\,s^{-1}}$
Internal Heating (Elsewhere)	ϕ	4×10^{-15}[h]	$\mathrm{K\,s^{-1}}$
Activation Energy	E^*	350	$\mathrm{kJ\,mol^{-1}}$
Activation Volume	V^*	6.8×10^{-6}	$\mathrm{m^3\,mol^{-1}}$
Viscosity Pre-Factor	$A^{Mant} \mid A^{Cont}$	$2.6 \times 10^{7} \mid 2.6 \times 10^{10}$	Pa s
Viscosity Bounds	μ_{min}-μ_{max}	10^{18}-10^{24}	Pa s
Water Content (Melting)	X_{H_2O}	300	ppm

[a] Artemieva (2009). [b] Ye et al. (2009). [c] Putirka (2016). [d] Sarafian et al. (2017). [e] Katsura et al. (2010). [f] Gibert et al. (2003). [g] $\equiv 1.3 \times 10^{-6}\,\mathrm{W\,m^{-3}}$ (Jaupart & Mareschal, 2005). [h] $\equiv 2 \times 10^{-8}\,\mathrm{W\,m^{-3}}$ (Pollack & Chapman, 1977).

Here, A is the viscosity pre-factor, E^* the activation energy, ρ_0 the reference density, g the acceleration of gravity, $\bar{z}$ the depth, V^* the activation volume, R the gas constant, T the temperature, and ψ the adiabatic gradient. We note that this formulation is identical to that used in Duvernay et al. (2021) for simulations without a low-viscosity channel. Free-slip velocity boundary conditions are imposed at the top of the domain together with a zero-slip base and lithostatic sidewalls that permit normal flow only. The temperature is set to 290 K at the surface and 1650 K — the upper mantle potential temperature — at 660 km depth; boundary conditions are free on all sidewalls. Internal heating is included throughout the domain, with a higher rate specified within the continental crust. Key model parameters are presented in Table 1.

Simulations incorporate a centred continental block (crust and lithospheric mantle), located between $x, y = 1250$ km and $x, y = 2750$ km, that is characterised by a lower density and higher viscosity relative to asthenospheric mantle (Table 1). Oceanic lithosphere surrounds the continent and is initialised using the thermal structure of a half-space cooling model of age 40 Myr: it is originally ∼90 km thick, as approximated by the depth of the 1620 K isotherm. The transition between ocean and continent is achieved by smooth 200 km–wide lithospheric steps, with the boundary between continental and oceanic material halfway along the step. We focus on two distinct continental geometries, both of which were analysed in Duvernay et al. (2021): (i) Case *U400* (Figure 2a), a 200 km–thick flat-bottom continent that features a 400 km–wide oceanic indent, and (ii) Case *Complex* (Figure 2b), a non-indented continental block with a heterogeneous, multi-scale lithospheric thickness distribution. The inclusion of an indent in the *U400* geometry mimics first-order characteristics of continental architectures imaged on Earth (e.g. Davies & Rawlinson, 2014; Zhang et al., 2014; Rawlinson et al., 2017; Klöcking et al., 2018; Hoggard, Czarnota, et al., 2020), whilst the *Complex* geometry better reflects the smaller-scale structure of Earth's continents at depth (e.g. Afonso et al., 2016; Rawlinson et al., 2017) (Figure 1). As these two continental configurations trigger edge-driven

Figures/IniContNEW.pdf

Figure 2. View from below of the initial lithosphere-asthenosphere boundary as delineated by the 1620 K isotherm. Red dots indicate locations of plume injection in our numerical experiments, with 1 corresponding to *U400_ Cont_ Step*, 2 to *U400_ Ocean_ Offshore*, 3 to *U400_ Cont_ Indent*, 4 to *U400_ Ocean_ Indent*, and 5 to *Complex_ Cont_ Centre*. Coloured squares denote probed areas investigated in Figure 6. (a) *U400* geometry. (b) *Complex* geometry. The dotted black line indicates the location of the slices presented in Figures S1 and S2.

magmatism (Duvernay et al., 2021), we run cases both with and without a mantle plume to isolate the plume's role in our quantitative diagnostics.

When incorporating a plume, it is injected at 660 km depth through a disc of radius $R_P = 200\,\text{km}$, on which temperature and vertical velocity boundary conditions are prescribed according to

$$B + C \times \exp\left[\left(\frac{d}{R_P}\right)^2 \ln\left(\frac{0.1}{T_P - T_M}\right)\right], \tag{2}$$

with d the distance to the centre of the disc and $T_P = 1800\,\text{K}$ the plume temperature. In the case of temperature, $B = T_M$ and $C = T_P - T_M$. For velocity, $B = 0$ and $C = v_P$, the injection velocity, set to $10\,\text{cm}\,\text{yr}^{-1}$; horizontal velocities are set to zero within the disc. The resulting plumes have an excess temperature of 150 K relative to background mantle, which is compatible with petrological estimates of 100 K–300 K (e.g. Herzberg et al., 2007; Putirka, 2008). Moreover, they have a mass flux of $\approx$500 kg s^{-1}, while recent estimates for active hotspots worldwide range from 200 kg s^{-1} to 4000 kg s^{-1}, with the highest values observed at Iceland and Hawaii (e.g. King & Adam, 2014; Hoggard, Parnell-Turner, & White, 2020). Our plumes, therefore, are representative of those at the lower end of the predicted range, which include a large number of magmatic hotspots both on continents and within the oceans.

The location of plume injection, relative to the continent, is varied (Figure 2), allowing us to examine a wide range of plausible interactions between a plume and overlying continental lithosphere. First, making use of the *U400* geometry, the plume's disc is placed at four different positions along $y = 2000\,\text{km}$, thus defining four cases: (i) *U400_ Cont_ Step*, where the plume is injected at $x = 1450\,\text{km}$ beneath the continent, adjacent to a long, linear lithospheric step; (ii) *U400_ Ocean_ Offshore*, where the plume is located at $x = 2850\,\text{km}$ offshore the oceanic indent; (iii) *U400_ Cont_ Indent*, with the plume centred

Table 2. *Summary of simulations examined*

Name	Continental geometry	Disc centre x-coordinate	Plume location
U400	*U400*	—	—
Complex	*Complex*	—	—
U400_ Cont_ Step	*U400*	1450 km	Below continent, far from indent
U400_ Ocean_ Offshore	*U400*	2850 km	Below ocean, offshore indent
U400_ Cont_ Indent	*U400*	2150 km	Below continent, nearby indent
U400_ Ocean_ Indent	*U400*	2500 km	Below ocean, below indent
Complex_ Cont_ Centre	*Complex*	2000 km	Below continent, centred

Note. Disc centre y-coordinate is set to 2000 km for all simulations incorporating a plume.

at $x = 2150$ km beneath the continent, adjacent to the indent; and (iv) *U400_ Ocean_ Indent*, where the plume rises at $x = 2500$ km directly beneath the oceanic indent. In addition, we examine a fifth plume model, *Complex_ Cont_ Centre*, where the plume is injected at $x, y = 2000$ km, centred beneath the *Complex* continental geometry. A summary of all cases examined is provided in Table 2.

3 Results

We first present results from our reference cases that do not include a mantle plume (Section 3.1). These allow us to isolate the effect of incorporating plumes in our subsequent simulations (Section 3.2). To illustrate the dynamics of our simulations, we display temporal snapshots of temperature, vertical velocity and melting rates, at either 120 km depth (*U400* geometry) or 180 km depth (*Complex* geometry), with the increased depth for the latter cases allowing us to focus on the interaction between the plume and the base of the heterogeneous continental lithosphere. In addition, for plume cases, we display melt production rates relative to the relevant reference case, highlighting the plume's impact.

3.1 Reference Cases

These cases are almost identical to those presented in Duvernay et al. (2021), differing only in the depth extent of the computational domain — 660 km here, as opposed to 1000 km — and the velocity boundary conditions on sidewalls — open to normal flow in the simulations examined herein, as opposed to free-slip. As illustrated in Figure 3a–i, for the *U400* geometry, edge-driven instabilities, induced by the negative buoyancy of oceanic lithosphere, develop along all lithospheric steps. These generate passive upwelling flows below adjacent oceanic lithosphere, forming convective rolls. We find that upwelling velocities are enhanced within the oceanic indent (Figure 3b), as the geometry of the inner corners facilitates the coalescence of upwelling currents (Davies & Rawlinson, 2014; Duvernay et al., 2021). As a result, melting rates are substantially higher close to the indent's inner corners over the first ∼20 Myr of model evolution (Figure 3f). At later stages (Figure 3j–o), melt production is more consistent across all steps (Figure 3l), owing to the sinking of primary instabilities and the growth of secondary instabilities, as reflected, for example, by intense offshore downwellings in Figure 3k, which generate shallow, focussed upwellings that sustain melting (Duvernay et al., 2021).

Comparable snapshots for the *Complex* continental geometry are presented in Figure 4. As with the previous case, instabilities develop all around the continent. During the first ∼10 Myr of model evolution (Figure 4a–c), negatively buoyant material sinks faster adjacent to thicker portions of the continent, which facilitate the development of

Figures/MosaicU400Geometry.pdf

Figure 3. Temporal evolution of the *U400* geometry in the absence of a mantle plume. The first and second columns display horizontal slices of temperature and vertical velocity at 120 km depth, whilst the third column shows instantaneous melting rates, integrated along the vertical axis (methodology described in Duvernay et al., 2021). The white/black contour delineates the continental boundary at the depth of the slice.

Figures/MosaicComplexGeometry.pdf

Figure 4. Temporal evolution of the *Complex* continental geometry simulation (similar to Figure 3). Horizontal slices and continental boundaries are displayed at 180 km depth to capture dynamics at the base of the heterogeneous continent.

instabilities. As a result, larger and more vigorous edge-driven cells initially develop adjacent to thicker continental lithosphere (Figures 4b and S1a). However, over the next ∼20 Myr, faster development of secondary instabilities enhances the vigour of edge-driven cells adjacent to thinner continental edges, beneath which modest upwelling flows subsequently develop (Figures 4d–i and S1b–c). Within the continent's interior, anomalous troughs in lithospheric thickness drive focussed upwellings that persist throughout the simulation, generating substantial decompression melting. Conversely, melting adjacent to lithospheric steps is modulated by the strength of surrounding instabilities and becomes negligible after ∼50 Myr (Figure 4o), owing to the thickening of oceanic lithosphere through thermal diffusion and fading of the primary instabilities that surround the continent, which limit decompression melting (Figures 4j–o and S1d–e). We note that the high viscosity of continental lithosphere prevents destabilisation of the continent's thicker region (Figure 4m–n).

3.2 Plume Cases

3.2.1 Below Continent, Away from Indent

We now consider scenarios incorporating a plume beneath the *U400* continental geometry. In the *U400_Cont_Step* case, the plume disc is located at $x = 1450$ km, close to a long, linear lithospheric step and far from the indent. As illustrated in Figure 5a–h, during the initial stages of plume ascent (≈10 Myr), the flow regime beneath and adjacent to the continent is reasonably consistent with the reference case (Figure 3): edge-driven instabilities develop at all lithospheric steps, and the largest upwelling velocities and melting rates are confined to the indent's inner corners. Nonetheless, as the plume's thermal anomaly approaches the base of the continent (Figure 6d), its buoyancy modifies the surrounding flow field and progressively enhances upwelling velocities at the adjacent step (Figure 5f). As a result, relative to the reference case, melt production increases at that step (Figures 5g–h and 6a) prior to any change in the temperature field associated with plume impingement at the LAB.

Plume arrival beneath the continent at 8–9 Myr causes buoyant material to spread in all directions. However, due to the proximity of the lithospheric step, spreading is asymmetric, with material preferentially flowing from thicker to thinner regions of the lithosphere (Figure 7). At the adjacent continental edge, this flow has analogous consequences to shear-driven upwelling (Duvernay et al., 2021), enhancing melting rates. We emphasise that these increased melting rates are apparent even prior to the arrival of the thermal anomaly (i.e. they are a direct consequence of increased upwelling rates rather than increased temperatures; Figures 5g–h and 6a), although they do increase further as this thermal anomaly emerges at the step (Figures 5k–l and 6a). Once beneath oceanic lithosphere, plume material moves away from the step, forming an expanding half-disc (Figure 5i–l). At the disc's leading edge, the positive buoyancy of plume material sweeps away the deepest portion of the overlying lithosphere, generating a 'curtain' of cold downwelling flow downstream of the spreading front (Figure 5i–j) and transient decompression melting upstream. Within the disc, away from the leading edge, vertical velocities and the associated melting tend towards zero (Figure 5n–o), owing to the prior removal and consequent stabilisation of overlying oceanic lithosphere.

Plume material accumulates alongside the continental step, generating gradients of temperature and vertical velocity to either side of the upwelling (Figure 5i–p). As a result, decompression melting concentrates in a linear trend along the continent's boundary, unlike the circular melt geometry expected upon direct plume impingement beneath oceanic lithosphere (e.g. Ribe & Christensen, 1999; Manglik & Christensen, 2006). We note that no melts are generated directly above the plume conduit in this case, as the thick continent keeps upwelling material below its solidus (Figure 5o), with limited erosion of overlying continental lithosphere observed. After 40 Myr (Figure 5q–t), both the

Figures/MosaicBelowContinentAlternative.pdf

Figure 5. Temporal evolution of the *U400_ Cont_ Step* simulation; the plume is injected at $x = 1450\,\mathrm{km}$, as indicated by the red circle. Illustration is similar to Figure 3, with an additional column displaying integrated melting rates relative to those of the corresponding reference case (*U400* geometry).

Figures/PlumeCurvesFilteredNEW.pdf

Figure 6. (a)–(c) Temporal evolution of the average melting rate recorded across all simulations within three selected $40{\times}40{\times}20\,\text{km}^3$ regions identified by coloured squares (Figure 2). (d) Temporal evolution across all plume simulations of the shallowest depth reached by the plume thermal anomaly within the computational domain.

Figures/Asymmetry.pdf

Figure 7. Horizontal cross-section at 220 km depth for case *U400_Cont_Step* illustrating the asymmetric spreading of plume material after it impinges beneath the continent. Background colours represent the x-component of velocity; labelled contours denote isotherms. Dotted blue and grey lines highlight the edge of the continent at 200 km and 140 km depth, respectively, and the red-filled circle depicts the location of the plume conduit.

Figures/U400_Plumes3D.pdf

Figure 8. Views from below of the 3-D interaction between a plume and the *U400* continental geometry. We use the 1620 K isotherm to represent the bottom surface of the continental lithosphere (blue tones) and oceanic lithosphere (light blue to white tones). Additionally, the isotherm also highlights thermal instabilities dripping in the upper mantle (dark blue to black tones) adjacent to the continent (primary instabilities) and offshore the continent (secondary instabilities); grey patches indicate thinner portions of the oceanic lithosphere (i.e. lithospheric erosion). The plume is depicted by the 1660 K isotherm, which is rendered half-transparent and coloured by vertical velocity. Areas experiencing melting are represented by individual particle dots, coloured by melting rate (no vertical integration). (a) *U400_ Cont_ Step*. (b) *U400_ Ocean_ Offshore*. (c) *U400_ Cont_ Indent*. (d) *U400_ Ocean_ Indent*.

primary melting zone adjacent to the step (Figure 6a) and the front of decompression melting linked to the expanding half-disc remain active, although the loss of buoyancy through thermal cooling progressively inhibits melting at the disc spreading front.

To complement the cross-sections of Figure 5, a 3-D snapshot of the final stage of the model at 40 Myr is included in Figure 8a. This illustration corroborates that plume flow mainly affects the dynamical regime and thermal structure in the plume conduit's vicinity. Where plume material emerges at the step, typical patterns expected from the combination of lithospheric cooling and edge-driven convection are absent. Along the rest of the continental boundary, including within the indent, the main characteristics of the flow regime and thermal structure remain consistent with the reference case (Figures 5q–t and 6b–c). Offshore the continent, within the spreading half-disc, the distribution of particles that record low-intensity melting rates indicates that plume material is close to internal destabilisation, characterised by the development of small-scale convection within the plume pancake (e.g. Ballmer et al., 2011).

3.2.2 Offshore Indent

In the *U400_Ocean_Offshore* case, the plume is injected offshore, outside the indent at $x = 2850$ km. As with the previous case, plume upwelling modifies the flow regime at the LAB as the buoyant anomaly approaches the lithosphere (Figures 9a–d and 6d). Above the plume, decompression melting is activated but, within the indent, existing edge-related upwellings at lithospheric steps are progressively suppressed by plume flow, leading to reduced melting rates relative to the reference case (Figure 9f–h).

Following impingement of the plume at the LAB (Figure 9e–h), material spreads radially to produce a circular decompression melting zone consistent with expectations of melting associated with a plume arriving beneath uniform oceanic lithosphere. Soon after, plume material reaches the continental boundary (Figure 9i–l), where it either enters the indent or gets redirected along the continent's outer steps, in the latter case triggering a front of enhanced melting that propagates with the flow (Figure 9i–p). The arrival of plume material within the indent drives intense horizontal motion and shuts off edge-driven convection and the associated melting (Figures 9k and 6b–c), leaving a region in its wake where vertical velocities and decompression melting have become negligible (Figures 9n–o and 6b–c). After reaching the indent's innermost step, plume material is forced beneath the continent due to ongoing inflow from the plume conduit and the associated dynamic pressure gradients (Figure S3d–e). At this stage, the dynamics within the indent contrast dramatically to both the reference and *U400_Cont_Step* cases, demonstrating that the flow regime and magmatic expression are transformed solely by changing the location of plume impingement at the LAB, relative to the continental lithosphere. Nonetheless, away from the plume's region of influence, the model's dynamics remain similar to the reference case (Figures 6a, 8b and 9t).

At 40 Myr (Figure 9q–t), within a disc surrounding the conduit, melting remains active directly above the plume conduit but is almost entirely suppressed elsewhere. Inside the indent, plume material is close to destabilisation, as illustrated by the alternating positives and negatives in the vertical velocity field, which trigger small pockets of localised melting (Figure 9r–s). This is corroborated by the companion 3-D view of the model's final stage in Figure 8b.

3.2.3 Below Continent, Close to Indent

In the *U400_Cont_Indent* case, the plume is injected below the continent at $x =$ 2150 km, adjacent to the indent. Similar to the *U400_Cont_Step* case (Figure 5), the initial 10 Myr of model evolution (Figure 10a–h) are comparable to the reference case, albeit with a substantial increase in melt production at the indent's innermost step (Fig-

Figures/MosaicOffshoreIndent.pdf

Figure 9. Temporal evolution of the *U400_ Ocean_ Offshore* case; the plume is injected at $x = 2850\,\mathrm{km}$. Illustration similar to Figure 5.

Figures/MosaicBelowContinent.pdf

Figure 10. Temporal evolution of the *U400_ Cont_ Indent* case; the plume is injected at $x = 2150\,\mathrm{km}$. Illustration similar to Figure 5.

ures 6b and 10g–h). Here, once again, flow driven by the plume has an analogous impact to shear-driven upwelling (Duvernay et al., 2021), enhancing upwelling velocities and the associated decompression melting. Owing to the thickness of the continent, plume material does not melt prior to or upon impingement at the LAB. Instead, it spreads preferentially towards the indent where it eventually emerges, generating melting that is substantially more intense than that generated solely through edge-driven convection (Figures 10i–l and 6b–c).

For the remainder of the simulation, plume material continues to flood into the indent, driving ongoing decompression melting at the indent's innermost step and along fronts that propagate outwards towards the oceanic domain (Figure 10m–p). At the indent's exit, the lateral space available (along the y-direction) for plume material increases and, accordingly, buoyant material that had accumulated along the indent's steps redistributes, flushing outwards into the oceanic realm through focussed upwellings that trigger further localised decompression melting. Moreover, the formation of these upwellings initiates small-scale convection within the plume pancake itself, promoting further localised melting in a domino effect.

After 40 Myr of model evolution (Figure 10q–t), decompression melting is present adjacent to the indent's inner steps and outer corners, continental outer steps connected to the indent, and also offshore, driven by small-scale convection and the complex destabilisation of plume material. These dynamics are further illustrated through a complementary 3-D view in Figure 8c, where plume material can be seen spreading as a thin layer beneath a large portion of the LAB. Preferential flow into, and subsequent melting within, the indent are also clearly highlighted. Destabilisation of the plume pancake is marked by the absence of decompression melting within well-defined pockets of downwelling flow. As with the previous cases considered, the flow regime and melting diagnostics are generally unaffected at steps far from the plume.

3.2.4 Below Indent

In the *U400_ Ocean_ Indent* case, the plume is injected directly beneath the indent at $x = 2500\,\mathrm{km}$. As in the *U400_ Ocean_ Offshore* case (Figure 9), the plume ascends rapidly and generates extensive melting upon impingement onto oceanic lithosphere (Figure 11a–h), with the main melting zone assuming an elliptical shape due to the geometry of the indent (Figure 11k). As the simulation evolves (Figure 11i–l), material is forced beneath the continent at the indent's steps (Figure 11j) and, accordingly, no decompression melting occurs in these regions (Figures 11k and 6c). We emphasize that this is opposite to the reference case (Figure 3), where melting within the indent occurs solely adjacent to these steps.

Similar to the *U400_ Cont_ Indent* case (Figure 10), plume material builds up within the indent, as it is largely prevented from spreading in all but one direction. Eventually, it flushes out around the indent's outer corners, generating focussed upwellings as it redistributes (Figure 11j–k). Relative to the *U400_ Cont_ Indent* case, upwellings and associated downwellings within the pancake are of greater intensity (Figure 11m–p). The resulting small-scale instabilities develop tangent to the indent's outer corners, leading to V-shaped decompression melting ridges (Figure 11q–t). This enhanced destabilisation is further illustrated in the associated 3-D snapshot (Figure 8d), where oblique zones of alternative upwelling and downwelling flow are apparent, along with the V-shaped melting ridges. The 3-D planform also demonstrates that relative to the *U400_ Cont_ Indent* case, plume material covers a smaller portion of the LAB (Figure 8c), as it accumulates within the indent and preferentially flushes into the oceanic realm.

Figures/MosaicBelowIndent.pdf

Figure 11. Temporal evolution of the *U400_ Ocean_ Indent* case; the plume is injected at $x = 2500\,\mathrm{km}$. Illustration similar to Figure 5.

Figures/MosaicComplexPlume.pdf

Figure 12. Temporal evolution of the *Complex_Cont_Centre* case; the plume is injected at $x, y = 2000\,\mathrm{km}$. Illustration similar to Figure 5, with the temperature and vertical velocity slices sampled at 180 km depth as in Figure 4.

Figures/Complex_Plume3D.pdf

Figure 13. View from below of the 3-D interaction between a plume and the *Complex* continental geometry. The 1620 K isotherm is used to represent the continental lithosphere (blue tones) and the oceanic lithosphere (light blue to white tones). Additionally, it also highlights thermal instabilities dripping in the upper mantle (dark blue to black) adjacent to the continent (primary instabilities) and offshore the continent (secondary instabilities); grey patches indicate lithospheric erosion. The plume is depicted by the 1660 K isotherm, which is rendered half-transparent and coloured by vertical velocity. Areas experiencing melting are represented by individual particle dots, coloured by melting rate (no integration).

3.2.5 Complex

We finally discuss the *Complex_ Cont_ Centre* case (Figure 12), where the plume is injected directly beneath the centre of the *Complex* continental geometry (Figure 2b). Unlike the plume scenarios discussed for the *U400* geometry, substantially enhanced melting rates are not observed adjacent to or within the continent during plume ascent, as the plume is located away from any lithospheric step or continental trough (Figure 12d). Upon impingement at the LAB ($\sim$10 Myr), plume material spreads below the continent, with the spreading direction controlled by the heterogeneous structure of the continental LAB (Figure 12e–f). In particular, plume material is forced around the region of thick continental lithosphere and progresses faster towards thinner portions of the continent. No decompression melting occurs above the conduit initially (Figure 12c), although the plume gradually erodes the base of the continent and eventually triggers melting, with melting rates increasing over time (Figure 12k). We note that melting above the conduit is possible in this case as overlying continental lithosphere is initially thinner at the same location relative to the *U400* geometry.

Following further spreading, plume material upwells within the two continental troughs, fuelling melting rates that far exceed those of the reference case (Figures 12l and 6b–c). Over the next ∼10 Myr (Figure 12m–p), plume spreading continues and, eventually, after ∼50 Myr, part of the plume pancake emerges at the lower continental boundary (negative-y direction), where it upwells at the lithospheric step and generates substantial melting (Figure 12s). Remarkably, at this stage, the plume is simultaneously producing melt at four distinct locations: above the conduit, in two pockets of thin lithosphere, and adjacent to the lower step, where plume material emerges almost 1000 km away from the conduit. The dynamics at this time are further illustrated in 3-D, on Figure 13, where preferred spreading directions and pockets of melting are clearly visible. We note that the spreading of plume material is hampered in the negative-x direction by the thick continental region, and it is also delayed as it passes through the two continental troughs. Away from where the plume emerges at the lower continental step, the flow regime and thermal structure adjacent to the continent are comparable to the reference case (Figure 12t).

4 Discussion

Using a series of 3-D geodynamical models, we have investigated the interaction between upwelling mantle plumes and the flow regime beneath and adjacent to continental lithosphere. Our motivation is to reveal how shallow convective processes, such as edge-driven convection, are influenced by the arrival of mantle plumes and to understand how these flow components combine, compete and interact to produce the key characteristics of intra-plate magmatism in the vicinity of Earth's highly heterogeneous continents. Our results have important implications for deciphering the spatio-temporal evolution of intra-plate magmatism in these complex tectonic and geological settings. In particular, they illustrate that the magmatic manifestation of mantle plumes within continental interiors or adjacent to continental margins differs significantly from that expected for plumes arriving beneath oceanic lithosphere, far from any plate boundary.

In the following sub-sections, we summarise the key findings of our simulations and discuss their broader implications for our understanding of intra-plate volcanism on Earth. We end by reviewing the limitations of our approach, how they may influence our results, and discuss potential avenues for future research.

4.1 Plumes Enhance Magmatism at Lithospheric Steps Several Million Years Before Plume Material Emerges at the Step

Shallow processes, such as edge-driven convection and shear-driven upwelling (e.g. King & Anderson, 1998; Conrad et al., 2010), have been invoked to explain intra-plate volcanism at a number of locations on Earth (e.g. Conrad et al., 2011; Davies & Rawlinson, 2014; Kaislaniemi & van Hunen, 2014; Ballmer, Conrad, et al., 2015). Usually, such volcanism lies close to a step-change in lithospheric thickness, which facilitates the development of convective cells, triggering decompression melting in the uppermost asthenosphere. Our previous work suggests that such edge-related magmatism applies only to Earth's lower-volume and shorter-lived intra-plate volcanic provinces (Duvernay et al., 2021). However, the simulations examined herein demonstrate that enhanced decompression melting can occur at lithospheric steps near an upwelling mantle plume as the plume approaches and impinges at the LAB. During their upper-mantle ascent, plumes modify the flow regime and drive more vigorous upwelling motion at adjacent lithospheric steps, substantially boosting decompression melting. For example, the volumetric magmatic production of the *U400_Cont_Step* case increases by up to 80 % relative to its reference case (Figure 5g-h, 3-D integrated melting rate at 10 Myr between $x = 1100$ km,

$y = 1850\,\mathrm{km}$ and $x = 1170\,\mathrm{km}$, $y = 2150\,\mathrm{km}$). In our models, such an increase in magmatic production occurs 5–10 Myr prior to the plume's thermal anomaly reaching the associated melting zone (e.g. Figures 6b 10h).

Such a boost in magmatic production could be critical to explaining the origins of intra-plate volcanism in regions where anomalously hot temperatures are not inferred from geochemical or seismological observations. Some of Earth's continental intra-plate volcanic provinces host low-volume, short-lived eruptions even though they lie reasonably close to mantle plumes (e.g. Ho et al., 2013; Cas et al., 2017; Ball et al., 2019). Our simulations suggest that many of these enigmatic volcanic provinces could result from the transient activation or enhancement of melting induced by a change in the flow field triggered by the adjacent mantle plume. Due to the interaction of plumes with the structure and motion of overlying plates, plume material may not always surface where the flow field promoted melting, resulting in short-lived volcanism that may be difficult to link directly to its primary driving mechanism.

4.2 Plume-Induced Melting May Have No Differentiating Geochemical Expression

The dynamical mechanisms that underpin the generation of volcanic rocks at Earth's surface can be inferred through geochemical analyses, which probe elemental and isotopic compositions (e.g. Dupré & Allègre, 1983; White et al., 1993; Tang et al., 2006; Klöcking et al., 2018; Ball et al., 2019). Contributions from mantle plumes are often identified based on geochemical signatures that differ from those typical of mid-ocean ridge basalts (e.g. Hart et al., 1992; Stracke et al., 2005). Our results, however, suggest that under certain circumstances, these geochemical approaches will be insensitive to the plume's contribution towards the generation of surface volcanism.

As noted in Section 4.1, mantle plumes can enhance decompression melting at lithospheric steps several million years before their thermal anomaly emerges at the step. In such a scenario, the modified flow field promotes higher-volume magmatism at these steps (e.g. the *U400_Cont_Step* case). However, since rock parcels passing through the melting zone do not come from the plume, melting temperatures and the resulting maximum melt fractions remain unchanged. As a result, the composition of erupted lavas does not show the geochemical signature of a mantle plume, despite the latter's important role in activating or enhancing decompression melting. Only if, or when, hot plume material emerges at the step would the erupted lavas display an evolution in their composition that would be detectable through geochemical analyses. Accordingly, it may not be possible for geochemical approaches, in isolation, to infer the important role of a mantle plume in the generation of intra-plate lavas. Studies that rule out a plume contribution to surface volcanism, based principally on the geochemical characteristics of surface lavas, may therefore have overlooked the plume's role in modulating the flow regime (e.g. Bradshaw et al., 1993; Barry et al., 2007).

4.3 Plumes Can Induce Simultaneous Melting in Several Locations, more than a Thousand Kilometres Apart

When a plume impinges onto the LAB, lateral currents associated with plume material spreading away from the plume conduit dominate the asthenospheric flow regime. Our simulations demonstrate that the spreading of plume material beneath heterogeneous lithosphere is anisotropic: it follows local pressure gradients controlled by the thickness and density of the overlying lithospheric lid (e.g. Sleep et al., 2002; Koptev et al., 2016). Accordingly, the location of plume impingement, relative to the local geometry of the LAB, determines the path taken by plume material, which, in turn, dictates where melting can occur.

When plumes impinge directly beneath thick continental keels, the pressure is likely high enough to suppress decompression melting immediately above the plume conduit (e.g. Niu, 2021). The absence of surface volcanism locally is therefore not a sufficient condition to rule out the presence of a plume (Davies, Rawlinson, et al., 2015). Nonetheless, spreading of plume material at the LAB can activate decompression melting in regions of thinner lithosphere several hundreds of kilometres away from the plume conduit. Without further observational constraints, volcanism at such distances from the seismological (e.g. Wolfe et al., 1997; French & Romanowicz, 2015) and topographical (e.g. Cadio et al., 2012; Davies et al., 2019) expressions of the plume will be challenging to link to underlying mantle dynamics.

Moreover, the farther plume material spreads from the conduit, the more heat it exchanges with the overlying lithosphere, and, thereby, the lower melt fractions and melting rates it can generate. Accordingly, low-intensity plume-derived melts produced far from their conduit may prove difficult to distinguish from melts derived purely through edge-driven processes (e.g. Figure 12s). Assessing the potential role of a plume may also be ambiguous if complex lithospheric structure forces plume-related volcanism to distribute adjacent to lithospheric steps, as observed in the *U400_Cont_Step* case, yielding a volcanic trend similar to that generated from shallow edge-driven processes (e.g. Duvernay et al., 2021). Therefore, Earth's continents, owing to their mechanical strength and non-uniform lithospheric structure, exert a primary control on the nature, location and principal characteristics of plume-related volcanism in continental settings. It follows that knowledge of regional lithospheric architecture becomes an essential prerequisite for identifying the dynamical mechanisms underpinning specific volcanic provinces, as emphasised by Davies and Rawlinson (2014) and Rawlinson et al. (2017).

4.4 The Arrival of Plume Material at Lithospheric Steps Can Completely Shut off Existing Magmatism

Changes in the asthenospheric flow field triggered by a plume can transform the dynamics in regions where edge-driven convection or shear-driven upwelling have previously sustained decompression melting. In particular, melting at lithospheric steps through edge-driven convection relies on passive return flows activated by negatively buoyant instabilities (e.g. Duvernay et al., 2021). Such return flows cannot develop if strong lateral currents, such as those induced by plume ascent and spreading, dominate the asthenospheric flow regime. As illustrated in the *U400_Ocean_Offshore* case (Figure 9), the arrival of a mantle plume offshore the continent, beneath a region of thin lithosphere, can completely shut off decompression melting at lithospheric steps by forcing material towards the continental boundary and, ultimately, downwards, below the continent. Such an effect is analogous to that occurring when asthenospheric shear drives flow towards lithospheric steps, as outlined by Davies and Rawlinson (2014) and Duvernay et al. (2021). This result is particularly counter-intuitive, as one would expect the excess heat carried by mantle plumes to facilitate decompression melting rather than act against it. Nonetheless, it may be critical in understanding why step-changes in lithospheric thickness, which should facilitate edge-driven convection, are not always associated with surface volcanism.

4.5 Plume Destabilisation Can Occur Through Interaction of Plume Flow with Surrounding Lithospheric Structure

In oceanic settings, buoyant plume material spreading in the immediate sub-lithospheric mantle assumes an elliptical shape, forming a structure commonly referred to as a plume pancake (e.g. Griffiths & Campbell, 1991; Ribe & Christensen, 1999). As noted above, the pancake cools down as it expands by exchanging heat with the overlying lithosphere. As a result, local anomalies in the temperature field develop and trigger the destabilisation of the buoyant structure through small-scale convection (e.g. Griffiths & Campbell, 1991). If the overlying lithospheric lid is thin enough, such dynamical instabilities can induce decompression melting in a geometrical pattern controlled by the plume's buoyancy flux and lithospheric motion (e.g. Ballmer et al., 2011).

Our results demonstrate that the destabilisation of a plume pancake can also stem from the interaction between buoyant material and the surrounding lithosphere. In particular, if the lithospheric structure channels plume material into confined regions, such as the indent of our *U400* lithospheric geometry, plume material accumulates, and areas of excess buoyancy develop. Where these narrow regions broaden, this enhanced buoyancy drives the re-distribution of plume material into adjacent asthenosphere, generating strong vertical currents that destabilise the entire structure. The resulting spatial distribution of small-scale convective patterns directly reflects the geometry of the LAB and its interaction with plume flow. In our simulations, structures such as linear ridges of partial melts form beneath thinner lithosphere, away from the plume conduit (e.g. the *U400_Ocean_Indent* case, Figure 11). Such complexities might be second-order effects that help explain the origin of transient volcanic events that lie offshore lithospheric structures similar to indents, such as along Australia's southeastern margin (Holford et al., 2012).

4.6 Potential Links Between Model Predictions and Earth's Observational Record

The analyses undertaken herein imply that significant decompression melting is unlikely to occur beneath deep continental roots, with plume material channelled towards regions of thinner lithosphere where it subsequently melts. This prediction is compatible with the observed global distribution of Neogene volcanism, which concentrates in areas of comparatively thin lithosphere (Figure 1). Accordingly, continental volcanic centres, generated by a mantle plume, may not always overlie the location of the plume conduit, resulting in intricate distributions of volcanism that are challenging to reconcile with underlying mantle dynamics.

The geographical distribution, geochronology and geochemistry of Earth's intraplate volcanic provinces provide a means to assess the applicability of our results. Whilst it is beyond the scope of the present study to examine every location in detail, there exist provinces that show characteristics consistent with those predicted by our models. For example, in eastern Australia, the Cosgrove track — Earth's longest continental hotspot track — marks the passage of a plume beneath thick continental lithosphere with a step-like structure (e.g. Fishwick et al., 2008; Davies, Rawlinson, et al., 2015). As a result, the volcanic track above the predicted path of the plume conduit is discontinuous, with wide volcanic gaps in regions of thick lithosphere. Nonetheless, a record of volcanism exists on a parallel trail to the east, where the lithosphere is thinner than inland (e.g. Davies, Rawlinson, et al., 2015; Meeuws et al., 2016; Rawlinson et al., 2017). These volcanic fields are offset from the re-constructed path of the Cosgrove plume, but their lavas display no systematic geochemical distinction in terms of major element, trace element and radiogenic isotope compositions relative to those formed atop the conduit (I. Jones et al., 2020). In the context of our results, this strongly suggests a direct association with the Cosgrove mantle plume for both tracks.

In the western Atlantic Ocean, the Vitória-Trindade Ridge represents a long-lived chain of age-progressive volcanic islands that extend from the eastern shore of South America to Martin Vaz Island, implying a link to an underlying mantle plume (dos Santos et al., 2021). The island track offshore connects to continental South America through the Abrolhos Volcanic Complex, a massive volcanic field that pre-dates the Vitória-Trindade Ridge. The Abrolhos Volcanic Complex recorded various stages of eruption between 35 and 70 Myr ago, representing a temporal duration comparable to the activity of the entire volcanic ridge (the last $\sim$35 Myr; dos Santos et al., 2021; Maia et al., 2021). Although it resembles the product of plume head impingement, dos Santos et al. (2021) suggest that it is likely not, an inference that our results support. The volcanic complex lies adjacent to the São Francisco Craton on land, which hosts several older occurrences of volcanism dated between 55–90 Myr ago, towards its western and southern boundaries (dos Santos et al., 2021). As a result, it is plausible that the Trindade plume impinged beneath the southwestern part of the São Francisco Craton, where volcanism was modest, given the thick overlying cratonic lithosphere. As South America was moving westwards away from Africa during the opening of the South Atlantic, the plume subsequently transited beneath the craton, prior to its emergence on the southeastern boundary of the craton, where it generated the extensive Abrolhos Volcanic Complex and the later Vitória-Trindade Ridge, which still erupts today at Martin Vaz Island (dos Santos et al., 2021).

In the North Atlantic Region, the Iceland plume is inferred to have first impinged Earth's lithosphere beneath Greenland (e.g. Marty et al., 1998; Meyer et al., 2007; Steinberger et al., 2019). While the exact path of the plume during the Cretaceous is not well-constrained, seismic tomography reveals that an east-west corridor of thinned lithosphere exists beneath Greenland, suggesting plume-driven thermo-mechanical erosion of the deeper lithosphere and, thereby, delineating a probable path for the Iceland plume (Lebedev et al., 2018). Interestingly, plume-related volcanism activated on both the eastern and western shores of Greenland about 62 Myr ago (Steinberger et al., 2019). While the presence of volcanism to the east — distributed parallel to the coastline and, therefore, indicative of the plume emerging at the continental boundary — agrees with the relative motion of the plume trending towards the current location of Iceland on the North Atlantic Ridge, volcanism along the western shore is more enigmatic, requiring the spreading of plume material beneath Greenland in the opposite direction (Steinberger et al., 2019). Such an observation correlates well with our results, where plume material spreading beneath a stable continent can enhance decompression melting at a continental boundary far from the plume conduit's location.

In Africa, volcanic fields such as Tibesti and the Northern Tanzanian Divergence have recorded evolutionary phases that display directional flow reminiscent of the emergence of a plume from beneath thicker lithosphere (e.g. Permenter & Oppenheimer, 2007; Mana et al., 2015), similar to the activation of enhanced melting within troughs in continental lithosphere highlighted herein. In Tibesti, successive volcanic phases, active in distinct parts of the region over the last 15 Myr, contributed to the build-up of the volcanic province. Eruptive history displays a progressive increase in erupted volumes followed by waning, and geochemical analyses of associated lavas highlight a significant range of geochemical signatures (Gourgaud & Vincent, 2004; Permenter & Oppenheimer, 2007; Deniel et al., 2015; Ball et al., 2019). Our results suggest that earlier, lower-volume volcanism could be linked to enhanced velocities ahead of a mantle plume, whilst later and more extensive volcanism could correspond to the arrival and progressive spreading of plume material at the LAB. Such a dynamic evolutionary regime could explain the large variability observed in the geochemistry of Tibesti lavas (e.g. Ball et al., 2019).

South of the border between Tanzania and Kenya, high-resolution seismic tomography images a broad mantle upwelling that interacts with the Tanzanian Craton (Clutier et al., 2021). The presence of the thick continental lithosphere deflects the ascent of the plume, which preferentially emerges at the craton's eastern margin (Koptev et al., 2015; Clutier et al., 2021). Geochronological analyses of the erupted products that distribute from the craton border to the west to Mount Kilimanjaro to the east, coupled with careful assessment of the tectonics of the encompassing region, reveal the presence of at least two volcanic trends, with different orientations, likely controlled by regional lithospheric structure (Le Gall et al., 2008; Mana et al., 2015). Additionally, geochemical signatures of lavas along each volcanic track display a progressive evolution, pointing towards potential mixing between two generating mechanisms (Mana et al., 2015), as suggested for Tibesti.

Finally, there are indications in the observational record that the interaction between plume flow and continental lithosphere can act against the development of convective instabilities adjacent to Earth's cratonic margins, thereby preventing decompression melting through mechanisms such as edge-driven convection. For example, the entire western margin of Africa hosts only limited Neogene volcanism, despite having long-lived cratonic margins (e.g. West African, Congo and Kaapvaal cratons), which should provide a favourable setting for edge-driven convection. Offshore, numerous volcanic ocean islands and seamounts, such as Canary, Cape Verde, the Cameroon Line, Saint Helena and Tristan-Gough, distribute between Azores to the North and Meteor to the South. Most have been linked to deep mantle upwellings associated with the African large low shear-wave velocity province (e.g. French & Romanowicz, 2015; Lei et al., 2020). In such a configuration, the impingement of many buoyant plumes offshore western Africa and their spreading in the sub-lithospheric mantle should drive asthenospheric flow from the Atlantic Ocean towards Africa. As a result, upwelling return flow associated with potential edge-driven instabilities along the cratonic margins of western Africa would be suppressed, potentially explaining the lack of volcanism at these locations over the Neogene.

4.7 Limitations and Future Work

Through their similarities with our previous suite of models (Duvernay et al., 2021), the present simulations share comparable limitations. In particular, melting at depth relies on a batch melting parameterisation of a peridotite assemblage, and our implementation does not account for changes in material properties, such as density and viscosity, that arise through melting. As such, we neglect complexities associated with multi-component melting (e.g. Shorttle et al., 2014) and potentially important feedbacks between melting and mantle dynamics (e.g. Gülcher et al., 2021). Furthermore, we do not simulate the effects of melt extraction and melt transport (Keller et al., 2017; Jain et al., 2019); this shortcoming needs to be considered when comparing our predicted melting rates with observations from the geological record.

In addition to our simplified treatment of melting, a number of assumptions have been made in our simulations. We use a diffusion creep rheology (thus neglecting the potentially substantial effects of dislocation creep), assume incompressibility and ignore the role of phase transitions. The impact of these assumptions should be analysed carefully in future work, although we expect the primary conclusions of our study to remain valid. Another potentially important aspect that we did not account for is the combined roles of plate motion and background asthenospheric flow, which will modulate the location and intensity of edge-driven instabilities, deflect mantle plumes during their ascent, and modify their spatio-temporal interaction with the LAB (e.g. Manglik & Christensen, 2006; Duvernay et al., 2021). Nonetheless, given the wide-ranging dynamics predicted in our simulations, we argue that this choice is justified, as it has allowed us to isolate and understand first-order features of these systems in the absence of further complexities. Despite this, there is little doubt that adding plate motion and asthenospheric flow to our models would shed additional light on plume-lithosphere interaction beneath continents and will likely be important in understanding differences in the volcanic record between fast-moving continents, such as Australia, and slow-moving continents, such as Africa.

The simulations examined herein incorporate mantle plumes. However, we only examined plumes of a specific buoyancy flux ($\sim$500 $\mathrm{kg\,s^{-1}}$), maintaining a fixed excess temperature (150 K), injection radius (200 km), and injection velocity (10 $\mathrm{cm\,yr^{-1}}$) across all simulations examined. We chose to focus on how the impingement location of a plume relative to a continent shapes the spatial interaction between these two entities at the LAB and the resulting magmatism, as opposed to the properties of the plume itself. Our results show that in a continental setting, the complex structure of the LAB is likely to play a crucial role in determining the nature and intricacies of plume-lithosphere interaction. They therefore demonstrate that the dynamic and magmatic expression of mantle plumes is not solely determined by their physical characteristics but also by the structure of overlying lithosphere. We speculate, however, that plumes with a higher buoyancy flux would enhance erosion of the LAB, more strongly modulate the regional flow field, enhance melting earlier during their ascent, and induce simultaneous volcanism at greater distances apart. Finally, we simulated purely thermal plumes, neglecting potential chemical heterogeneities. Although accounting for denser or more viscous materials in the plume conduit can alter the dynamics of the buoyant upwelling (e.g. Ballmer et al., 2013; T. Jones et al., 2016; Farnetani et al., 2018), it is unlikely that such features will strongly modulate the interaction between plumes and overlying continental lithosphere. Nonetheless, the presence of more fusible lithologies would likely enhance melt production (e.g. Shorttle et al., 2014) and should be considered in future studies.

5 Conclusions

Using a series of geodynamical models, we have investigated the interaction between upwelling mantle plumes and heterogeneous continental lithosphere to understand how melt-generating processes combine and control magmatism in some of Earth's most complex geological settings.

We find that pressures beneath thick continental cratons are sufficient to inhibit decompression melting immediately above plume upwellings. However, the heterogeneous structure of continental lithosphere gives rise to pressure gradients that channel plume material away from the conduit, concentrating it beneath thinner portions of the lithosphere where decompression melting can occur. In some scenarios, such anisotropic spreading of plume material can lead to simultaneous magmatism in regions located over 1000 km apart.

Our results illustrate how potential locations for plume-induced decompression melting are controlled by the structure of the lithosphere at depth and the location of plume impingement: in the absence of surface plate motions and background mantle flow, it is primarily the topography of the lithosphere-asthenosphere boundary that controls the spreading path of plumes and, hence, where the solidus is eventually crossed. Our results also demonstrate that overlying lithospheric structure ultimately dictates the geometry of magmatism: we find that the magmatic expression of plumes regularly concentrates adjacent to lithospheric steps, where it may be challenging to distinguish from that arising through edge-driven convection. Distinguishing between both driving mechanisms becomes even more challenging when plume-driven flow enhances magmatism at lithospheric steps several million years before the buoyant plume material enters the melting zone. In this scenario, erupted lavas will have no differentiating geochemical signature, despite the crucial role of the plume in activating melting.

Quite counter-intuitively, we find that if plumes impinge in regions of thinner lithosphere, the resulting asthenospheric flow regime can force material downwards and beneath the continent at lithospheric steps, shutting off pre-existing edge-related magmatism. In addition, under certain conditions, the interaction between plume material and lithospheric structure can induce internal destabilisation of the plume pancake, driving complex time-dependent magmatic patterns at the surface.

In conclusion, our study, which produces spatial and temporal magmatic patterns compatible with those observed on Earth, demonstrates that continental magmatism is likely the product of complex, time-dependent interactions between cratonic lithosphere, mantle plumes, and shallower dynamical processes, such as edge-driven convection. In turn, it emphasises the challenge of linking continental magmatism to underlying mantle dynamics and motivates an inter-disciplinary approach in future studies.

Acknowledgments

T.D. is funded by an ANU PhD Scholarship (International) Full-Time (737/2018). D.R.D., S.C.K. and T.D. acknowledge support from the Australian Research Council (ARC), under DP170100058. D.R.D. also acknowledges support from the Australian Research Data Commons (ARDC), under the G-Adopt platform grant PL031. C.R.M was funded by an Australian Government Research Training Program Domestic Scholarship. Numerical simulations were undertaken on the NCI National Facility in Canberra, Australia, which is supported by the Australian Commonwealth Government. The Fluidity computational modelling framework, including source code and documentation, is available from `https://fluidityproject.github.io/`; the release (tag 4.1.19) used for the simulations presented herein has been archived at Zenodo (Kramer et al., 2021). Similarly, example input files required to reproduce the simulations presented herein have been made available (Duvernay, 2022). The authors would like to thank Patrick Ball, Ian Campbell, Caroline Eakin, Siavash Ghelichkan, Mark Hoggard, Brian Kennett, Marthe Klöcking, Nick Rawlinson and Cian Wilson for fruitful discussions at various stages of this research. Figures have been prepared using Matplotlib, Cartopy, ParaView and Inkscape.

References

Afonso, J. C., Rawlinson, N., Yang, Y., Schutt, D. L., Jones, A. G., Fullea, J., & Griffin, W. L. (2016). 3-D multiobservable probabilistic inversion for the compositional and thermal structure of the lithosphere and upper mantle: III. Thermochemical tomography in the Western-Central US. *Journal of Geophysical Research: Solid Earth*, *121*(10), 7337–7370.

Artemieva, I. M. (2009). The continental lithosphere: reconciling thermal, seismic, and petrologic data. *Lithos*, *109*(1-2), 23–46.

Ashwal, L. D., & Burke, K. (1989). African lithospheric structure, volcanism, and topography. *Earth and Planetary Science Letters*, *96*(1-2), 8–14.

Austermann, J., Kaye, B. T., Mitrovica, J. X., & Huybers, P. (2014). A statistical analysis of the correlation between large igneous provinces and lower mantle seismic structure. *Geophysical Journal International*, *197*(1), 1–9.

Ball, P., White, N., Maclennan, J., & Stephenson, S. (2021). Global influence of mantle temperature and plate thickness on intraplate volcanism. *Nature communications*, *12*(1), 1–13.

Ball, P., White, N., Masoud, A., Nixon, S., Hoggard, M., Maclennan, J., … Kröpelin, S. (2019). Quantifying asthenospheric and lithospheric controls on mafic magmatism across North Africa. *Geochemistry, Geophysics, Geosystems*, *20*(7), 3520–3555.

Ballmer, M. D., Conrad, C. P., Smith, E. I., & Johnsen, R. (2015). Intraplate volcanism at the edges of the Colorado Plateau sustained by a combination of triggered edge-driven convection and shear-driven upwelling. *Geochemistry, Geophysics, Geosystems*, *16*(2), 366–379.

Ballmer, M. D., Ito, G., & Cheng, C. (2015). Asymmetric dynamical behavior of thermochemical plumes and implications for Hawaiian lava composition. *Hawaiian Volcanoes: From Source to Surface*, *208*, 35.

Ballmer, M. D., Ito, G., Van Hunen, J., & Tackley, P. J. (2011). Spatial and temporal variability in Hawaiian hotspot volcanism induced by small-scale convection. *Nature Geoscience*, *4*(7), 457–460.

Ballmer, M. D., Ito, G., Wolfe, C. J., & Solomon, S. C. (2013). Double layering of a thermochemical plume in the upper mantle beneath Hawaii. *Earth and Planetary Science Letters*, *376*, 155–164.

Barry, T., Ivanov, A., Rasskazov, S., Demonterova, E., Dunai, T., Davies, G., & Harrison, D. (2007). Helium isotopes provide no evidence for deep mantle involvement in widespread Cenozoic volcanism across Central Asia. *Lithos*, *95*(3-4), 415–424.

Bird, P. (2003). An updated digital model of plate boundaries. *Geochemistry, Geophysics, Geosystems*, *4*(3).

Bradshaw, T., Hawkesworth, C., & Gallagher, K. (1993). Basaltic volcanism in the Southern Basin and Range: no role for a mantle plume. *Earth and Planetary Science Letters*, *116*(1-4), 45–62.

Bredow, E., Steinberger, B., Gassmöller, R., & Dannberg, J. (2017). How plume-ridge interaction shapes the crustal thickness pattern of the Réunion hotspot track. *Geochemistry, Geophysics, Geosystems*, *18*(8), 2930–2948.

Cadio, C., Ballmer, M. D., Panet, I., Diament, M., & Ribe, N. (2012). New constraints on the origin of the Hawaiian swell from wavelet analysis of the geoid to topography ratio. *Earth and Planetary Science Letters*, *359*, 40–54.

Cas, R., Van Otterloo, J., Blaikie, T., & Van Den Hove, J. (2017). The dynamics of a very large intra-plate continental basaltic volcanic province, the Newer Volcanics Province, SE Australia, and implications for other provinces. *Geological Society, London, Special Publications*, *446*(1), 123–172.

Clutier, A., Gautier, S., & Tiberi, C. (2021). Hybrid local and teleseismic P-wave tomography in North Tanzania: role of inherited structures and magmatism on continental rifting. *Geophysical Journal International*, *224*(3), 1588–1606.

Conrad, C. P., Bianco, T. A., Smith, E. I., & Wessel, P. (2011). Patterns of intraplate volcanism controlled by asthenospheric shear. *Nature Geoscience*, *4*(5), 317–321.

Conrad, C. P., Wu, B., Smith, E. I., Bianco, T. A., & Tibbetts, A. (2010). Shear-driven upwelling induced by lateral viscosity variations and asthenospheric shear: A mechanism for intraplate volcanism. *Physics of the Earth and Planetary Interiors*, *178*(3-4), 162–175.

Courtillot, V., Davaille, A., Besse, J., & Stock, J. (2003). Three distinct types of hotspots in the Earth's mantle. *Earth and Planetary Science Letters*, *205*(3-4), 295–308.

Crisp, J. A. (1984). Rates of magma emplacement and volcanic output. *Journal of Volcanology and Geothermal Research*, *20*(3-4), 177–211.

Davies, D. R., & Davies, J. H. (2009). Thermally-driven mantle plumes reconcile multiple hot-spot observations. *Earth and Planetary Science Letters*, *278*(1-2), 50–54.

Davies, D. R., Goes, S., & Sambridge, M. (2015). On the relationship between volcanic hotspot locations, the reconstructed eruption sites of large igneous provinces and deep mantle seismic structure. *Earth and Planetary Science Letters*, *411*, 121–130.

Davies, D. R., & Rawlinson, N. (2014). On the origin of recent intraplate volcanism in Australia. *Geology*, *42*(12), 1031–1034.

Davies, D. R., Rawlinson, N., Iaffaldano, G., & Campbell, I. H. (2015). Lithospheric controls on magma composition along Earth's longest continental hotspot track. *Nature*, *525*(7570), 511–514.

Davies, D. R., Valentine, A., Kramer, S. C., Rawlinson, N., Hoggard, M., Eakin, C., & Wilson, C. (2019). Earth's multi-scale topographic response to global mantle flow. *Nature Geoscience*, *12*(10), 845–850.

Davies, D. R., Wilson, C. R., & Kramer, S. C. (2011). Fluidity: A fully unstructured anisotropic adaptive mesh computational modeling framework for geodynamics. *Geochemistry, Geophysics, Geosystems*, *12*(6).

Demidjuk, Z., Turner, S., Sandiford, M., George, R., Foden, J., & Etheridge, M. (2007). U-series isotope and geodynamic constraints on mantle melting processes beneath the Newer Volcanic Province in South Australia. *Earth and Planetary Science Letters*, *261*(3), 517–533.

Deniel, C., Vincent, P., Beauvilain, A., & Gourgaud, A. (2015). The Cenozoic volcanic province of Tibesti (Sahara of Chad): major units, chronology, and structural features. *Bulletin of Volcanology*, *77*(9), 74.

dos Santos, A. C., Mata, J., Jourdan, F., de Oliveira Rodrigues, S. W., Monteiro, L. G. P., Guedes, E., … Geraldes, M. C. (2021). Martin Vaz island geochronology: Constraint on the Trindade Mantle Plume track from the youngest and easternmost volcanic episodes. *Journal of South American Earth Sciences*, *106*, 103090.

Duncan, R. A., & Richards, M. (1991). Hotspots, mantle plumes, flood basalts, and true polar wander. *Reviews of Geophysics*, *29*(1), 31–50.

Dupré, B., & Allègre, C. J. (1983). Pb–Sr isotope variation in Indian Ocean basalts and mixing phenomena. *Nature*, *303*(5913), 142–146.

Duvernay, T. (2022, January). *Patol75/Continental-Magmatism-The-Surface-Manifestation-Of-Dynamic-Interactions-Between- Cratonic-Lithosphere: Submission to Geochemistry, Geophysics, Geosystems.* Zenodo. Retrieved from `https://doi.org/10.5281/zenodo.5847709` doi: 10.5281/zenodo.5847709

Duvernay, T., Davies, D. R., Mathews, C. R., Gibson, A. H., & Kramer, S. C. (2021). Linking intra-plate volcanism to lithospheric structure and asthenospheric flow. *Geochemistry, Geophysics, Geosystems*, e2021GC009953.

Ebinger, C. J., & Sleep, N. (1998). Cenozoic magmatism throughout east Africa resulting from impact of a single plume. *Nature*, *395*(6704), 788–791.

Farnetani, C. G., Hofmann, A. W., Duvernay, T., & Limare, A. (2018). Dynamics of rheological heterogeneities in mantle plumes. *Earth and Planetary Science Letters*, *499*, 74–82.

Farrington, R., Stegman, D., Moresi, L., Sandiford, M., & May, D. (2010). Interactions of 3D mantle flow and continental lithosphere near passive margins. *Tectonophysics*, *483*(1-2), 20–28.

Fishwick, S., Heintz, M., Kennett, B., Reading, A., & Yoshizawa, K. (2008). Steps in lithospheric thickness within eastern Australia, evidence from surface wave tomography. *Tectonics*, *27*(4).

Fishwick, S., & Rawlinson, N. (2012). 3-D structure of the Australian lithosphere from evolving seismic datasets. *Australian Journal of Earth Sciences*, *59*(6), 809–826.

French, S. W., & Romanowicz, B. (2015). Broad plumes rooted at the base of the Earth's mantle beneath major hotspots. *Nature*, *525*(7567), 95.

Gassmöller, R., Dannberg, J., Bredow, E., Steinberger, B., & Torsvik, T. H. (2016). Major influence of plume-ridge interaction, lithosphere thickness variations, and global mantle flow on hotspot volcanism—the example of Tristan. *Geochemistry, Geophysics, Geosystems*, *17*(4), 1454–1479.

Gibert, B., Seipold, U., Tommasi, A., & Mainprice, D. (2003). Thermal diffusivity of upper mantle rocks: Influence of temperature, pressure, and the deformation fabric. *Journal of Geophysical Research: Solid Earth*, *108*(B8).

Gourgaud, A., & Vincent, P. (2004). Petrology of two continental alkaline intraplate series at Emi Koussi volcano, Tibesti, Chad. *Journal of volcanology and geothermal research*, *129*(4), 261–290.

Griffiths, R., & Campbell, I. (1991). Interaction of mantle plume heads with the Earth's surface and onset of small-scale convection. *Journal of Geophysical Research: Solid Earth*, *96*(B11), 18295–18310.

Gülcher, A. J. P., Ballmer, M. D., & Tackley, P. J. (2021). Coupled dynamics and evolution of primordial and recycled heterogeneity in Earth's lower mantle. *Solid Earth*, *12*(9), 2087–2107.

Hart, S., Hauri, E., Oschmann, L., & Whitehead, J. (1992). Mantle plumes and entrainment: isotopic evidence. *Science*, *256*(5056), 517–520.

Herzberg, C., Asimow, P. D., Arndt, N., Niu, Y., Lesher, C., Fitton, J., … Saunders, A. (2007). Temperatures in ambient mantle and plumes: Constraints from basalts, picrites, and komatiites. *Geochemistry, Geophysics, Geosystems*, *8*(2).

Ho, K.-S., Ge, W.-C., Chen, J.-C., You, C.-F., Yang, H.-J., & Zhang, Y.-L. (2013).

Late Cenozoic magmatic transitions in the central Great Xing'an Range, Northeast China: Geochemical and isotopic constraints on petrogenesis. *Chemical Geology*, *352*, 1–18.

Hoggard, M. J., Czarnota, K., Richards, F. D., Huston, D. L., Jaques, A. L., & Ghelichkhan, S. (2020). Global distribution of sediment-hosted metals controlled by craton edge stability. *Nature Geoscience*, *13*(7), 504–510.

Hoggard, M. J., Parnell-Turner, R., & White, N. (2020). Hotspots and mantle plumes revisited: Towards reconciling the mantle heat transfer discrepancy. *Earth and Planetary Science Letters*, *542*, 116317.

Holford, S., Schofield, N., MacDonald, J., Duddy, I., & Green, P. (2012). Seismic analysis of igneous systems in sedimentary basins and their impacts on hydrocarbon prospectivity: Examples from the southern Australian margin. *The APPEA Journal*, *52*(1), 229–252.

Ito, G., Lin, J., & Gable, C. W. (1996). Dynamics of mantle flow and melting at a ridge-centered hotspot: Iceland and the Mid-Atlantic Ridge. *Earth and Planetary Science Letters*, *144*(1-2), 53–74.

Jain, C., Rozel, A. B., Tackley, P. J., Sanan, P., & Gerya, T. V. (2019). Growing primordial continental crust self-consistently in global mantle convection models. *Gondwana Research*, *73*, 96–122.

Jaupart, C., & Mareschal, J. (2005). Production from heat flow data. *The Crust*, *3*, 65–84.

Jellinek, A. M., & Manga, M. (2004). Links between long-lived hot spots, mantle plumes, D", and plate tectonics. *Reviews of Geophysics*, *42*(3).

Johnson, R. W., Johnson, R. W., Knutson, J., & Taylor, S. R. (1989). *Intraplate volcanism: in eastern Australia and New Zealand*. Cambridge University Press.

Jones, I., Ubide, T., Crossingham, T., Wilding, B., & Verdel, C. (2020). Evidence of a common source component for east Australian Cenozoic mafic magmatism. *Lithos*, *354*, 105254.

Jones, T., Davies, D. R., Campbell, I., Iaffaldano, G., Yaxley, G., Kramer, S. C., & Wilson, C. (2017). The concurrent emergence and causes of double volcanic hotspot tracks on the Pacific plate. *Nature*, *545*(7655), 472.

Jones, T., Davies, D. R., Campbell, I., Wilson, C., & Kramer, S. C. (2016). Do mantle plumes preserve the heterogeneous structure of their deep-mantle source? *Earth and Planetary Science Letters*, *434*, 10–17.

Kaislaniemi, L., & van Hunen, J. (2014). Dynamics of lithospheric thinning and mantle melting by edge-driven convection: Application to Moroccan Atlas mountains. *Geochemistry, Geophysics, Geosystems*, *15*(8), 3175–3189.

Katsura, T., Yoneda, A., Yamazaki, D., Yoshino, T., & Ito, E. (2010). Adiabatic temperature profile in the mantle. *Physics of the Earth and Planetary Interiors*, *183*(1-2), 212–218.

Katz, R. F., Spiegelman, M., & Langmuir, C. H. (2003). A new parameterization of hydrous mantle melting. *Geochemistry, Geophysics, Geosystems*, *4*(9).

Keller, T., Katz, R. F., & Hirschmann, M. M. (2017). Volatiles beneath mid-ocean ridges: Deep melting, channelised transport, focusing, and metasomatism. *Earth and Planetary Science Letters*, *464*, 55–68.

Kennett, B., & Davies, D. (2020). Intra-plate volcanism in North Queensland and eastern new Guinea: A cryptic mantle plume? *Gondwana Research*, *79*, 209–216.

King, S. D. (2007). Hotspots and edge-driven convection. *Geology*, *35*(3), 223–226.

King, S. D., & Adam, C. (2014). Hotspot swells revisited. *Physics of the Earth and Planetary Interiors*, *235*, 66–83.

King, S. D., & Anderson, D. L. (1998). Edge-driven convection. *Earth and Planetary Science Letters*, *160*(3-4), 289–296.

King, S. D., & Ritsema, J. (2000). African hot spot volcanism: small-scale convection in the upper mantle beneath cratons. *Science*, *290*(5494), 1137–1140.

Klöcking, M., White, N., Maclennan, J., McKenzie, D., & Fitton, J. (2018). Quantitative relationships between basalt geochemistry, shear wave velocity, and asthenospheric temperature beneath western North America. *Geochemistry, Geophysics, Geosystems*, *19*(9), 3376–3404.

Koptev, A., Burov, E., Calais, E., Leroy, S., Gerya, T., Guillou-Frottier, L., & Cloetingh, S. (2016). Contrasted continental rifting via plume-craton interaction: Applications to Central East African Rift. *Geoscience Frontiers*, *7*(2), 221–236.

Koptev, A., Calais, E., Burov, E., Leroy, S., & Gerya, T. (2015). Dual continental rift systems generated by plume–lithosphere interaction. *Nature Geoscience*, *8*(5), 388.

Kramer, S. C., Greaves, T., Funke, S. W., Wilson, C., Avdis, A., Davies, R., … Ham, D. A. (2021, August). *Fluidityproject/fluidity: Zenodo release.* Zenodo. Retrieved from `https://doi.org/10.5281/zenodo.5221157` doi: 10.5281/zenodo.5221157

Kramer, S. C., Wilson, C. R., & Davies, D. R. (2012). An implicit free surface algorithm for geodynamical simulations. *Physics of the Earth and Planetary Interiors*, *194*, 25–37.

Lebedev, S., Schaeffer, A. J., Fullea, J., & Pease, V. (2018). Seismic tomography of the Arctic region: Inferences for the thermal structure and evolution of the lithosphere. *Geological Society, London, Special Publications*, *460*(1), 419–440.

Le Gall, B., Nonnotte, P., Rolet, J., Benoit, M., Guillou, H., Mousseau-Nonnotte, M., … Déverchère, J. (2008). Rift propagation at craton margin.: Distribution of faulting and volcanism in the North Tanzanian Divergence (East Africa) during Neogene times. *Tectonophysics*, *448*(1-4), 1–19.

Lei, W., Ruan, Y., Bozdağ, E., Peter, D., Lefebvre, M., Komatitsch, D., … Pugmire, D. (2020). Global adjoint tomography—model GLAD-M25. *Geophysical Journal International*, *223*(1), 1–21.

Maia, T. M., dos Santos, A. C., Rocha-Júnior, E. R. V., de Morisson Valeriano, C., Mendes, J. C., Jeck, I. K., … Mohriak, W. U. (2021). First petrologic data for Vitória Seamount, Vitória-Trindade Ridge, South Atlantic: a contribution to the Trindade mantle plume evolution. *Journal of South American Earth Sciences*, *109*, 103304.

Mana, S., Furman, T., Turrin, B. D., Feigenson, M. D., & Swisher, C. C. (2015). Magmatic activity across the East African North Tanzanian divergence zone. *Journal of the Geological Society*, *172*(3), 368–389.

Manglik, A., & Christensen, U. (2006). Effect of lithospheric root on decompression melting in plume–lithosphere interaction models. *Geophysical Journal International*, *164*(1), 259–270.

Marty, B., Upton, B. G., & Ellam, R. M. (1998). Helium isotopes in early Tertiary basalts, northeast Greenland: Evidence for 58 Ma plume activity in the North Atlantic–Iceland volcanic province. *Geology*, *26*(5), 407–410.

Mathews, C. (2021). *Methods for tracking material properties within an unstructured, adaptive mesh computational modelling framework, with application to simulating the development of seismic anisotropy at spreading centres and transform faults* (Unpublished doctoral dissertation). Research School of Earth Sciences, ANU Colleges of Science, The Australian National University.

McKenzie, D. (1984). The generation and compaction of partially molten rock. *Journal of Petrology*, *25*(3), 713–765.

McNab, F., Ball, P., Hoggard, M., & White, N. (2018). Neogene uplift and magmatism of Anatolia: Insights from drainage analysis and basaltic geochemistry. *Geochemistry, Geophysics, Geosystems*, *19*(1), 175–213.

Meeuws, F. J., Holford, S. P., Foden, J. D., & Schofield, N. (2016). Distribution, chronology and causes of Cretaceous–Cenozoic magmatism along the magma-poor rifted southern Australian margin: Links between mantle melting and basin formation. *Marine and Petroleum Geology*, *73*, 271–298.

Meyer, R., Van Wijk, J., & Gernigon, L. (2007). The North Atlantic Igneous Province: A review of models for its formation. *Special Papers-Geological Society of America*, *430*, 525.

Missenard, Y., & Cadoux, A. (2012). Can Moroccan Atlas lithospheric thinning and volcanism be induced by edge-driven convection? *Terra Nova*, *24*(1), 27–33.

Morgan, W. J. (1971). Convection plumes in the lower mantle. *Nature*, *230*(5288), 42.

Nikogosian, I., Gartner, A. B., Van Bergen, M., Mason, P., & Van Hinsbergen, D. J. (2018). Mantle sources of recent Anatolian intraplate magmatism: A regional plume or local tectonic origin? *Tectonics*, *37*(12), 4535–4566.

Niu, Y. (2021). Lithosphere thickness controls the extent of mantle melting, depth of melt extraction and basalt compositions in all tectonic settings on Earth–a review and new perspectives. *Earth-Science Reviews*, 103614.

Nyblade, A. A., & Sleep, N. H. (2003). Long lasting epeirogenic uplift from mantle plumes and the origin of the Southern African Plateau. *Geochemistry, Geophysics, Geosystems*, *4*(12).

Özdemir, Y., & Güleç, N. (2014). Geological and geochemical evolution of the Quaternary Süphan Stratovolcano, Eastern Anatolia, Turkey: evidence for the lithosphere–asthenosphere interaction in post-collisional volcanism. *Journal of Petrology*, *55*(1), 37–62.

Permenter, J. L., & Oppenheimer, C. (2007). Volcanoes of the Tibesti massif (Chad, northern Africa). *Bulletin of volcanology*, *69*(6), 609–626.

Pollack, H. N., & Chapman, D. S. (1977). On the regional variation of heat flow, geotherms, and lithospheric thickness. *Tectonophysics*, *38*(3-4), 279–296.

Putirka, K. (2008). Excess temperatures at ocean islands: Implications for mantle layering and convection. *Geology*, *36*(4), 283–286.

Putirka, K. (2016). Rates and styles of planetary cooling on Earth, Moon, Mars, and Vesta, using new models for oxygen fugacity, ferric-ferrous ratios, olivine-liquid Fe-Mg exchange, and mantle potential temperature. *American Mineralogist*, *101*(4), 819–840.

Rawlinson, N., Davies, D. R., & Pilia, S. (2017). The mechanisms underpinning Cenozoic intraplate volcanism in eastern Australia: Insights from seismic tomography and geodynamic modeling. *Geophysical Research Letters*, *44*(19), 9681–9690.

Ribe, N., & Christensen, U. (1999). The dynamical origin of Hawaiian volcanism. *Earth and Planetary Science Letters*, *171*(4), 517–531.

Ritsema, J., Deuss, a. A., Van Heijst, H., & Woodhouse, J. (2011). S40RTS: a degree-40 shear-velocity model for the mantle from new Rayleigh wave dispersion, teleseismic traveltime and normal-mode splitting function measurements. *Geophysical Journal International*, *184*(3), 1223–1236.

Sarafian, E., Gaetani, G. A., Hauri, E. H., & Sarafian, A. R. (2017). Experimental constraints on the damp peridotite solidus and oceanic mantle potential temperature. *Science*, *355*(6328), 942–945.

Sengör, A., & Burke, K. (1978). Relative timing of rifting and volcanism on Earth and its tectonic implications. *Geophysical Research Letters*, *5*(6), 419–421.

Shorttle, O., Maclennan, J., & Lambart, S. (2014). Quantifying lithological variability in the mantle. *Earth and Planetary Science Letters*, *395*, 24–40.

Sleep, N., Ebinger, C., & Kendall, J.-M. (2002). Deflection of mantle plume material by cratonic keels. *Geological Society, London, Special Publications*, *199*(1), 135–150.

Smith, R. B., Jordan, M., Steinberger, B., Puskas, C. M., Farrell, J., Waite, G. P., . . . O'Connell, R. (2009). Geodynamics of the Yellowstone hotspot and mantle plume: Seismic and GPS imaging, kinematics, and mantle flow. *Journal of Volcanology and Geothermal Research*, *188*(1-3), 26–56.

Steinberger, B. (2000). Plumes in a convecting mantle: Models and observations for individual hotspots. *Journal of Geophysical Research: Solid Earth*, *105*(B5), 11127–11152.

Steinberger, B., Bredow, E., Lebedev, S., Schaeffer, A., & Torsvik, T. H. (2019). Widespread volcanism in the Greenland–North Atlantic region explained by the Iceland plume. *Nature Geoscience*, *12*(1), 61–68.

Stracke, A., Hofmann, A. W., & Hart, S. R. (2005). FOZO, HIMU, and the rest of the mantle zoo. *Geochemistry, Geophysics, Geosystems*, *6*(5).

Tang, Y.-J., Zhang, H.-F., & Ying, J.-F. (2006). Asthenosphere–lithospheric mantle interaction in an extensional regime: implication from the geochemistry of Cenozoic basalts from Taihang Mountains, North China Craton. *Chemical Geology*, *233*(3-4), 309–327.

Tatsumi, Y., Hamilton, D., & Nesbitt, R. (1986). Chemical characteristics of fluid phase released from a subducted lithosphere and origin of arc magmas: evidence from high-pressure experiments and natural rocks. *Journal of Volcanology and Geothermal Research*, *29*(1-4), 293–309.

Turcotte, D., & Oxburgh, E. R. (1978). Intra-plate volcanism. *Philosophical Transactions of the Royal Society of London. Series A, Mathematical and Physical Sciences*, *288*(1355), 561–579.

van den Hove, J. C., Van Otterloo, J., Betts, P. G., Ailleres, L., & Cas, R. A. (2017). Controls on volcanism at intraplate basaltic volcanic fields. *Earth and Planetary Science Letters*, *459*, 36–47.

Wellman, P., & McDougall, I. (1974). Cainozoic igneous activity in eastern Australia. *Tectonophysics*, *23*(1-2), 49–65.

White, W. M., McBirney, A. R., & Duncan, R. A. (1993). Petrology and geochemistry of the Galápagos Islands: Portrait of a pathological mantle plume. *Journal of Geophysical Research: Solid Earth*, *98*(B11), 19533–19563.

Wilson, C. (2009). *Modelling multiple-material flows on adaptive unstructured meshes* (Unpublished doctoral dissertation). Imperial College London.

Wolfe, C. J., Bjarnason, I. T., VanDecar, J. C., & Solomon, S. C. (1997). Seismic structure of the Iceland mantle plume. *Nature*, *385*(6613), 245–247.

Ye, Y., Schwering, R. A., & Smyth, J. R. (2009). Effects of hydration on thermal expansion of forsterite, wadsleyite, and ringwoodite at ambient pressure. *American Mineralogist*, *94*(7), 899–904.

Zhang, R., Wu, Q., Sun, L., He, J., & Gao, Z. (2014). Crustal and lithospheric structure of Northeast China from S-wave receiver functions. *Earth and Planetary Science Letters*, *401*, 196–205.

Continental Magmatism: The Surface Manifestation of Dynamic Interactions Between Cratonic Lithosphere, Mantle Plumes and Edge-Driven Convection

Thomas Duvernay[1], D. Rhodri Davies[1], Christopher R. Mathews[1], Angus H. Gibson[1], Stephan C. Kramer[2]

[1]Research School of Earth Sciences, Australian National University, Canberra, ACT, Australia
[2]Department of Earth Science and Engineering, Imperial College London, London, UK

Key Points:

- The interaction between mantle plumes and continental lithosphere produces complex spatial and temporal magmatic trends at the surface.
- Lithospheric thickness gradients channel plume material towards areas of thin lithosphere, facilitating melting far from the plume conduit.
- Magmatic contributions from edge-driven convection and mantle plumes can be challenging to distinguish in continental settings.

Corresponding author: Thomas Duvernay, `thomas.duvernay@anu.edu.au`

Abstract

Several of Earth's intra-plate volcanic provinces occur within or adjacent to continental lithosphere, with many believed to mark the surface expression of upwelling mantle plumes. Nonetheless, studies of plume-derived magmatism have generally focussed on ocean-island volcanism, where the overlying rigid lithosphere is of uniform thickness. Here, we investigate the interaction between mantle plumes and heterogeneous continental lithosphere using a series of geodynamical models. Our results demonstrate that the spatio-temporal magmatic expression of plumes in these continental settings is complex and strongly depends on the location of plume impingement, differing substantially from that expected beneath oceanic lithosphere. Where plumes ascend beneath thick continental cratons, the overlying lid locally limits decompression melting. However, gradients in lithospheric thickness channel plume material towards regions of thinner lithosphere, activating magmatism away from the plume conduit, sometimes simultaneously at locations more than a thousand kilometres apart. This magmatism regularly concentrates at lithospheric steps, where it may be difficult to distinguish from that arising through edge-driven convection, especially if differentiating geochemical signatures are absent, as implied by some of our results. If plumes impinge in regions of thinner lithosphere, the resulting asthenospheric flow regime can force material downwards at lithospheric steps, shutting off pre-existing edge-related magmatism. In addition, under certain conditions, the interaction between plume material and lithospheric structure can induce internal destabilisation of the plume pancake, driving complex time-dependent magmatic patterns at the surface. Our study highlights the challenges associated with linking continental magmatism to underlying mantle dynamics and motivates an inter-disciplinary approach in future studies.

Plain Language Summary

As explained by the theory of plate tectonics, most of Earth's volcanism concentrates on the boundaries between lithospheric plates. However, a significant class of volcanism occurs within plate interiors. This volcanism is usually associated with the ascent of mantle plumes — buoyant upwellings of hot rock that rise through the mantle towards Earth's surface. Yet, the exact link between mantle plumes and surface volcanism is not fully understood, particularly in continental regions where Earth's outermost shell — the lithosphere — exhibits substantial variations in thickness and composition, owing to a complex and protracted evolutionary history. In the present study, we use multi-resolution 3-D computational models to simulate the interaction between mantle plumes and heterogeneous continental lithosphere to demonstrate how the structure and geometry of this overlying lithospheric 'lid' shape the volcanic response at Earth's surface. Our results provide new pathways towards understanding the link between surface volcanism and underlying dynamical processes within Earth's interior.

1 Introduction

Volcanism on Earth is conceptualised within the framework of plate tectonics, which describes the planet's outermost shell — the lithosphere — as a collection of mobile, rigid plates separated by discrete tectonic boundaries. Relative motion between these surface plates induces melting in the sub-lithospheric mantle, either through passive decompression at a mid-ocean ridge (e.g. Sengör & Burke, 1978) or enrichment in volatile elements at a subduction zone (e.g. Tatsumi et al., 1986). Such plate boundary settings host most of Earth's magmatic activity (e.g. Crisp, 1984), although a significant class of volcanism occurs within plate interiors (Figure 1). This so-called intra-plate volcanism is difficult to reconcile with plate tectonic theory (e.g. Turcotte & Oxburgh, 1978). Our current understanding of its origins relies on the notion of upwelling convective currents within Earth's mantle, both at small and large scales, which lead to decompression melting in

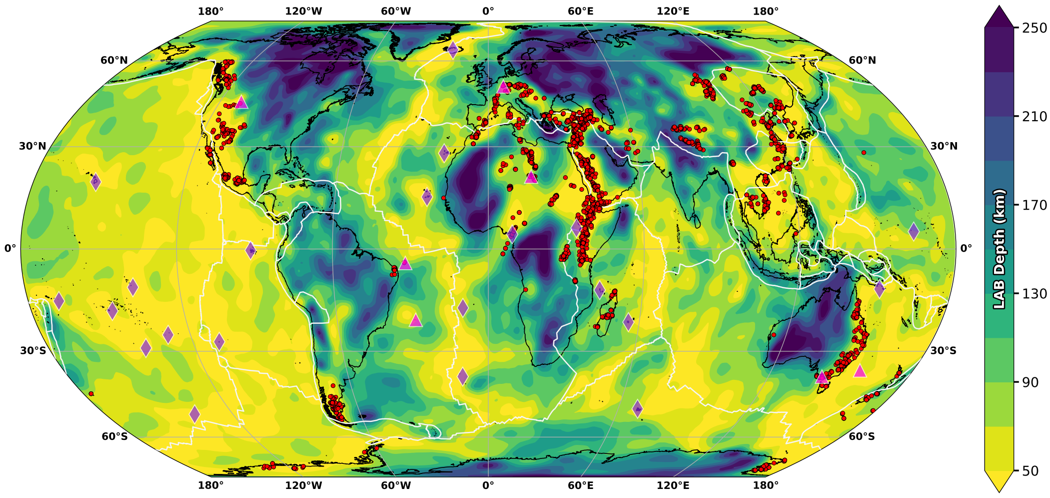

Figure 1. Intra-plate volcanism in the context of lithospheric structure. Background colours show a seismically-derived estimate of lithospheric thickness from Davies et al. (2019). White segments, sourced from Bird (2003), delimit tectonic plate boundaries. Purple diamonds indicate the location of primary and clearly resolved plumes, based upon full-waveform seismic tomography (French & Romanowicz, 2015); additional magenta triangles denote intra-plate volcanic regions from the catalogue of Steinberger (2000) that display a clear, long-lived age progression for over 15 Myr, which strongly supports generation by deep-rooted mantle plumes (e.g. Courtillot et al., 2003). Red dots mark Neogene volcanic occurrences on continents, as compiled by Ball et al. (2021), which are generally restricted to thinner regions of lithosphere. The figure highlights several areas where upwelling mantle plumes rise in close proximity to cratonic lithosphere, for example, within and adjacent to the African, North American and Australian continents.

the shallow asthenosphere that is largely independent of surface plate motions (e.g. Ito et al., 1996; King & Anderson, 1998; Ribe & Christensen, 1999; King & Ritsema, 2000; Jellinek & Manga, 2004; Farrington et al., 2010; Conrad et al., 2011; Kaislaniemi & van Hunen, 2014; Duvernay et al., 2021).

Large-scale upwelling flow takes the form of mantle plumes — buoyant parcels of hot rock that rise from a thermal boundary layer at the core-mantle boundary towards Earth's surface (e.g. Morgan, 1971). The vigorous ascent of plumes through the upper mantle, as well as their rooting in the higher-viscosity lower mantle, ensures that their location remains stable relative to overlying lithosphere, providing a straightforward explanation for age-progressive volcanism both in the oceans and on continents (e.g. Morgan, 1971; Duncan & Richards, 1991; Davies, Rawlinson, et al., 2015). Smaller-scale convective motions occur shallower and manifest, for example, as edge-driven flows that develop adjacent to lithospheric steps (e.g. King & Anderson, 1998). More precisely, in the context of passive margins, denser oceanic lithosphere destabilises and sinks through the underlying asthenosphere, driving an upwelling return flow in the form of a convective cell that facilitates modest decompression melting (e.g. Duvernay et al., 2021). Alternatively, the presence of favourably oriented asthenospheric shear can stimulate similar ascending currents and associated magmatism where the lithosphere rapidly thins (e.g. Conrad et al., 2010; Duvernay et al., 2021). In combination, these shallow mechanisms are postulated to explain intra-continental and continental margin volcanism at a number of locations (e.g. King & Ritsema, 2000; Demidjuk et al., 2007; King, 2007; Conrad et al., 2011; Missenard & Cadoux, 2012; Davies & Rawlinson, 2014; Klöcking et al., 2018).

The role of mantle plumes in generating ocean island volcanism is becoming increasingly well understood (e.g. Davies & Davies, 2009; Ballmer et al., 2011; Ballmer, Ito, & Cheng, 2015; Gassmöller et al., 2016; Bredow et al., 2017; T. Jones et al., 2017). However, their contribution towards continental volcanism remains unclear, given difficulties in separating plume-related magmatism from that produced by the shallower mechanisms described above (e.g. King, 2007). Figure 1 illustrates that most Neogene continental volcanic provinces (Ball et al., 2021) are located in regions of comparatively thin lithosphere (generally less than ~ 90 km thick), adjacent to step-changes in lithospheric thickness. Whilst such settings are favourable for edge- and shear-driven mechanisms (e.g. Conrad et al., 2011; Duvernay et al., 2021), Figure 1 also illustrates that many of these volcanic regions lie in close proximity to mantle plumes. Decompression melting is unlikely at the high pressures underlying continental cratons (e.g. Davies, Rawlinson, et al., 2015; Niu, 2021), and, thus, it has been argued that the preferential occurrence of volcanism in areas of thinner continental lithosphere is due to the channelling of plume material into these regions (e.g. Ebinger & Sleep, 1998; Sleep et al., 2002; Nyblade & Sleep, 2003; Manglik & Christensen, 2006). Accordingly, the relative contributions of edge-related mechanisms and mantle plumes remain unclear and are likely variable across different volcanic provinces. Pulling apart these contributions is challenging, particularly since they may interact, as is hinted by the observational record in several places (e.g. Ebinger & Sleep, 1998; Nyblade & Sleep, 2003; Davies, Rawlinson, et al., 2015; Kennett & Davies, 2020).

Among the intra-plate volcanic provinces highlighted in Figure 1, several show evidence of an interplay between edge-related convective instabilities and mantle plumes. In eastern Australia, the combination of age-progressive and non-age-progressive volcanism, onshore and offshore of a continent with a step-like lithospheric architecture (e.g. Fishwick et al., 2008; Fishwick & Rawlinson, 2012; Rawlinson et al., 2017), makes it challenging to identify and isolate the dynamical mechanisms controlling Cenozoic volcanism (e.g. Wellman & McDougall, 1974; Johnson et al., 1989; Davies & Rawlinson, 2014; Davies, Rawlinson, et al., 2015; Kennett & Davies, 2020; Ball et al., 2021). To add further complexity, even the age-progressive volcanic chains, postulated to be the surface expression of mantle plumes, display volcanic gaps in regions of thick lithosphere, indicating that lithospheric thickness variations control where plume-related melting can occur and where the resulting melts can rise to the surface (e.g. Davies, Rawlinson, et al., 2015; Niu, 2021; Ball et al., 2021). The African continent hosts several volcanic provinces adjacent to ancient cratonic terrains and is underlain by one of the two deep-mantle, large low seismic velocity provinces that spawn several of Earth's mantle plumes (e.g. Ashwal & Burke, 1989; Ritsema et al., 2011; Austermann et al., 2014; Davies, Goes, & Sambridge, 2015). Africa, therefore, constitutes a setting in which multiple mechanisms, both shallow and deep-rooted, likely combine to dictate the nature and characteristics of surface volcanism (e.g. Ebinger & Sleep, 1998; Nyblade & Sleep, 2003; Ball et al., 2019). In western North America, the presence of the Yellowstone caldera and its associated 15 Myr age-progressive volcanic track (e.g. Smith et al., 2009) contrasts with the occurrence of many smaller non-age-progressive volcanic fields, including those surrounding the Colorado Plateau (e.g. Afonso et al., 2016; Klöcking et al., 2018). The extensive Abrolhos Volcanic Complex on the South American continent, where volcanism was locked to the moving plate from 70 Myr to 35 Myr, prior to its emergence at the age-progressive Vitória-Trindade Ridge (dos Santos et al., 2021), hints at a complex dynamical regime modulated by cratonic lithosphere, edge-related processes and upwelling mantle flow. Finally, in Anatolia, another continental region with significant variations in lithospheric thickness, the origin of recent Neogene volcanism is debated, with studies advocating an interaction between ascending plume-like flow and lithospheric instabilities (e.g. Özdemir & Güleç, 2014; McNab et al., 2018; Nikogosian et al., 2018).

The intricacies that characterise many volcanic provinces at Earth's surface illustrate that additional efforts are required to obtain a deeper understanding of how plumes interact with continental lithosphere and the associated shallow convective processes to control the generation of intra-plate volcanism within Earth's highly heterogeneous continents. However, despite recent modelling and observational efforts to constrain the nature and dynamics of shallow convective flows (e.g. Kaislaniemi & van Hunen, 2014; van den Hove et al., 2017; Duvernay et al., 2021), few studies have systematically analysed their interaction with upwelling mantle plumes, particularly in a highly heterogeneous continental setting (e.g. Farrington et al., 2010; Koptev et al., 2015). The examples described above suggest that such interactions could be critical to controlling the distribution and intensity of intra-plate volcanism in these settings.

In this study, through a series of numerical simulations, we analyse the interaction between mantle plumes and continental lithospheric structure and the resulting impact on shallow convective processes. Our study builds on Duvernay et al. (2021), where edge-driven convection and shear-driven upwelling were examined in isolation, allowing us to illustrate how the incorporation of plumes can explain complex magmatic patterns observed within and adjacent to Earth's continents, as described above. Our simulations incorporate continents of different geometries and include variations in the depth and architecture of the continental lithosphere-asthenosphere boundary (LAB) consistent with those imaged on Earth (e.g. Afonso et al., 2016; Rawlinson et al., 2017). For each simulation, the plume's location relative to the continent is varied, allowing us to examine plume-lithosphere interaction across a wide range of configurations.

Our results demonstrate that even when plumes impinge beneath regions of thicker lithosphere, magmatism concentrates beneath thinner lithosphere, consistent with the volcanic record displayed in Figure 1: lithospheric structure channels the spread of plume material towards regions of thinner lithosphere, where it melts. Importantly, this highlights how the locus of plume arrival, relative to the continent, determines the magmatic response. Moreover, we emphasise that plumes impinging beneath continental interior can trigger melting simultaneously in distinct regions, sometimes located several hundreds of kilometres away from the conduit and over a thousand kilometres apart. Plumes can also shut off pre-existing decompression melting zones at lithospheric steps by driving lateral flow towards the steps, impeding previous ascending currents. Our findings provide fundamental new insight into the generation of intra-plate volcanism within Earth's continents and shed light on the critical processes and interactions that shape the magmatic response to underlying dynamics.

2 Methods

The simulations presented here build on those of Duvernay et al. (2021). They utilise Fluidity — a finite element, control-volume computational modelling framework (e.g. Davies et al., 2011; Kramer et al., 2012, 2021) — to solve the equations governing incompressible (Boussinesq) mantle dynamics. Simulations are run within a 3-D Cartesian box of dimensions 4000:4000:660 km (x:y:z) and take advantage of Fluidity's anisotropic, unstructured, adaptive meshing capabilities. Furthermore, they exploit Fluidity's multi-material (Wilson, 2009) and particle-in-cell (Mathews, 2021) functionalities to track, respectively, individual materials — continental crust, continental lithosphere and oceanic lithosphere/mantle, which can have distinct material properties — and melt production across the computational domain. Melt productivity is calculated using the parameterisation of Katz et al. (2003), which is coupled to a modified version of the framework of McKenzie (1984), as described in Duvernay et al. (2021).

In all simulations, deformation is accommodated through diffusion creep, and the associated viscosity is defined using a classical Arrhenius law that is both pressure- and temperature-dependent,

$$\mu = A \times \exp\left(\frac{E^* + \rho_0 g \overline{z}\, V^*}{R(T + \psi \overline{z})}\right). \tag{1}$$

Table 1. *Model parameters common to all simulations*

Name	Symbol	Value	Units
Reference Density	$\rho_0^{Mant} \mid \rho_0^{Cont} \mid \rho_0^{Crust}$	3370 | 3300 | 2900[a]	$\mathrm{kg\,m^{-3}}$
Gravity	g	9.8	$\mathrm{m\,s^{-2}}$
Gas Constant	R	8.3145	$\mathrm{J\,K^{-1}\,mol^{-1}}$
Thermal Expansion	α	3×10^{-5}[b]	$\mathrm{K^{-1}}$
Surface Temperature	T_S	290	K
Mantle Temperature	T_M	1650[c,d]	K
Plume Temperature	T_P	1800	K
Plume Injection Velocity	v_P	10	$\mathrm{cm\,yr^{-1}}$
Plume Disc Radius	R_P	200	km
Adiabatic Gradient	ψ	4×10^{-4}[e]	$\mathrm{K\,m^{-1}}$
Thermal Diffusion	κ	6×10^{-7}[f]	$\mathrm{m^2\,s^{-1}}$
Internal Heating (Crust)	ϕ	2.6×10^{-13}[g]	$\mathrm{K\,s^{-1}}$
Internal Heating (Elsewhere)	ϕ	4×10^{-15}[h]	$\mathrm{K\,s^{-1}}$
Activation Energy	E^*	350	$\mathrm{kJ\,mol^{-1}}$
Activation Volume	V^*	6.8×10^{-6}	$\mathrm{m^3\,mol^{-1}}$
Viscosity Pre-Factor	$A^{Mant} \mid A^{Cont}$	$2.6 \times 10^{7} \mid 2.6 \times 10^{10}$	Pa s
Viscosity Bounds	μ_{min}-μ_{max}	10^{18}-10^{24}	Pa s
Water Content (Melting)	X_{H_2O}	300	ppm

[a] Artemieva (2009). [b] Ye et al. (2009). [c] Putirka (2016). [d] Sarafian et al. (2017). [e] Katsura et al. (2010). [f] Gibert et al. (2003). [g] $\equiv 1.3 \times 10^{-6}\,\mathrm{W\,m^{-3}}$ (Jaupart & Mareschal, 2005). [h] $\equiv 2 \times 10^{-8}\,\mathrm{W\,m^{-3}}$ (Pollack & Chapman, 1977).

Here, A is the viscosity pre-factor, E^* the activation energy, ρ_0 the reference density, g the acceleration of gravity, $\bar{z}$ the depth, V^* the activation volume, R the gas constant, T the temperature, and ψ the adiabatic gradient. We note that this formulation is identical to that used in Duvernay et al. (2021) for simulations without a low-viscosity channel. Free-slip velocity boundary conditions are imposed at the top of the domain together with a zero-slip base and lithostatic sidewalls that permit normal flow only. The temperature is set to 290 K at the surface and 1650 K — the upper mantle potential temperature — at 660 km depth; boundary conditions are left free on all sidewalls. Internal heating is included throughout the domain, with a higher rate specified within the continental crust. Key model parameters are presented in Table 1.

Simulations incorporate a centred continental block (crust and lithospheric mantle), located between $x, y = 1250$ km and $x, y = 2750$ km, that is characterised by a lower density and higher viscosity relative to asthenospheric mantle (Table 1). Oceanic lithosphere surrounds the continent and is initialised using the thermal structure of a half-space cooling model of age 40 Myr: it is originally $\sim$90 km thick, as approximated by the depth of the 1620 K isotherm. The transition between ocean and continent is achieved by smooth 200 km–wide lithospheric steps, with the boundary between continental and oceanic material halfway along the step. We focus on two distinct continental geometries, both of which were analysed in Duvernay et al. (2021): (i) Case *U400* (Figure 2a), a 200 km–thick flat-bottom continent that features a 400 km–wide oceanic indent, and (ii) Case *Complex* (Figure 2b), a non-indented continental block with a heterogeneous, multi-scale lithospheric thickness distribution. The inclusion of an indent in the *U400* geometry mimics first-order characteristics of continental architectures imaged on Earth (e.g. Davies & Rawlinson, 2014; Zhang et al., 2014; Rawlinson et al., 2017; Klöcking et al., 2018; Hoggard, Czarnota, et al., 2020), whilst the *Complex* geometry better reflects the smaller-scale structure of Earth's continents at depth (e.g. Afonso et al., 2016; Rawlinson et al., 2017) (Figure 1). As these two continental configurations trigger edge-driven

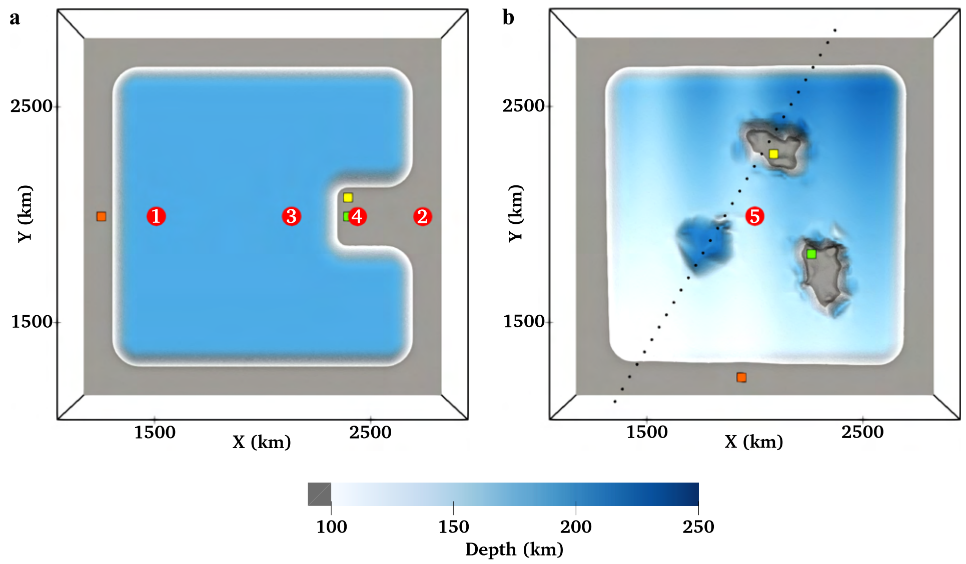

Figure 2. View from below of the initial lithosphere-asthenosphere boundary as delineated by the 1620 K isotherm. Red dots indicate locations of plume injection in our numerical experiments, with 1 corresponding to *U400_Cont_Step*, 2 to *U400_Ocean_Offshore*, 3 to *U400_Cont_Indent*, 4 to *U400_Ocean_Indent*, and 5 to *Complex_Cont_Centre*. Coloured squares denote probed areas investigated in Figure 6. (a) *U400* geometry. (b) *Complex* geometry. The dotted black line indicates the location of the slices presented in Figures S1 and S2.

magmatism (Duvernay et al., 2021), we run cases both with and without a mantle plume to isolate the plume's role in our quantitative diagnostics.

When incorporating a plume, it is injected at 660 km depth through a disc of radius $R_P = 200$ km, on which temperature and vertical velocity boundary conditions are prescribed according to

$$B + C \times \exp\left[\left(\frac{d}{R_P}\right)^2 \ln\left(\frac{0.1}{T_P - T_M}\right)\right], \tag{2}$$

with d the distance to the centre of the disc and $T_P = 1800$ K the plume temperature. In the case of temperature, $B = T_M$ and $C = T_P - T_M$. For velocity, $B = 0$ and $C = v_P$, the injection velocity, set to 10 cm yr^{-1}; horizontal velocities are set to zero within the disc. The resulting plumes have an excess temperature of 150 K relative to background mantle, which is compatible with petrological estimates of 100 K–300 K (e.g. Herzberg et al., 2007; Putirka, 2008). Moreover, they have a mass flux of ≈500 kg s^{-1}, while recent estimates for active hotspots worldwide range from 200 kg s^{-1} to 4000 kg s^{-1}, with the highest values observed at Iceland and Hawaii (e.g. King & Adam, 2014; Hoggard, Parnell-Turner, & White, 2020). Our plumes, therefore, are representative of those at the lower end of the predicted range, which include a large number of magmatic hotspots both on continents and within the oceans.

The location of plume injection, relative to the continent, is varied (Figure 2), allowing us to examine a wide range of plausible interactions between a plume and overlying continental lithosphere. First, making use of the *U400* geometry, the plume's disc is placed at four different positions along $y = 2000$ km, thus defining four cases: (i) *U400_Cont_Step*, where the plume is injected at $x = 1450$ km beneath the continent, adjacent to a long, linear lithospheric step; (ii) *U400_Ocean_Offshore*, where the plume is located at $x =$ 2850 km offshore the oceanic indent; (iii) *U400_Cont_Indent*, with the plume centred

Table 2. *Summary of simulations examined*

Name	Continental geometry	Disc centre x-coordinate	Plume location
U400	*U400*	—	—
Complex	*Complex*	—	—
U400_ Cont_ Step	*U400*	1450 km	Below continent, far from indent
U400_ Ocean_ Offshore	*U400*	2850 km	Below ocean, offshore indent
U400_ Cont_ Indent	*U400*	2150 km	Below continent, nearby indent
U400_ Ocean_ Indent	*U400*	2500 km	Below ocean, below indent
Complex_ Cont_ Centre	*Complex*	2000 km	Below continent, centred

Note. Disc centre y-coordinate is set to 2000 km for all simulations incorporating a plume.

at $x = 2150$ km beneath the continent, adjacent to the indent; and (iv) *U400_ Ocean_ Indent*, where the plume rises at $x = 2500$ km directly beneath the oceanic indent. In addition, we examine a fifth plume model, *Complex_ Cont_ Centre*, where the plume is injected at $x, y = 2000$ km, centred beneath the *Complex* continental geometry. A summary of all cases examined is provided in Table 2.

3 Results

We first present results from our reference cases that do not include a mantle plume (Section 3.1). These allow us to isolate the effect of incorporating plumes in our subsequent simulations (Section 3.2). To illustrate the dynamics of our simulations, we display temporal snapshots of temperature, vertical velocity and melting rates, at either 120 km depth (*U400* geometry) or 180 km depth (*Complex* geometry), with the increased depth for the latter cases allowing us to focus on the interaction between the plume and the base of the heterogeneous continental lithosphere. In addition, for plume cases, we display melt production rates relative to the relevant reference case, highlighting the plume's impact.

3.1 Reference Cases

These cases are almost identical to those presented in Duvernay et al. (2021), differing only in the depth extent of the computational domain — 660 km here, as opposed to 1000 km — and the velocity boundary conditions on sidewalls — open to normal flow in the simulations examined herein, as opposed to free-slip. As illustrated in Figure 3a–i, for the *U400* geometry, edge-driven instabilities, induced by the negative buoyancy of oceanic lithosphere, develop along all lithospheric steps. These generate passive upwelling flows below adjacent oceanic lithosphere, forming convective rolls. We find that upwelling velocities are enhanced within the oceanic indent (Figure 3b), as the geometry of the inner corners facilitates the coalescence of upwelling currents (Davies & Rawlinson, 2014; Duvernay et al., 2021). As a result, melting rates are substantially higher close to the indent's inner corners over the first ∼20 Myr of model evolution (Figure 3f). At later stages (Figure 3j–o), melt production is more consistent across all steps (Figure 3l), owing to the sinking of primary instabilities and the growth of secondary instabilities, as reflected, for example, by intense offshore downwellings in Figure 3k, which generate shallow, focussed upwellings that sustain melting (Duvernay et al., 2021).

Comparable snapshots for the *Complex* continental geometry are presented in Figure 4. As with the previous case, instabilities develop all around the continent. During the first ∼10 Myr of model evolution (Figure 4a–c), negatively buoyant material sinks faster adjacent to thicker portions of the continent, which facilitate the development of

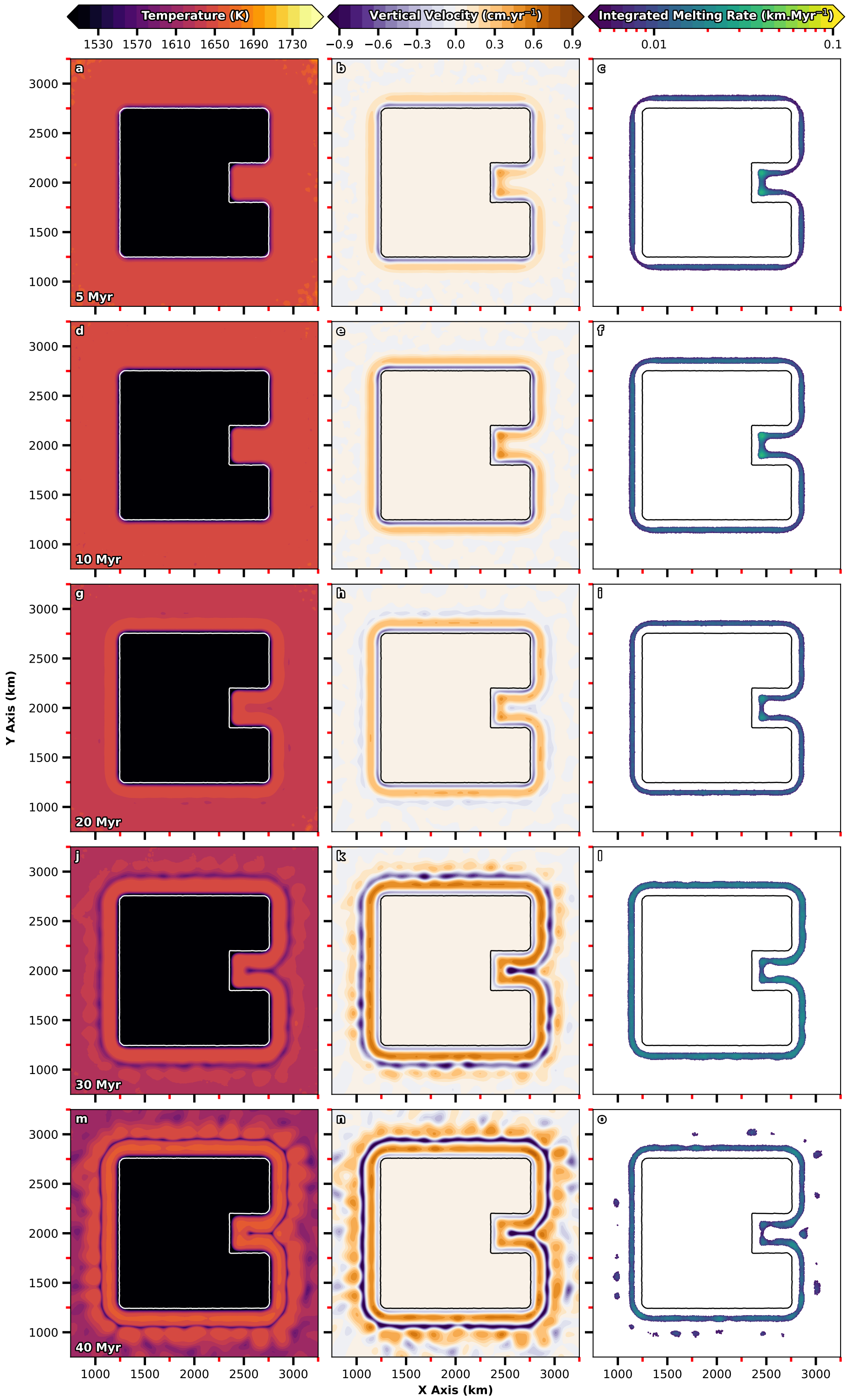

Figure 3. Temporal evolution of the *U400* geometry in the absence of a mantle plume. The first and second columns display horizontal slices of temperature and vertical velocity at 120 km depth, whilst the third column shows instantaneous melting rates, integrated along the vertical axis (methodology described in Duvernay et al., 2021). The white/black contour delineates the continental boundary at the depth of the slice.

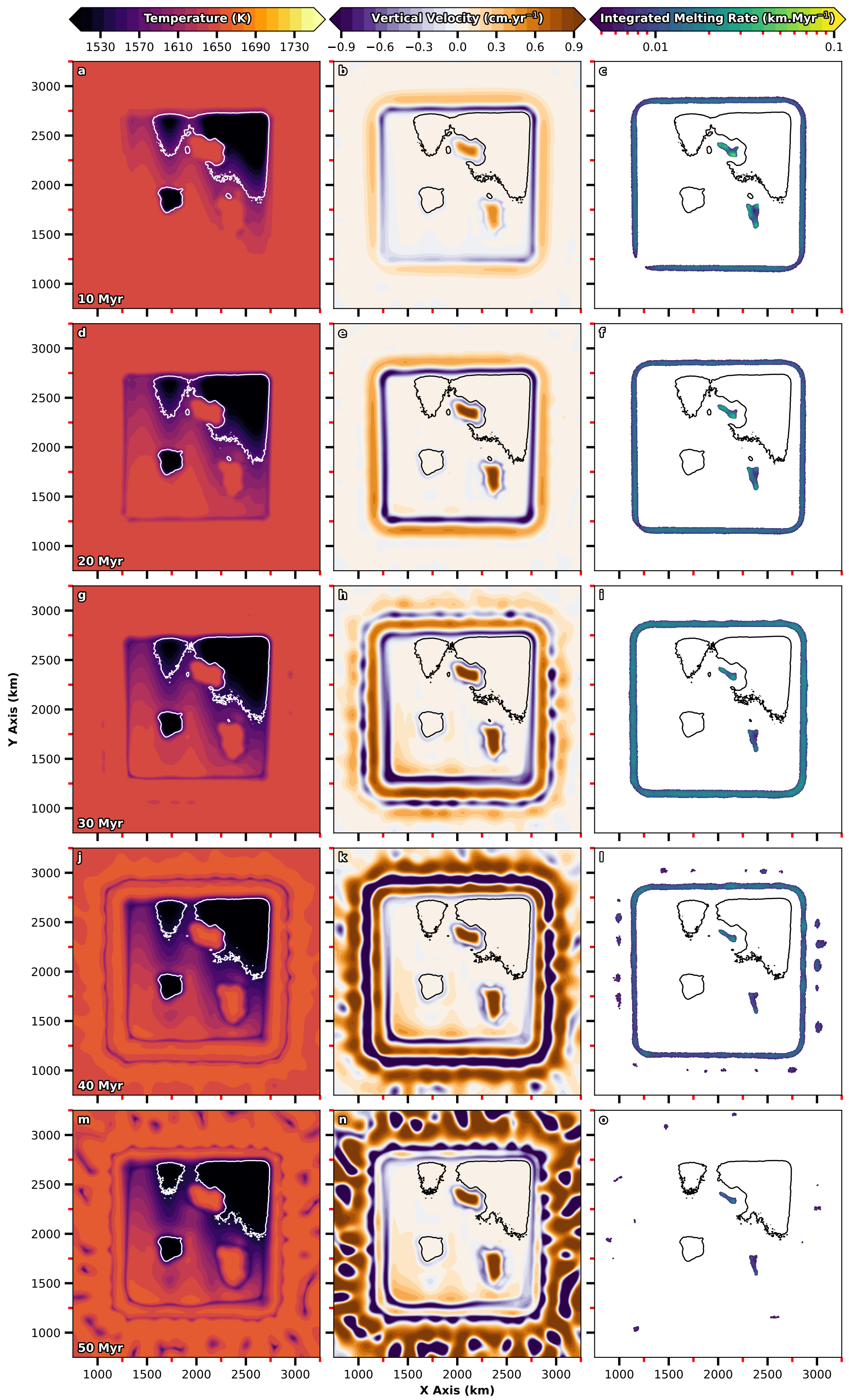

Figure 4. Temporal evolution of the *Complex* continental geometry simulation (similar to Figure 3). Horizontal slices and continental boundaries are displayed at 180 km depth to capture dynamics at the base of the heterogeneous continent.

instabilities. As a result, larger and more vigorous edge-driven cells initially develop adjacent to thicker continental lithosphere (Figures 4b and S1a). However, over the next ~20 Myr, faster development of secondary instabilities enhances the vigour of edge-driven cells adjacent to thinner continental edges, beneath which modest upwelling flows subsequently develop (Figures 4d–i and S1b–c). Within the continent's interior, anomalous troughs in lithospheric thickness drive focussed upwellings that persist throughout the simulation, generating substantial decompression melting. Conversely, melting adjacent to lithospheric steps is modulated by the strength of surrounding instabilities and becomes negligible after ~50 Myr (Figure 4o), owing to the thickening of oceanic lithosphere through thermal diffusion and fading of the primary instabilities that surround the continent, which limit decompression melting (Figures 4j–o and S1d–e). We note that the high viscosity of continental lithosphere prevents destabilisation of the continent's thicker region (Figure 4m–n).

3.2 Plume Cases

3.2.1 Below Continent, Away from Indent

We now consider scenarios incorporating a plume beneath the *U400* continental geometry. In the *U400_Cont_Step* case, the plume disc is located at $x = 1450$ km, close to a long, linear lithospheric step and far from the indent. As illustrated in Figure 5a–h, during the initial stages of plume ascent (≈10 Myr), the flow regime beneath and adjacent to the continent is reasonably consistent with the reference case (Figure 3): edge-driven instabilities develop at all lithospheric steps, and the largest upwelling velocities and melting rates are confined to the indent's inner corners. Nonetheless, as the plume's thermal anomaly approaches the base of the continent (Figure 6d), its buoyancy modifies the surrounding flow field and progressively enhances upwelling velocities at the adjacent step (Figure 5f). As a result, relative to the reference case, melt production increases at that step (Figures 5g–h and 6a) prior to any change in the temperature field associated with plume impingement at the LAB.

Plume arrival beneath the continent at 8–9 Myr causes buoyant material to spread in all directions. However, due to the proximity of the lithospheric step, spreading is asymmetric, with material preferentially flowing from thicker to thinner regions of the lithosphere (Figure 7). At the adjacent continental edge, this flow has analogous consequences to shear-driven upwelling (Duvernay et al., 2021), enhancing melting rates. We emphasise that these increased melting rates are apparent even prior to the arrival of the thermal anomaly (i.e. they are a direct consequence of increased upwelling rates rather than increased temperatures; Figures 5g–h and 6a), although they do increase further as this thermal anomaly emerges at the step (Figures 5k–l and 6a). Once beneath oceanic lithosphere, plume material moves away from the step, forming an expanding half-disc (Figure 5i–l). At the disc's leading edge, the positive buoyancy of plume material sweeps away the deepest portion of the overlying lithosphere, generating a 'curtain' of cold downwelling flow downstream of the spreading front (Figure 5i–j) and transient decompression melting upstream. Within the disc, away from the leading edge, vertical velocities and the associated melting tend towards zero (Figure 5n–o), owing to the prior removal and consequent stabilisation of overlying oceanic lithosphere.

Plume material accumulates alongside the continental step, generating gradients of temperature and vertical velocity to either side of the upwelling (Figure 5i–p). As a result, decompression melting concentrates in a linear trend along the continent's boundary, unlike the circular melt geometry expected upon direct plume impingement beneath oceanic lithosphere (e.g. Ribe & Christensen, 1999; Manglik & Christensen, 2006). We note that no melts are generated directly above the plume conduit in this case, as the thick continent keeps upwelling material below its solidus (Figure 5o), with limited erosion of overlying continental lithosphere observed. After 40 Myr (Figure 5q–t), both the

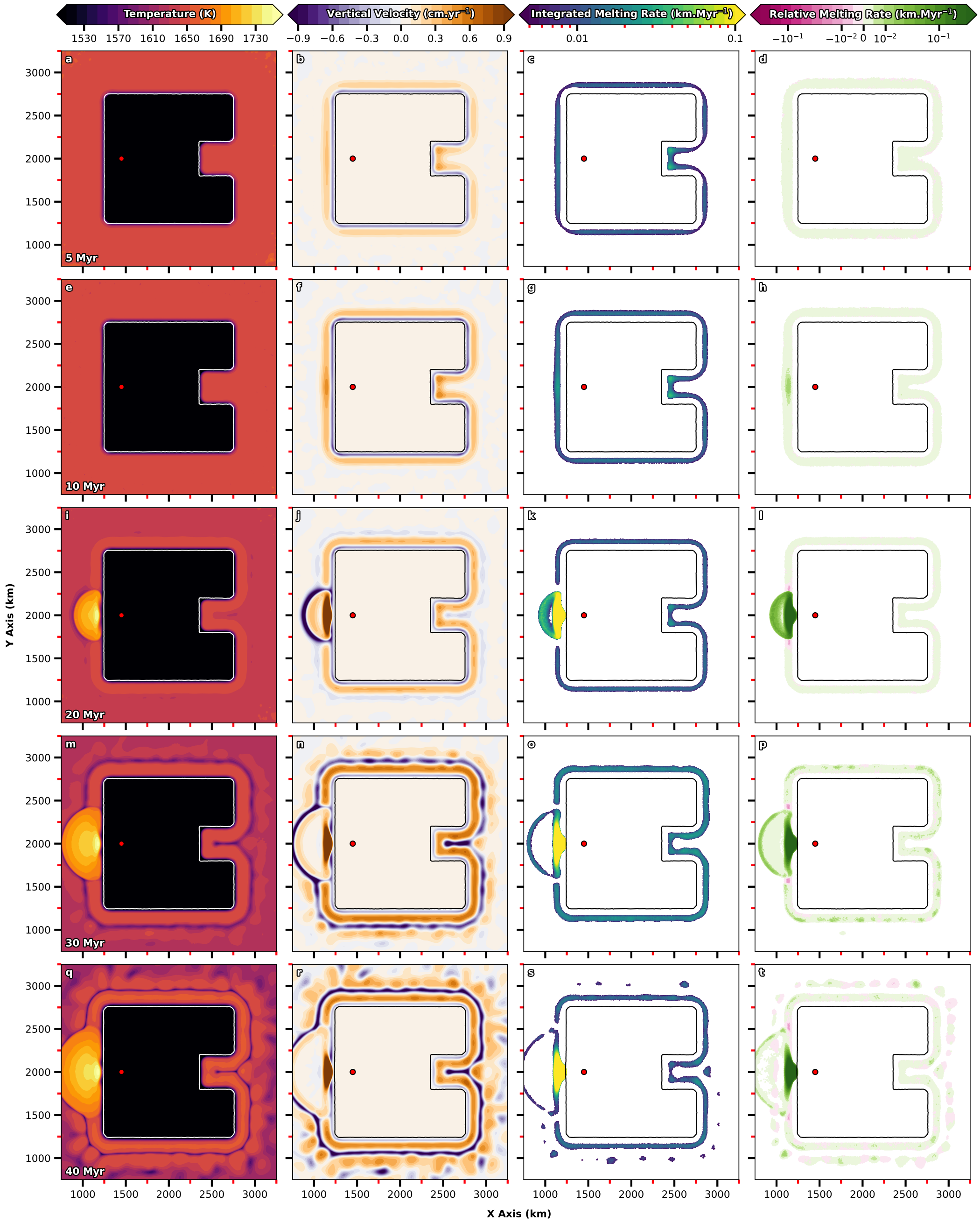

Figure 5. Temporal evolution of the *U400_Cont_Step* simulation; the plume is injected at $x = 1450\,\mathrm{km}$, as indicated by the red circle. Illustration is similar to Figure 3, with an additional column displaying integrated melting rates relative to those of the corresponding reference case (*U400* geometry).

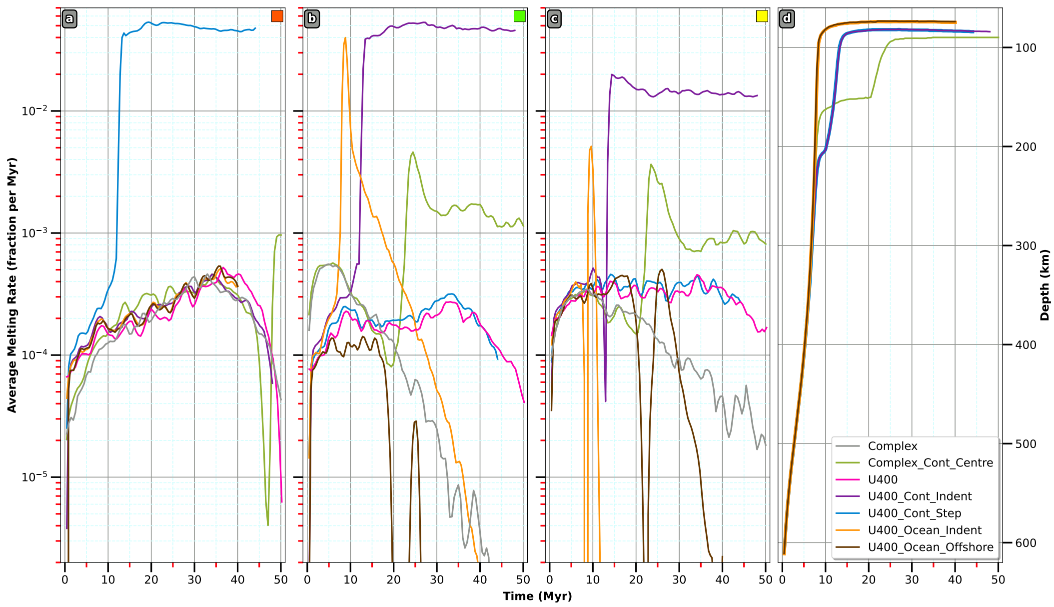

Figure 6. (a)–(c) Temporal evolution of the average melting rate recorded across all simulations within three selected $40 \times 40 \times 20\,\mathrm{km}^3$ regions identified by coloured squares (Figure 2). (d) Temporal evolution across all plume simulations of the shallowest depth reached by the plume thermal anomaly within the computational domain.

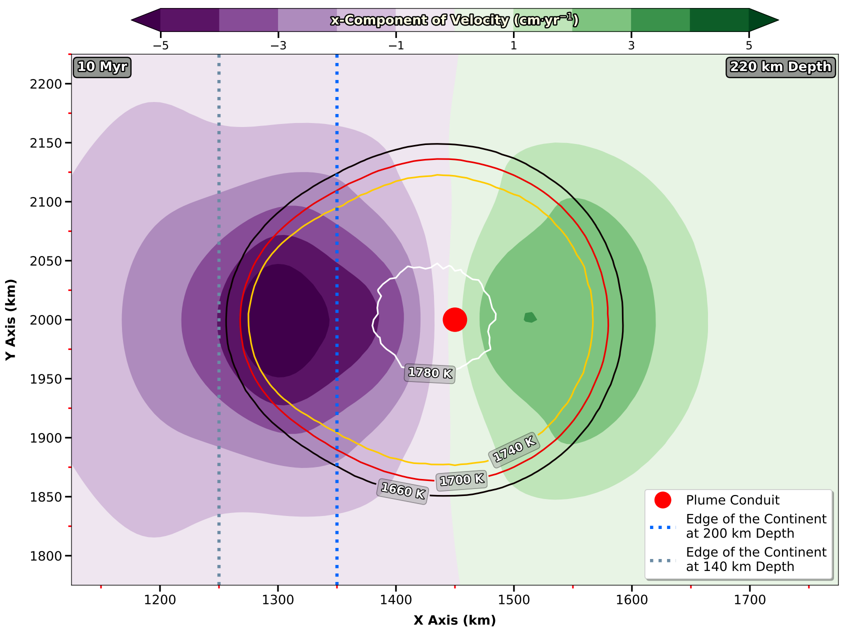

Figure 7. Horizontal cross-section at 220 km depth for case *U400_Cont_Step* illustrating the asymmetric spreading of plume material after it impinges beneath the continent. Background colours represent the x-component of velocity; labelled contours denote isotherms. Dotted blue and grey lines highlight the edge of the continent at 200 km and 140 km depth, respectively, and the red-filled circle depicts the location of the plume conduit.

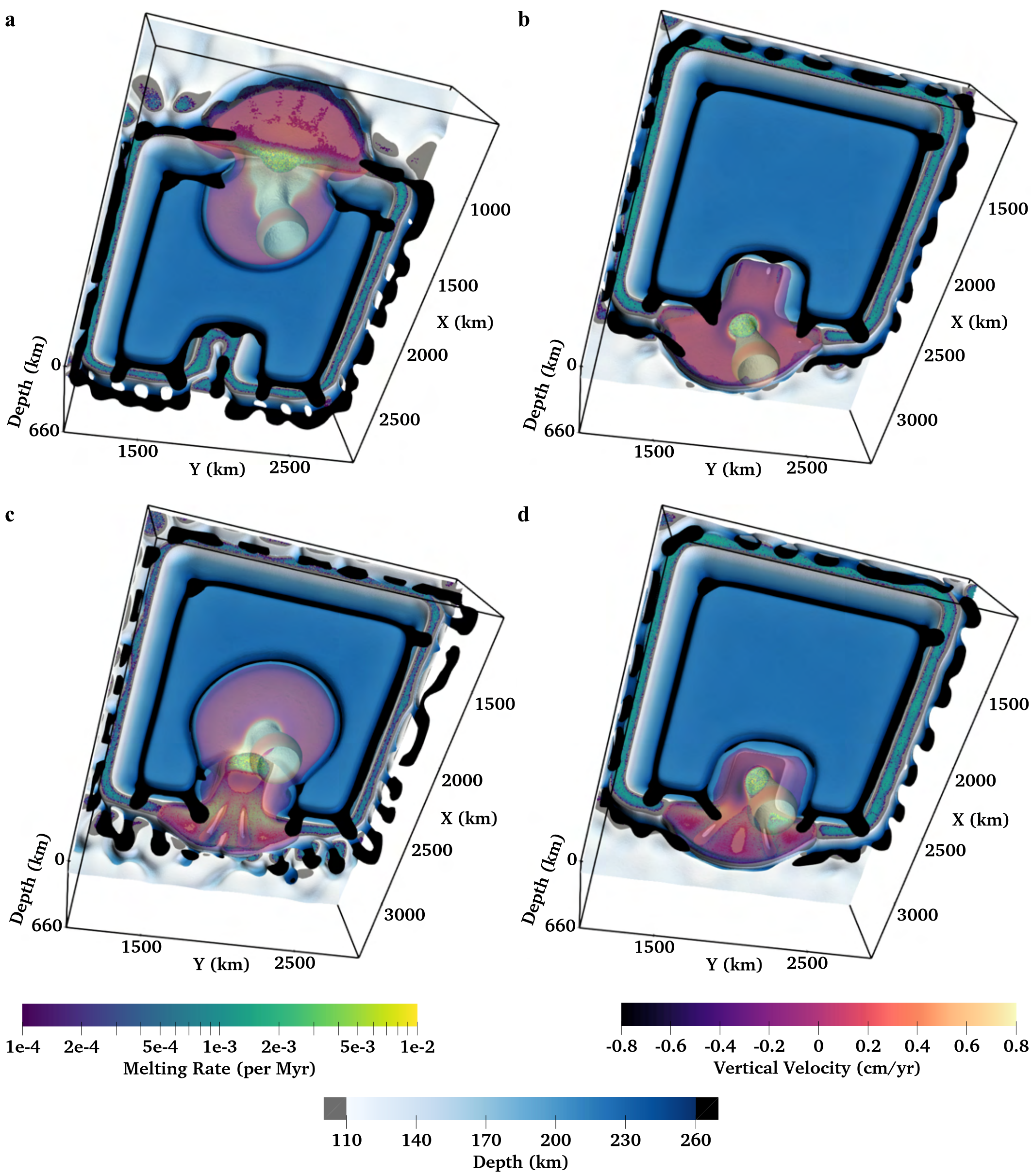

Figure 8. Views from below of the 3-D interaction between a plume and the *U400* continental geometry. We use the 1620 K isotherm to represent the bottom surface of the continental lithosphere (blue tones) and oceanic lithosphere (light blue to white tones). Additionally, the isotherm also highlights thermal instabilities dripping in the upper mantle (dark blue to black tones) adjacent to the continent (primary instabilities) and offshore the continent (secondary instabilities); grey patches indicate thinner portions of the oceanic lithosphere (i.e. lithospheric erosion). The plume is depicted by the 1660 K isotherm, which is rendered half-transparent and coloured by vertical velocity. Areas experiencing melting are represented by individual particle dots, coloured by melting rate (no vertical integration). (a) *U400_ Cont_ Step*. (b) *U400_ Ocean_ Offshore*. (c) *U400_ Cont_ Indent*. (d) *U400_ Ocean_ Indent*.

primary melting zone adjacent to the step (Figure 6a) and the front of decompression melting linked to the expanding half-disc remain active, although the loss of buoyancy through thermal cooling progressively inhibits melting at the disc spreading front.

To complement the cross-sections of Figure 5, a 3-D snapshot of the final stage of the model at 40 Myr is included in Figure 8a. This illustration corroborates that plume flow mainly affects the dynamical regime and thermal structure in the plume conduit's vicinity. Where plume material emerges at the step, typical patterns expected from the combination of lithospheric cooling and edge-driven convection are absent. Along the rest of the continental boundary, including within the indent, the main characteristics of the flow regime and thermal structure remain consistent with the reference case (Figures 5q–t and 6b–c). Offshore the continent, within the spreading half-disc, the distribution of particles that record low-intensity melting rates indicates that plume material is close to internal destabilisation, characterised by the development of small-scale convection within the plume pancake (e.g. Ballmer et al., 2011).

3.2.2 Offshore Indent

In the *U400_Ocean_Offshore* case, the plume is injected offshore, outside the indent at $x = 2850$ km. As with the previous case, plume upwelling modifies the flow regime at the LAB as the buoyant anomaly approaches the lithosphere (Figures 9a–d and 6d). Above the plume, decompression melting is activated but, within the indent, existing edge-related upwellings at lithospheric steps are progressively suppressed by plume flow, leading to reduced melting rates relative to the reference case (Figure 9f–h).

Following impingement of the plume at the LAB (Figure 9e–h), material spreads radially to produce a circular decompression melting zone consistent with expectations of melting associated with a plume arriving beneath uniform oceanic lithosphere. Soon after, plume material reaches the continental boundary (Figure 9i–l), where it either enters the indent or gets redirected along the continent's outer steps, in the latter case triggering a front of enhanced melting that propagates with the flow (Figure 9i–p). The arrival of plume material within the indent drives intense horizontal motion and shuts off edge-driven convection and the associated melting (Figures 9k and 6b–c), leaving a region in its wake where vertical velocities and decompression melting have become negligible (Figures 9n–o and 6b–c). After reaching the indent's innermost step, plume material is forced beneath the continent due to ongoing inflow from the plume conduit and the associated dynamic pressure gradients (Figure S3d–e). At this stage, the dynamics within the indent contrast dramatically to both the reference and *U400_Cont_Step* cases, demonstrating that the flow regime and magmatic expression are transformed solely by changing the location of plume impingement at the LAB, relative to the continental lithosphere. Nonetheless, away from the plume's region of influence, the model's dynamics remain similar to the reference case (Figures 6a, 8b and 9t).

At 40 Myr (Figure 9q–t), within a disc surrounding the conduit, melting remains active directly above the plume conduit but is almost entirely suppressed elsewhere. Inside the indent, plume material is close to destabilisation, as illustrated by the alternating positives and negatives in the vertical velocity field, which trigger small pockets of localised melting (Figure 9r–s). This is corroborated by the companion 3-D view of the model's final stage in Figure 8b.

3.2.3 Below Continent, Close to Indent

In the *U400_Cont_Indent* case, the plume is injected below the continent at $x = 2150$ km, adjacent to the indent. Similar to the *U400_Cont_Step* case (Figure 5), the initial 10 Myr of model evolution (Figure 10a–h) are comparable to the reference case, albeit with a substantial increase in melt production at the indent's innermost step (Fig-

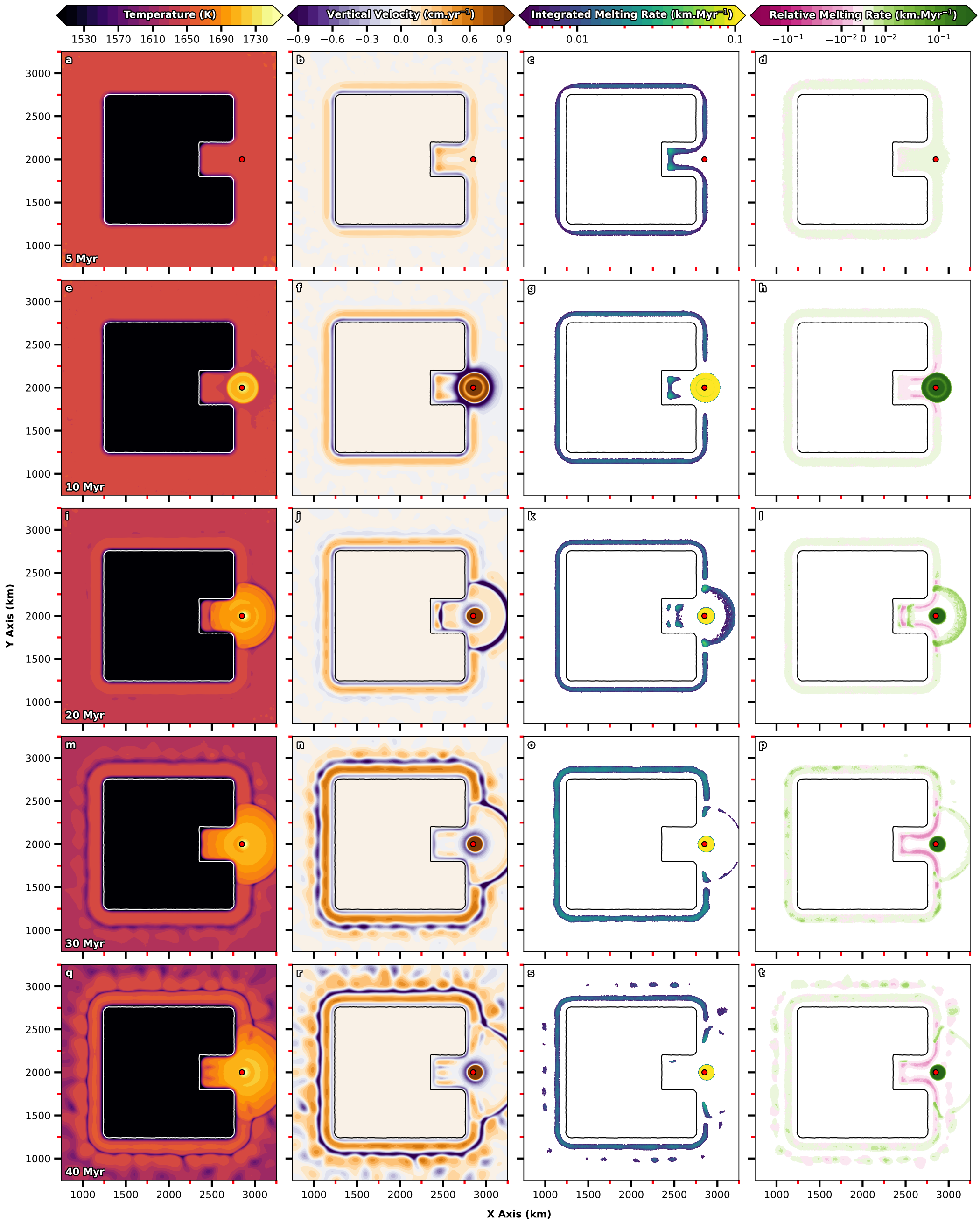

Figure 9. Temporal evolution of the *U400_ Ocean_ Offshore* case; the plume is injected at $x = 2850\,\mathrm{km}$. Illustration similar to Figure 5.

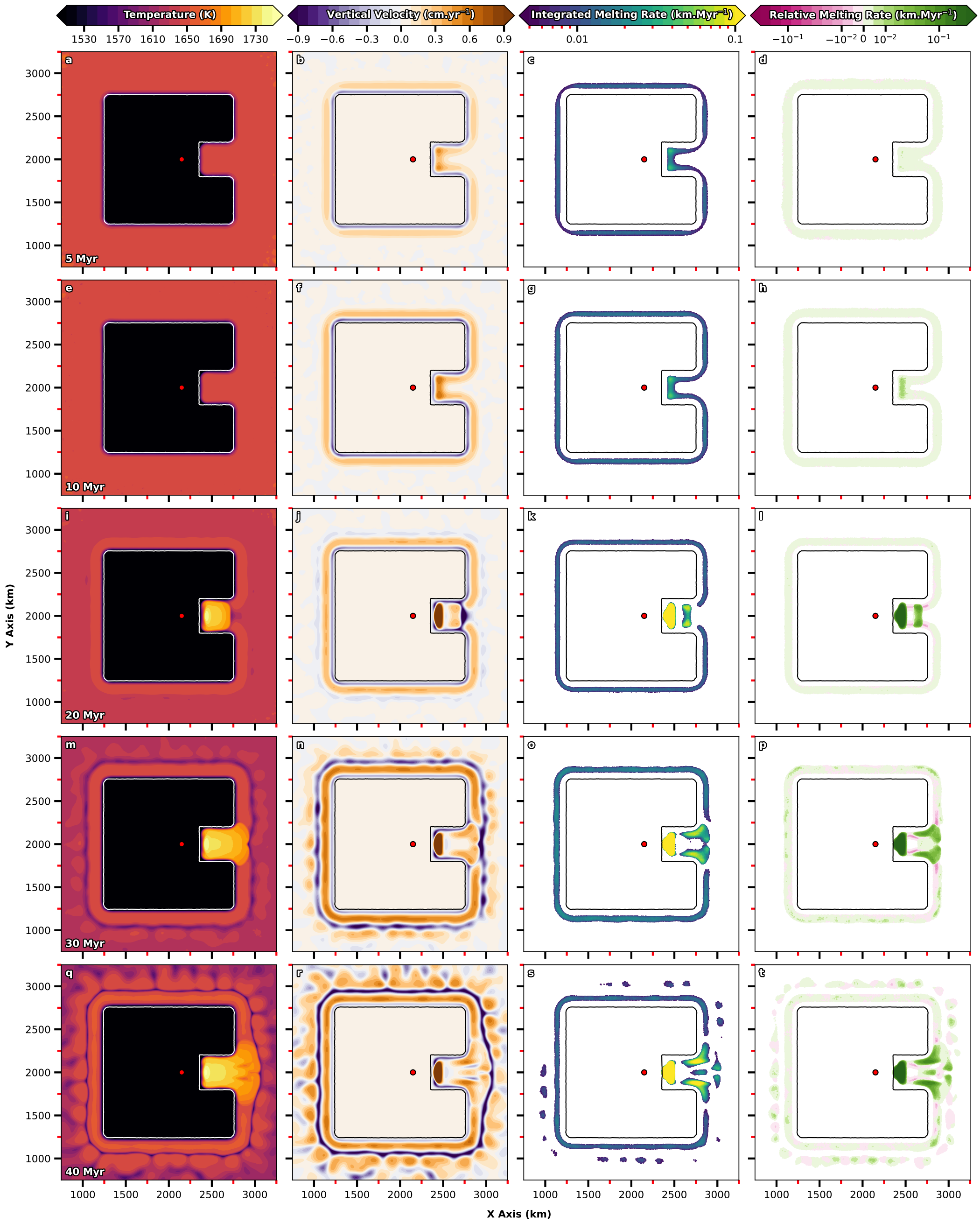

Figure 10. Temporal evolution of the *U400_Cont_Indent* case; the plume is injected at $x = 2150\,\text{km}$. Illustration similar to Figure 5.

ures 6b and 10g–h). Here, once again, flow driven by the plume has an analogous impact to shear-driven upwelling (Duvernay et al., 2021), enhancing upwelling velocities and the associated decompression melting. Owing to the thickness of the continent, plume material does not melt prior to or upon impingement at the LAB. Instead, it spreads preferentially towards the indent where it eventually emerges, generating melting that is substantially more intense than that generated solely through edge-driven convection (Figures 10i–l and 6b–c).

For the remainder of the simulation, plume material continues to flood into the indent, driving ongoing decompression melting at the indent's innermost step and along fronts that propagate outwards towards the oceanic domain (Figure 10m–p). At the indent's exit, the lateral space available (along the y-direction) for plume material increases and, accordingly, buoyant material that had accumulated along the indent's steps redistributes, flushing outwards into the oceanic realm through focussed upwellings that trigger further localised decompression melting. Moreover, the formation of these upwellings initiates small-scale convection within the plume pancake itself, promoting further localised melting in a domino effect.

After 40 Myr of model evolution (Figure 10q–t), decompression melting is present adjacent to the indent's inner steps and outer corners, continental outer steps connected to the indent, and also offshore, driven by small-scale convection and the complex destabilisation of plume material. These dynamics are further illustrated through a complementary 3-D view in Figure 8c, where plume material can be seen spreading as a thin layer beneath a large portion of the LAB. Preferential flow into, and subsequent melting within, the indent are also clearly highlighted. Destabilisation of the plume pancake is marked by the absence of decompression melting within well-defined pockets of downwelling flow. As with the previous cases considered, the flow regime and melting diagnostics are generally unaffected at steps far from the plume.

3.2.4 Below Indent

In the *U400_ Ocean_ Indent* case, the plume is injected directly beneath the indent at $x = 2500$ km. As in the *U400_ Ocean_ Offshore* case (Figure 9), the plume ascends rapidly and generates extensive melting upon impingement onto oceanic lithosphere (Figure 11a–h), with the main melting zone assuming an elliptical shape due to the geometry of the indent (Figure 11k). As the simulation evolves (Figure 11i–l), material is forced beneath the continent at the indent's steps (Figure 11j) and, accordingly, no decompression melting occurs in these regions (Figures 11k and 6c). We emphasize that this is opposite to the reference case (Figure 3), where melting within the indent occurs solely adjacent to these steps.

Similar to the *U400_ Cont_ Indent* case (Figure 10), plume material builds up within the indent, as it is largely prevented from spreading in all but one direction. Eventually, it flushes out around the indent's outer corners, generating focussed upwellings as it redistributes (Figure 11j–k). Relative to the *U400_ Cont_ Indent* case, upwellings and associated downwellings within the pancake are of greater intensity (Figure 11m–p). The resulting small-scale instabilities develop tangent to the indent's outer corners, leading to V-shaped decompression melting ridges (Figure 11q–t). This enhanced destabilisation is further illustrated in the associated 3-D snapshot (Figure 8d), where oblique zones of alternative upwelling and downwelling flow are apparent, along with the V-shaped melting ridges. The 3-D planform also demonstrates that relative to the *U400_ Cont_ Indent* case, plume material covers a smaller portion of the LAB (Figure 8c), as it accumulates within the indent and preferentially flushes into the oceanic realm.

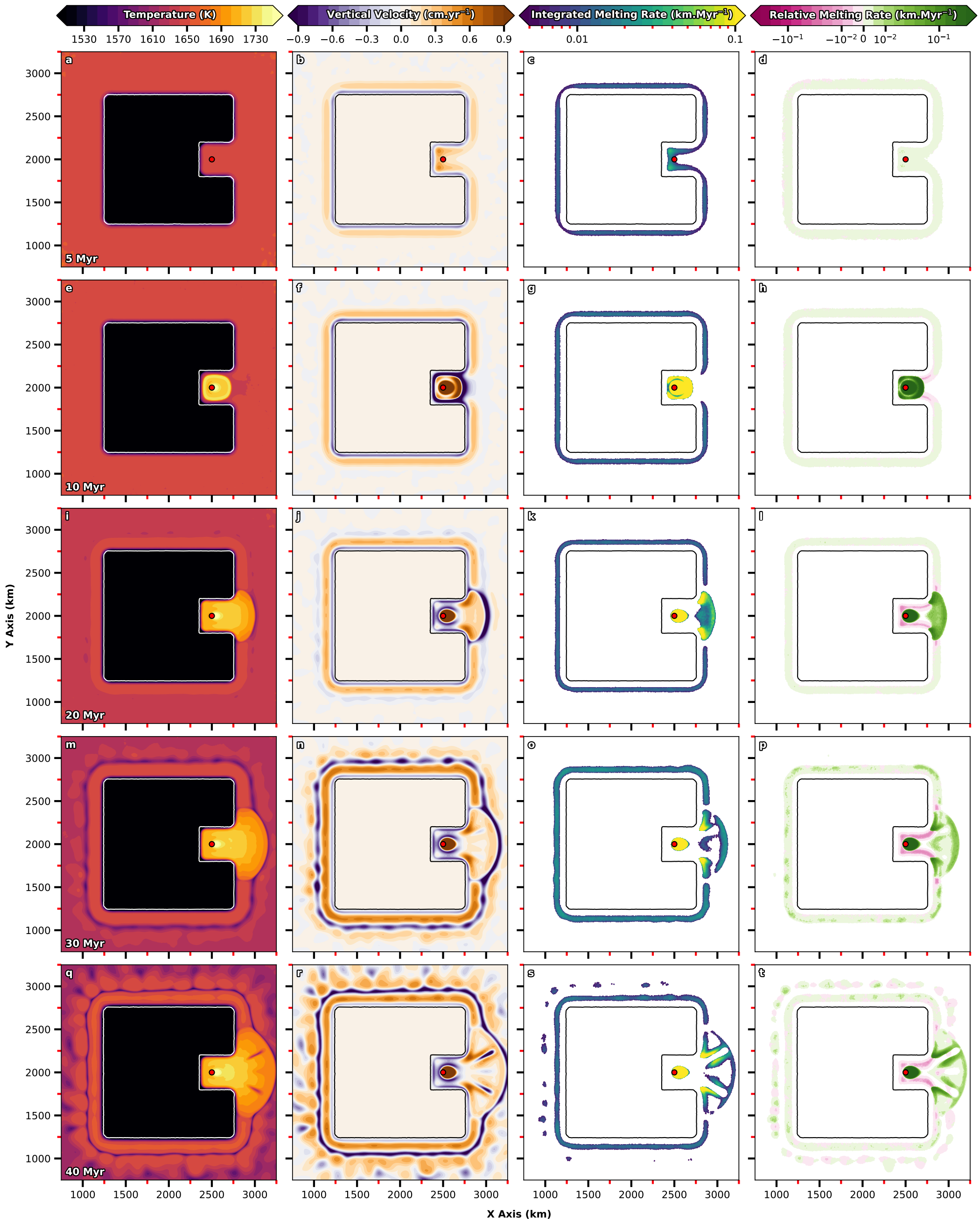

Figure 11. Temporal evolution of the *U400_Ocean_Indent* case; the plume is injected at $x = 2500\,\text{km}$. Illustration similar to Figure 5.

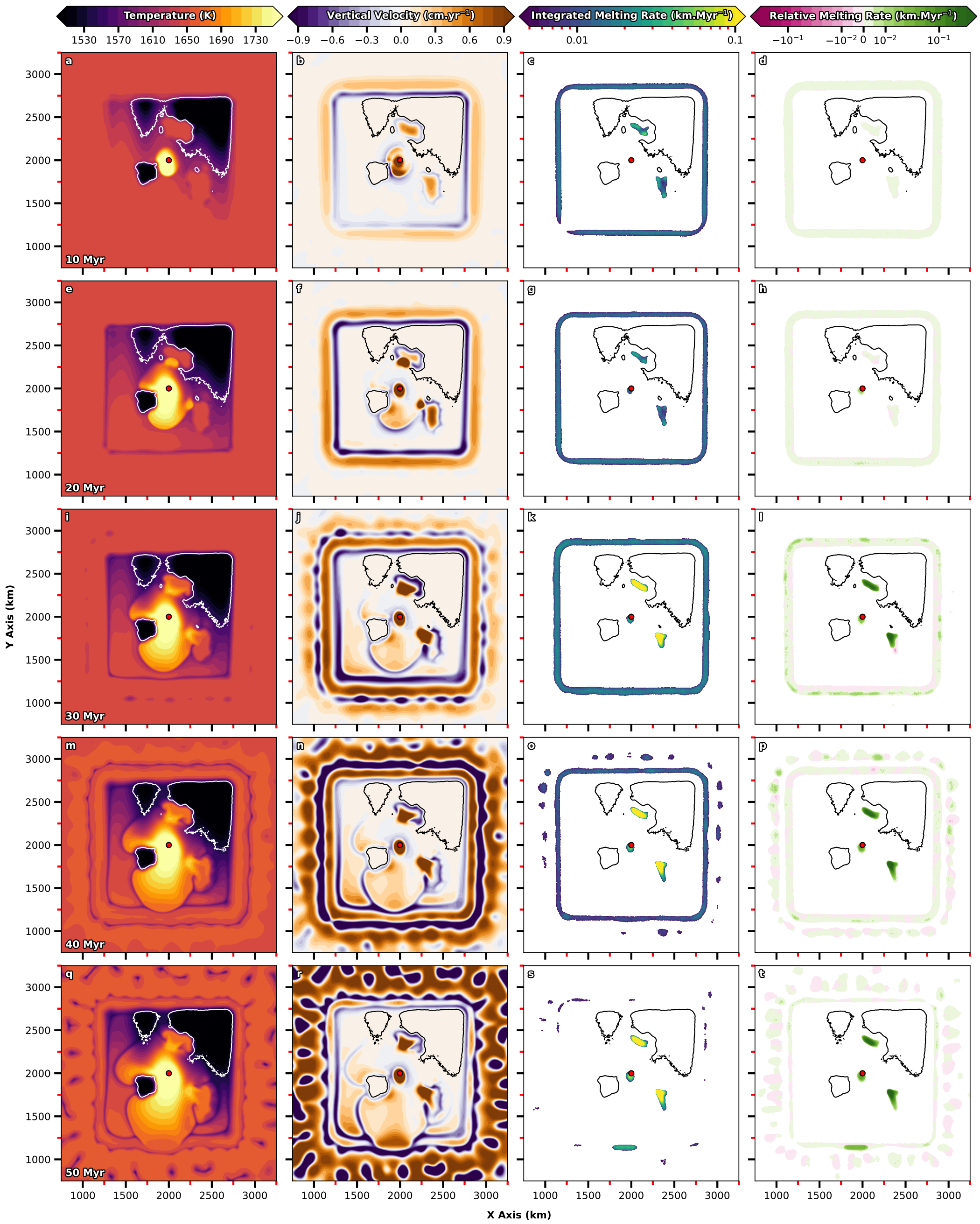

Figure 12. Temporal evolution of the *Complex_Cont_Centre* case; the plume is injected at $x, y = 2000\,\mathrm{km}$. Illustration similar to Figure 5, with the temperature and vertical velocity slices sampled at 180 km depth as in Figure 4.

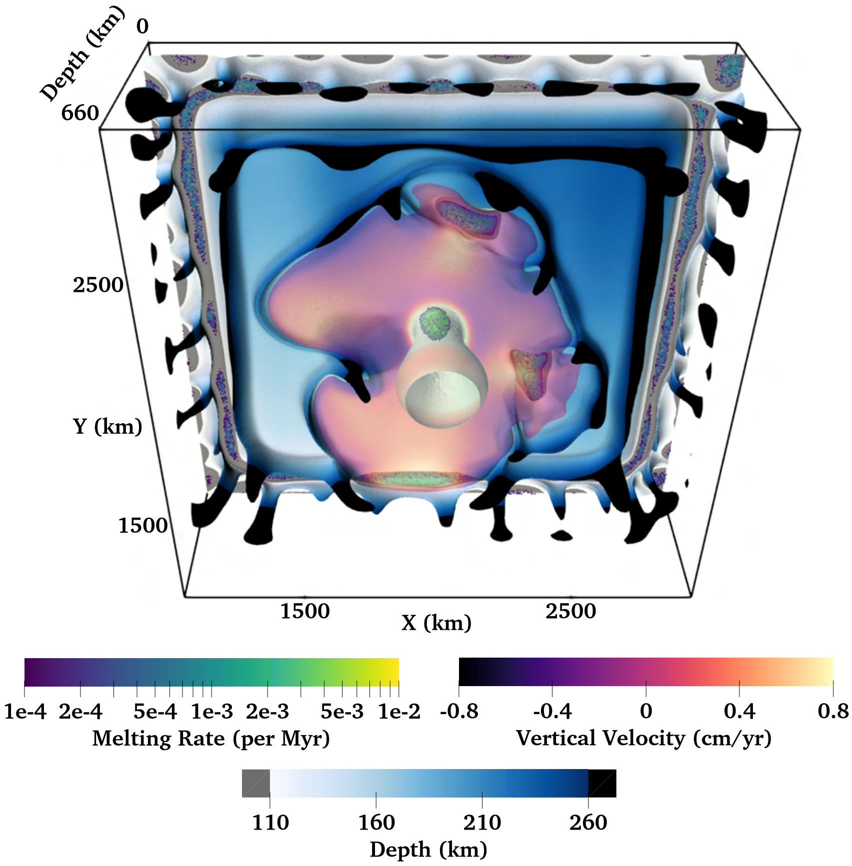

Figure 13. View from below of the 3-D interaction between a plume and the *Complex* continental geometry. The 1620 K isotherm is used to represent the continental lithosphere (blue tones) and the oceanic lithosphere (light blue to white tones). Additionally, it also highlights thermal instabilities dripping in the upper mantle (dark blue to black) adjacent to the continent (primary instabilities) and offshore the continent (secondary instabilities); grey patches indicate lithospheric erosion. The plume is depicted by the 1660 K isotherm, which is rendered half-transparent and coloured by vertical velocity. Areas experiencing melting are represented by individual particle dots, coloured by melting rate (no integration).

3.2.5 Complex

We finally discuss the *Complex_ Cont_ Centre* case (Figure 12), where the plume is injected directly beneath the centre of the *Complex* continental geometry (Figure 2b). Unlike the plume scenarios discussed for the *U400* geometry, substantially enhanced melting rates are not observed adjacent to or within the continent during plume ascent, as the plume is located away from any lithospheric step or continental trough (Figure 12d). Upon impingement at the LAB (~10 Myr), plume material spreads below the continent, with the spreading direction controlled by the heterogeneous structure of the continental LAB (Figure 12e–f). In particular, plume material is forced around the region of thick continental lithosphere and progresses faster towards thinner portions of the continent. No decompression melting occurs above the conduit initially (Figure 12c), although the plume gradually erodes the base of the continent and eventually triggers melting, with melting rates increasing over time (Figure 12k). We note that melting above the conduit is possible in this case as overlying continental lithosphere is initially thinner at the same location relative to the *U400* geometry.

Following further spreading, plume material upwells within the two continental troughs, fuelling melting rates that far exceed those of the reference case (Figures 12l and 6b–c). Over the next ~10 Myr (Figure 12m–p), plume spreading continues and, eventually, after ~50 Myr, part of the plume pancake emerges at the lower continental boundary (negative-y direction), where it upwells at the lithospheric step and generates substantial melting (Figure 12s). Remarkably, at this stage, the plume is simultaneously producing melt at four distinct locations: above the conduit, in two pockets of thin lithosphere, and adjacent to the lower step, where plume material emerges almost 1000 km away from the conduit. The dynamics at this time are further illustrated in 3-D, on Figure 13, where preferred spreading directions and pockets of melting are clearly visible. We note that the spreading of plume material is hampered in the negative-x direction by the thick continental region, and it is also delayed as it passes through the two continental troughs. Away from where the plume emerges at the lower continental step, the flow regime and thermal structure adjacent to the continent are comparable to the reference case (Figure 12t).

4 Discussion

Using a series of 3-D geodynamical models, we have investigated the interaction between upwelling mantle plumes and the flow regime beneath and adjacent to continental lithosphere. Our motivation is to reveal how shallow convective processes, such as edge-driven convection, are influenced by the arrival of mantle plumes and to understand how these flow components combine, compete and interact to produce the key characteristics of intra-plate magmatism in the vicinity of Earth's highly heterogeneous continents. Our results have important implications for deciphering the spatio-temporal evolution of intra-plate magmatism in these complex tectonic and geological settings. In particular, they illustrate that the magmatic manifestation of mantle plumes within continental interiors or adjacent to continental margins differs significantly from that expected for plumes arriving beneath oceanic lithosphere, far from any plate boundary.

In the following sub-sections, we summarise the key findings of our simulations and discuss their broader implications for our understanding of intra-plate volcanism on Earth. We end by reviewing the limitations of our approach, how they may influence our results, and discuss potential avenues for future research.

4.1 Plumes Enhance Magmatism at Lithospheric Steps Several Million Years Before Plume Material Emerges at the Step

Shallow processes, such as edge-driven convection and shear-driven upwelling (e.g. King & Anderson, 1998; Conrad et al., 2010), have been invoked to explain intra-plate volcanism at a number of locations on Earth (e.g. Conrad et al., 2011; Davies & Rawlinson, 2014; Kaislaniemi & van Hunen, 2014; Ballmer, Conrad, et al., 2015). Usually, such volcanism lies close to a step-change in lithospheric thickness, which facilitates the development of convective cells, triggering decompression melting in the uppermost asthenosphere. Our previous work suggests that such edge-related magmatism applies only to Earth's lower-volume and shorter-lived intra-plate volcanic provinces (Duvernay et al., 2021). However, the simulations examined herein demonstrate that enhanced decompression melting can occur at lithospheric steps near an upwelling mantle plume as the plume approaches and impinges at the LAB. During their upper-mantle ascent, plumes modify the flow regime and drive more vigorous upwelling motion at adjacent lithospheric steps, substantially boosting decompression melting. For example, the volumetric magmatic production of the *U400_Cont_Step* case increases by up to 80 % relative to its reference case (Figure 5g-h, 3-D integrated melting rate at 10 Myr between $x = 1100$ km,

$y = 1850$ km and $x = 1170$ km, $y = 2150$ km). In our models, such an increase in magmatic production occurs 5–10 Myr prior to the plume's thermal anomaly reaching the associated melting zone (e.g. Figures 6b 10h).

Such a boost in magmatic production could be critical to explaining the origins of intra-plate volcanism in regions where anomalously hot temperatures are not inferred from geochemical or seismological observations. Some of Earth's continental intra-plate volcanic provinces host low-volume, short-lived eruptions even though they lie reasonably close to mantle plumes (e.g. Ho et al., 2013; Cas et al., 2017; Ball et al., 2019). Our simulations suggest that many of these enigmatic volcanic provinces could result from the transient activation or enhancement of melting induced by a change in the flow field triggered by the adjacent mantle plume. Due to the interaction of plumes with the structure and motion of overlying plates, plume material may not always surface where the flow field promoted melting, resulting in short-lived volcanism that may be difficult to link directly to its primary driving mechanism.

4.2 Plume-Induced Melting May Have No Differentiating Geochemical Expression

The dynamical mechanisms that underpin the generation of volcanic rocks at Earth's surface can be inferred through geochemical analyses, which probe elemental and isotopic compositions (e.g. Dupré & Allègre, 1983; White et al., 1993; Tang et al., 2006; Klöcking et al., 2018; Ball et al., 2019). Contributions from mantle plumes are often identified based on geochemical signatures that differ from those typical of mid-ocean ridge basalts (e.g. Hart et al., 1992; Stracke et al., 2005). Our results, however, suggest that under certain circumstances, these geochemical approaches will be insensitive to the plume's contribution towards the generation of surface volcanism.

As noted in Section 4.1, mantle plumes can enhance decompression melting at lithospheric steps several million years before their thermal anomaly emerges at the step. In such a scenario, the modified flow field promotes higher-volume magmatism at these steps (e.g. the *U400_Cont_Step* case). However, since rock parcels passing through the melting zone do not come from the plume, melting temperatures and the resulting maximum melt fractions remain unchanged. As a result, the composition of erupted lavas does not show the geochemical signature of a mantle plume, despite the latter's important role in activating or enhancing decompression melting. Only if, or when, hot plume material emerges at the step would the erupted lavas display an evolution in their composition that would be detectable through geochemical analyses. Accordingly, it may not be possible for geochemical approaches, in isolation, to infer the important role of a mantle plume in the generation of intra-plate lavas. Studies that rule out a plume contribution to surface volcanism, based principally on the geochemical characteristics of surface lavas, may therefore have overlooked the plume's role in modulating the flow regime (e.g. Bradshaw et al., 1993; Barry et al., 2007).

4.3 Plumes Can Induce Simultaneous Melting in Several Locations, more than a Thousand Kilometres Apart

When a plume impinges onto the LAB, lateral currents associated with plume material spreading away from the plume conduit dominate the asthenospheric flow regime. Our simulations demonstrate that the spreading of plume material beneath heterogeneous lithosphere is anisotropic: it follows local pressure gradients controlled by the thickness and density of the overlying lithospheric lid (e.g. Sleep et al., 2002; Koptev et al., 2016). Accordingly, the location of plume impingement, relative to the local geometry of the LAB, determines the path taken by plume material, which, in turn, dictates where melting can occur.

When plumes impinge directly beneath thick continental keels, the pressure is likely high enough to suppress decompression melting immediately above the plume conduit (e.g. Niu, 2021). The absence of surface volcanism locally is therefore not a sufficient condition to rule out the presence of a plume (Davies, Rawlinson, et al., 2015). Nonetheless, spreading of plume material at the LAB can activate decompression melting in regions of thinner lithosphere several hundreds of kilometres away from the plume conduit. Without further observational constraints, volcanism at such distances from the seismological (e.g. Wolfe et al., 1997; French & Romanowicz, 2015) and topographical (e.g. Cadio et al., 2012; Davies et al., 2019) expressions of the plume will be challenging to link to underlying mantle dynamics.

Moreover, the farther plume material spreads from the conduit, the more heat it exchanges with the overlying lithosphere, and, thereby, the lower melt fractions and melting rates it can generate. Accordingly, low-intensity plume-derived melts produced far from their conduit may prove difficult to distinguish from melts derived purely through edge-driven processes (e.g. Figure 12s). Assessing the potential role of a plume may also be ambiguous if complex lithospheric structure forces plume-related volcanism to distribute adjacent to lithospheric steps, as observed in the *U400_Cont_Step* case, yielding a volcanic trend similar to that generated from shallow edge-driven processes (e.g. Duvernay et al., 2021). Therefore, Earth's continents, owing to their mechanical strength and non-uniform lithospheric structure, exert a primary control on the nature, location and principal characteristics of plume-related volcanism in continental settings. It follows that knowledge of regional lithospheric architecture becomes an essential prerequisite for identifying the dynamical mechanisms underpinning specific volcanic provinces, as emphasised by Davies and Rawlinson (2014) and Rawlinson et al. (2017).

4.4 The Arrival of Plume Material at Lithospheric Steps Can Completely Shut off Existing Magmatism

Changes in the asthenospheric flow field triggered by a plume can transform the dynamics in regions where edge-driven convection or shear-driven upwelling have previously sustained decompression melting. In particular, melting at lithospheric steps through edge-driven convection relies on passive return flows activated by negatively buoyant instabilities (e.g. Duvernay et al., 2021). Such return flows cannot develop if strong lateral currents, such as those induced by plume ascent and spreading, dominate the asthenospheric flow regime. As illustrated in the *U400_Ocean_Offshore* case (Figure 9), the arrival of a mantle plume offshore the continent, beneath a region of thin lithosphere, can completely shut off decompression melting at lithospheric steps by forcing material towards the continental boundary and, ultimately, downwards, below the continent. Such an effect is analogous to that occurring when asthenospheric shear drives flow towards lithospheric steps, as outlined by Davies and Rawlinson (2014) and Duvernay et al. (2021). This result is particularly counter-intuitive, as one would expect the excess heat carried by mantle plumes to facilitate decompression melting rather than act against it. Nonetheless, it may be critical in understanding why step-changes in lithospheric thickness, which should facilitate edge-driven convection, are not always associated with surface volcanism.

4.5 Plume Destabilisation Can Occur Through Interaction of Plume Flow with Surrounding Lithospheric Structure

In oceanic settings, buoyant plume material spreading in the immediate sub-lithospheric mantle assumes an elliptical shape, forming a structure commonly referred to as a plume pancake (e.g. Griffiths & Campbell, 1991; Ribe & Christensen, 1999). As noted above, the pancake cools down as it expands by exchanging heat with the overlying lithosphere. As a result, local anomalies in the temperature field develop and trigger the destabilisation of the buoyant structure through small-scale convection (e.g. Griffiths & Campbell, 1991). If the overlying lithospheric lid is thin enough, such dynamical instabilities can induce decompression melting in a geometrical pattern controlled by the plume's buoyancy flux and lithospheric motion (e.g. Ballmer et al., 2011).

Our results demonstrate that the destabilisation of a plume pancake can also stem from the interaction between buoyant material and the surrounding lithosphere. In particular, if the lithospheric structure channels plume material into confined regions, such as the indent of our *U400* lithospheric geometry, plume material accumulates, and areas of excess buoyancy develop. Where these narrow regions broaden, this enhanced buoyancy drives the re-distribution of plume material into adjacent asthenosphere, generating strong vertical currents that destabilise the entire structure. The resulting spatial distribution of small-scale convective patterns directly reflects the geometry of the LAB and its interaction with plume flow. In our simulations, structures such as linear ridges of partial melts form beneath thinner lithosphere, away from the plume conduit (e.g. the *U400_Ocean_Indent* case, Figure 11). Such complexities might be second-order effects that help explain the origin of transient volcanic events that lie offshore lithospheric structures similar to indents, such as along Australia's southeastern margin (Holford et al., 2012).

4.6 Potential Links Between Model Predictions and Earth's Observational Record

The analyses undertaken herein imply that significant decompression melting is unlikely to occur beneath deep continental roots, with plume material channelled towards regions of thinner lithosphere where it subsequently melts. This prediction is compatible with the observed global distribution of Neogene volcanism, which concentrates in areas of comparatively thin lithosphere (Figure 1). Accordingly, continental volcanic centres, generated by a mantle plume, may not always overlie the location of the plume conduit, resulting in intricate distributions of volcanism that are challenging to reconcile with underlying mantle dynamics.

The geographical distribution, geochronology and geochemistry of Earth's intraplate volcanic provinces provide a means to assess the applicability of our results. Whilst it is beyond the scope of the present study to examine every location in detail, there exist provinces that show characteristics consistent with those predicted by our models. For example, in eastern Australia, the Cosgrove track — Earth's longest continental hotspot track — marks the passage of a plume beneath thick continental lithosphere with a step-like structure (e.g. Fishwick et al., 2008; Davies, Rawlinson, et al., 2015). As a result, the volcanic track above the predicted path of the plume conduit is discontinuous, with wide volcanic gaps in regions of thick lithosphere. Nonetheless, a record of volcanism exists on a parallel trail to the east, where the lithosphere is thinner than inland (e.g. Davies, Rawlinson, et al., 2015; Meeuws et al., 2016; Rawlinson et al., 2017). These volcanic fields are offset from the re-constructed path of the Cosgrove plume, but their lavas display no systematic geochemical distinction in terms of major element, trace element and radiogenic isotope compositions relative to those formed atop the conduit (I. Jones et al., 2020). In the context of our results, this strongly suggests a direct association with the Cosgrove mantle plume for both tracks.

In the western Atlantic Ocean, the Vitória-Trindade Ridge represents a long-lived chain of age-progressive volcanic islands that extend from the eastern shore of South America to Martin Vaz Island, implying a link to an underlying mantle plume (dos Santos et al., 2021). The island track offshore connects to continental South America through the Abrolhos Volcanic Complex, a massive volcanic field that pre-dates the Vitória-Trindade Ridge. The Abrolhos Volcanic Complex recorded various stages of eruption between 35 and 70 Myr ago, representing a temporal duration comparable to the activity of the entire volcanic ridge (the last $\sim$35 Myr; dos Santos et al., 2021; Maia et al., 2021). Although it resembles the product of plume head impingement, dos Santos et al. (2021) suggest that it is likely not, an inference that our results support. The volcanic complex lies adjacent to the São Francisco Craton on land, which hosts several older occurrences of volcanism dated between 55–90 Myr ago, towards its western and southern boundaries (dos Santos et al., 2021). As a result, it is plausible that the Trindade plume impinged beneath the southwestern part of the São Francisco Craton, where volcanism was modest, given the thick overlying cratonic lithosphere. As South America was moving westwards away from Africa during the opening of the South Atlantic, the plume subsequently transited beneath the craton, prior to its emergence on the southeastern boundary of the craton, where it generated the extensive Abrolhos Volcanic Complex and the later Vitória-Trindade Ridge, which still erupts today at Martin Vaz Island (dos Santos et al., 2021).

In the North Atlantic Region, the Iceland plume is inferred to have first impinged Earth's lithosphere beneath Greenland (e.g. Marty et al., 1998; Meyer et al., 2007; Steinberger et al., 2019). While the exact path of the plume during the Cretaceous is not well-constrained, seismic tomography reveals that an east-west corridor of thinned lithosphere exists beneath Greenland, suggesting plume-driven thermo-mechanical erosion of the deeper lithosphere and, thereby, delineating a probable path for the Iceland plume (Lebedev et al., 2018). Interestingly, plume-related volcanism activated on both the eastern and western shores of Greenland about 62 Myr ago (Steinberger et al., 2019). While the presence of volcanism to the east — distributed parallel to the coastline and, therefore, indicative of the plume emerging at the continental boundary — agrees with the relative motion of the plume trending towards the current location of Iceland on the North Atlantic Ridge, volcanism along the western shore is more enigmatic, requiring the spreading of plume material beneath Greenland in the opposite direction (Steinberger et al., 2019). Such an observation correlates well with our results, where plume material spreading beneath a stable continent can enhance decompression melting at a continental boundary far from the plume conduit's location.

In Africa, volcanic fields such as Tibesti and the Northern Tanzanian Divergence have recorded evolutionary phases that display directional flow reminiscent of the emergence of a plume from beneath thicker lithosphere (e.g. Permenter & Oppenheimer, 2007; Mana et al., 2015), similar to the activation of enhanced melting within troughs in continental lithosphere highlighted herein. In Tibesti, successive volcanic phases, active in distinct parts of the region over the last 15 Myr, contributed to the build-up of the volcanic province. Eruptive history displays a progressive increase in erupted volumes followed by waning, and geochemical analyses of associated lavas highlight a significant range of geochemical signatures (Gourgaud & Vincent, 2004; Permenter & Oppenheimer, 2007; Deniel et al., 2015; Ball et al., 2019). Our results suggest that earlier, lower-volume volcanism could be linked to enhanced velocities ahead of a mantle plume, whilst later and more extensive volcanism could correspond to the arrival and progressive spreading of plume material at the LAB. Such a dynamic evolutionary regime could explain the large variability observed in the geochemistry of Tibesti lavas (e.g. Ball et al., 2019).

South of the border between Tanzania and Kenya, high-resolution seismic tomography images a broad mantle upwelling that interacts with the Tanzanian Craton (Clutier et al., 2021). The presence of the thick continental lithosphere deflects the ascent of the plume, which preferentially emerges at the craton's eastern margin (Koptev et al., 2015; Clutier et al., 2021). Geochronological analyses of the erupted products that distribute from the craton border to the west to Mount Kilimanjaro to the east, coupled with careful assessment of the tectonics of the encompassing region, reveal the presence of at least two volcanic trends, with different orientations, likely controlled by regional lithospheric structure (Le Gall et al., 2008; Mana et al., 2015). Additionally, geochemical signatures of lavas along each volcanic track display a progressive evolution, pointing towards potential mixing between two generating mechanisms (Mana et al., 2015), as suggested for Tibesti.

Finally, there are indications in the observational record that the interaction between plume flow and continental lithosphere can act against the development of convective instabilities adjacent to Earth's cratonic margins, thereby preventing decompression melting through mechanisms such as edge-driven convection. For example, the entire western margin of Africa hosts only limited Neogene volcanism, despite having long-lived cratonic margins (e.g. West African, Congo and Kaapvaal cratons), which should provide a favourable setting for edge-driven convection. Offshore, numerous volcanic ocean islands and seamounts, such as Canary, Cape Verde, the Cameroon Line, Saint Helena and Tristan-Gough, distribute between Azores to the North and Meteor to the South. Most have been linked to deep mantle upwellings associated with the African large low shear-wave velocity province (e.g. French & Romanowicz, 2015; Lei et al., 2020). In such a configuration, the impingement of many buoyant plumes offshore western Africa and their spreading in the sub-lithospheric mantle should drive asthenospheric flow from the Atlantic Ocean towards Africa. As a result, upwelling return flow associated with potential edge-driven instabilities along the cratonic margins of western Africa would be suppressed, potentially explaining the lack of volcanism at these locations over the Neogene.

4.7 Limitations and Future Work

Through their similarities with our previous suite of models (Duvernay et al., 2021), the present simulations share comparable limitations. In particular, melting at depth relies on a batch melting parameterisation of a peridotite assemblage, and our implementation does not account for changes in material properties, such as density and viscosity, that arise through melting. As such, we neglect complexities associated with multi-component melting (e.g. Shorttle et al., 2014) and potentially important feedbacks between melting and mantle dynamics (e.g. Gülcher et al., 2021). Furthermore, we do not simulate the effects of melt extraction and melt transport (Keller et al., 2017; Jain et al., 2019); this shortcoming needs to be considered when comparing our predicted melting rates with observations from the geological record.

In addition to our simplified treatment of melting, a number of assumptions have been made in our simulations. We use a diffusion creep rheology (thus neglecting the potentially substantial effects of dislocation creep), assume incompressibility and ignore the role of phase transitions. The impact of these assumptions should be analysed carefully in future work, although we expect the primary conclusions of our study to remain valid. Another potentially important aspect that we did not account for is the combined roles of plate motion and background asthenospheric flow, which will modulate the location and intensity of edge-driven instabilities, deflect mantle plumes during their ascent, and modify their spatio-temporal interaction with the LAB (e.g. Manglik & Christensen, 2006; Duvernay et al., 2021). Nonetheless, given the wide-ranging dynamics predicted in our simulations, we argue that this choice is justified, as it has allowed us to isolate and understand first-order features of these systems in the absence of further complexities. Despite this, there is little doubt that adding plate motion and asthenospheric flow to our models would shed additional light on plume-lithosphere interaction beneath continents and will likely be important in understanding differences in the volcanic record between fast-moving continents, such as Australia, and slow-moving continents, such as Africa.

The simulations examined herein incorporate mantle plumes. However, we only examined plumes of a specific buoyancy flux ($\sim$500 $\mathrm{kg\,s^{-1}}$), maintaining a fixed excess temperature (150 K), injection radius (200 km), and injection velocity (10 $\mathrm{cm\,yr^{-1}}$) across all simulations examined. We chose to focus on how the impingement location of a plume relative to a continent shapes the spatial interaction between these two entities at the LAB and the resulting magmatism, as opposed to the properties of the plume itself. Our results show that in a continental setting, the complex structure of the LAB is likely to play a crucial role in determining the nature and intricacies of plume-lithosphere interaction. They therefore demonstrate that the dynamic and magmatic expression of mantle plumes is not solely determined by their physical characteristics but also by the structure of overlying lithosphere. We speculate, however, that plumes with a higher buoyancy flux would enhance erosion of the LAB, more strongly modulate the regional flow field, enhance melting earlier during their ascent, and induce simultaneous volcanism at greater distances apart. Finally, we simulated purely thermal plumes, neglecting potential chemical heterogeneities. Although accounting for denser or more viscous materials in the plume conduit can alter the dynamics of the buoyant upwelling (e.g. Ballmer et al., 2013; T. Jones et al., 2016; Farnetani et al., 2018), it is unlikely that such features will strongly modulate the interaction between plumes and overlying continental lithosphere. Nonetheless, the presence of more fusible lithologies would likely enhance melt production (e.g. Shorttle et al., 2014) and should be considered in future studies.

5 Conclusions

Using a series of geodynamical models, we have investigated the interaction between upwelling mantle plumes and heterogeneous continental lithosphere to understand how melt-generating processes combine and control magmatism in some of Earth's most complex geological settings.

We find that pressures beneath thick continental cratons are sufficient to inhibit decompression melting immediately above plume upwellings. However, the heterogeneous structure of continental lithosphere gives rise to pressure gradients that channel plume material away from the conduit, concentrating it beneath thinner portions of the lithosphere where decompression melting can occur. In some scenarios, such anisotropic spreading of plume material can lead to simultaneous magmatism in regions located over 1000 km apart.

Our results illustrate how potential locations for plume-induced decompression melting are controlled by the structure of the lithosphere at depth and the location of plume impingement: in the absence of surface plate motions and background mantle flow, it is primarily the topography of the lithosphere-asthenosphere boundary that controls the spreading path of plumes and, hence, where the solidus is eventually crossed. Our results also demonstrate that overlying lithospheric structure ultimately dictates the geometry of magmatism: we find that the magmatic expression of plumes regularly concentrates adjacent to lithospheric steps, where it may be challenging to distinguish from that arising through edge-driven convection. Distinguishing between both driving mechanisms becomes even more challenging when plume-driven flow enhances magmatism at lithospheric steps several million years before the buoyant plume material enters the melting zone. In this scenario, erupted lavas will have no differentiating geochemical signature, despite the crucial role of the plume in activating melting.

Quite counter-intuitively, we find that if plumes impinge in regions of thinner lithosphere, the resulting asthenospheric flow regime can force material downwards and beneath the continent at lithospheric steps, shutting off pre-existing edge-related magmatism. In addition, under certain conditions, the interaction between plume material and lithospheric structure can induce internal destabilisation of the plume pancake, driving complex time-dependent magmatic patterns at the surface.

In conclusion, our study, which produces spatial and temporal magmatic patterns compatible with those observed on Earth, demonstrates that continental magmatism is likely the product of complex, time-dependent interactions between cratonic lithosphere, mantle plumes, and shallower dynamical processes, such as edge-driven convection. In turn, it emphasises the challenge of linking continental magmatism to underlying mantle dynamics and motivates an inter-disciplinary approach in future studies.

Acknowledgments

T.D. is funded by an ANU PhD Scholarship (International) Full-Time (737/2018). D.R.D., S.C.K. and T.D. acknowledge support from the Australian Research Council (ARC), under DP170100058. D.R.D. also acknowledges support from the Australian Research Data Commons (ARDC), under the G-Adopt platform grant PL031. C.R.M was funded by an Australian Government Research Training Program Domestic Scholarship. Numerical simulations were undertaken on the NCI National Facility in Canberra, Australia, which is supported by the Australian Commonwealth Government. The Fluidity computational modelling framework, including source code and documentation, is available from `https://fluidityproject.github.io/`; the release (tag 4.1.19) used for the simulations presented herein has been archived at Zenodo (Kramer et al., 2021). Similarly, example input files required to reproduce the simulations presented herein have been made available (Duvernay, 2022). The authors would like to thank Patrick Ball, Ian Campbell, Caroline Eakin, Siavash Ghelichkan, Mark Hoggard, Brian Kennett, Marthe Klöcking, Nick Rawlinson and Cian Wilson for fruitful discussions at various stages of this research. Figures have been prepared using Matplotlib, Cartopy, ParaView and Inkscape.

References

Afonso, J. C., Rawlinson, N., Yang, Y., Schutt, D. L., Jones, A. G., Fullea, J., & Griffin, W. L. (2016). 3-D multiobservable probabilistic inversion for the compositional and thermal structure of the lithosphere and upper mantle: III. Thermochemical tomography in the Western-Central US. *Journal of Geophysical Research: Solid Earth*, *121*(10), 7337–7370.

Artemieva, I. M. (2009). The continental lithosphere: reconciling thermal, seismic, and petrologic data. *Lithos*, *109*(1-2), 23–46.

Ashwal, L. D., & Burke, K. (1989). African lithospheric structure, volcanism, and topography. *Earth and Planetary Science Letters*, *96*(1-2), 8–14.

Austermann, J., Kaye, B. T., Mitrovica, J. X., & Huybers, P. (2014). A statistical analysis of the correlation between large igneous provinces and lower mantle seismic structure. *Geophysical Journal International*, *197*(1), 1–9.

Ball, P., White, N., Maclennan, J., & Stephenson, S. (2021). Global influence of mantle temperature and plate thickness on intraplate volcanism. *Nature communications*, *12*(1), 1–13.

Ball, P., White, N., Masoud, A., Nixon, S., Hoggard, M., Maclennan, J., . . . Kröpelin, S. (2019). Quantifying asthenospheric and lithospheric controls on mafic magmatism across North Africa. *Geochemistry, Geophysics, Geosystems*, *20*(7), 3520–3555.

Ballmer, M. D., Conrad, C. P., Smith, E. I., & Johnsen, R. (2015). Intraplate volcanism at the edges of the Colorado Plateau sustained by a combination of triggered edge-driven convection and shear-driven upwelling. *Geochemistry, Geophysics, Geosystems*, *16*(2), 366–379.

Ballmer, M. D., Ito, G., & Cheng, C. (2015). Asymmetric dynamical behavior of thermochemical plumes and implications for Hawaiian lava composition. *Hawaiian Volcanoes: From Source to Surface*, *208*, 35.

Ballmer, M. D., Ito, G., Van Hunen, J., & Tackley, P. J. (2011). Spatial and temporal variability in Hawaiian hotspot volcanism induced by small-scale convection. *Nature Geoscience*, *4*(7), 457–460.

Ballmer, M. D., Ito, G., Wolfe, C. J., & Solomon, S. C. (2013). Double layering of a thermochemical plume in the upper mantle beneath Hawaii. *Earth and Planetary Science Letters*, *376*, 155–164.

Barry, T., Ivanov, A., Rasskazov, S., Demonterova, E., Dunai, T., Davies, G., & Harrison, D. (2007). Helium isotopes provide no evidence for deep mantle involvement in widespread Cenozoic volcanism across Central Asia. *Lithos*, *95*(3-4), 415–424.

Bird, P. (2003). An updated digital model of plate boundaries. *Geochemistry, Geophysics, Geosystems*, *4*(3).

Bradshaw, T., Hawkesworth, C., & Gallagher, K. (1993). Basaltic volcanism in the Southern Basin and Range: no role for a mantle plume. *Earth and Planetary Science Letters*, *116*(1-4), 45–62.

Bredow, E., Steinberger, B., Gassmöller, R., & Dannberg, J. (2017). How plume-ridge interaction shapes the crustal thickness pattern of the Réunion hotspot track. *Geochemistry, Geophysics, Geosystems*, *18*(8), 2930–2948.

Cadio, C., Ballmer, M. D., Panet, I., Diament, M., & Ribe, N. (2012). New constraints on the origin of the Hawaiian swell from wavelet analysis of the geoid to topography ratio. *Earth and Planetary Science Letters*, *359*, 40–54.

Cas, R., Van Otterloo, J., Blaikie, T., & Van Den Hove, J. (2017). The dynamics of a very large intra-plate continental basaltic volcanic province, the Newer Volcanics Province, SE Australia, and implications for other provinces. *Geological Society, London, Special Publications*, *446*(1), 123–172.

Clutier, A., Gautier, S., & Tiberi, C. (2021). Hybrid local and teleseismic P-wave tomography in North Tanzania: role of inherited structures and magmatism on continental rifting. *Geophysical Journal International*, *224*(3), 1588–1606.

Conrad, C. P., Bianco, T. A., Smith, E. I., & Wessel, P. (2011). Patterns of intraplate volcanism controlled by asthenospheric shear. *Nature Geoscience*, *4*(5), 317–321.

Conrad, C. P., Wu, B., Smith, E. I., Bianco, T. A., & Tibbetts, A. (2010). Shear-driven upwelling induced by lateral viscosity variations and asthenospheric shear: A mechanism for intraplate volcanism. *Physics of the Earth and Planetary Interiors*, *178*(3-4), 162–175.

Courtillot, V., Davaille, A., Besse, J., & Stock, J. (2003). Three distinct types of hotspots in the Earth's mantle. *Earth and Planetary Science Letters*, *205*(3-4), 295–308.

Crisp, J. A. (1984). Rates of magma emplacement and volcanic output. *Journal of Volcanology and Geothermal Research*, *20*(3-4), 177–211.

Davies, D. R., & Davies, J. H. (2009). Thermally-driven mantle plumes reconcile multiple hot-spot observations. *Earth and Planetary Science Letters*, *278*(1-2), 50–54.

Davies, D. R., Goes, S., & Sambridge, M. (2015). On the relationship between volcanic hotspot locations, the reconstructed eruption sites of large igneous provinces and deep mantle seismic structure. *Earth and Planetary Science Letters*, *411*, 121–130.

Davies, D. R., & Rawlinson, N. (2014). On the origin of recent intraplate volcanism in Australia. *Geology*, *42*(12), 1031–1034.

Davies, D. R., Rawlinson, N., Iaffaldano, G., & Campbell, I. H. (2015). Lithospheric controls on magma composition along Earth's longest continental hotspot track. *Nature*, *525*(7570), 511–514.

Davies, D. R., Valentine, A., Kramer, S. C., Rawlinson, N., Hoggard, M., Eakin, C., & Wilson, C. (2019). Earth's multi-scale topographic response to global mantle flow. *Nature Geoscience*, *12*(10), 845–850.

Davies, D. R., Wilson, C. R., & Kramer, S. C. (2011). Fluidity: A fully unstructured anisotropic adaptive mesh computational modeling framework for geodynamics. *Geochemistry, Geophysics, Geosystems*, *12*(6).

Demidjuk, Z., Turner, S., Sandiford, M., George, R., Foden, J., & Etheridge, M. (2007). U-series isotope and geodynamic constraints on mantle melting processes beneath the Newer Volcanic Province in South Australia. *Earth and Planetary Science Letters*, *261*(3), 517–533.

Deniel, C., Vincent, P., Beauvilain, A., & Gourgaud, A. (2015). The Cenozoic volcanic province of Tibesti (Sahara of Chad): major units, chronology, and structural features. *Bulletin of Volcanology*, *77*(9), 74.

dos Santos, A. C., Mata, J., Jourdan, F., de Oliveira Rodrigues, S. W., Monteiro, L. G. P., Guedes, E., ... Geraldes, M. C. (2021). Martin Vaz island geochronology: Constraint on the Trindade Mantle Plume track from the youngest and easternmost volcanic episodes. *Journal of South American Earth Sciences*, *106*, 103090.

Duncan, R. A., & Richards, M. (1991). Hotspots, mantle plumes, flood basalts, and true polar wander. *Reviews of Geophysics*, *29*(1), 31–50.

Dupré, B., & Allègre, C. J. (1983). Pb–Sr isotope variation in Indian Ocean basalts and mixing phenomena. *Nature*, *303*(5913), 142–146.

Duvernay, T. (2022, January). *Patol75/Continental-Magmatism-The-Surface-Manifestation-Of-Dynamic-Interactions-Between- Cratonic-Lithosphere: Submission to Geochemistry, Geophysics, Geosystems.* Zenodo. Retrieved from `https://doi.org/10.5281/zenodo.5847709` doi: 10.5281/zenodo.5847709

Duvernay, T., Davies, D. R., Mathews, C. R., Gibson, A. H., & Kramer, S. C. (2021). Linking intra-plate volcanism to lithospheric structure and asthenospheric flow. *Geochemistry, Geophysics, Geosystems*, e2021GC009953.

Ebinger, C. J., & Sleep, N. (1998). Cenozoic magmatism throughout east Africa resulting from impact of a single plume. *Nature*, *395*(6704), 788–791.

Farnetani, C. G., Hofmann, A. W., Duvernay, T., & Limare, A. (2018). Dynamics of rheological heterogeneities in mantle plumes. *Earth and Planetary Science Letters*, *499*, 74–82.

Farrington, R., Stegman, D., Moresi, L., Sandiford, M., & May, D. (2010). Interactions of 3D mantle flow and continental lithosphere near passive margins. *Tectonophysics*, *483*(1-2), 20–28.

Fishwick, S., Heintz, M., Kennett, B., Reading, A., & Yoshizawa, K. (2008). Steps in lithospheric thickness within eastern Australia, evidence from surface wave tomography. *Tectonics*, *27*(4).

Fishwick, S., & Rawlinson, N. (2012). 3-D structure of the Australian lithosphere from evolving seismic datasets. *Australian Journal of Earth Sciences*, *59*(6), 809–826.

French, S. W., & Romanowicz, B. (2015). Broad plumes rooted at the base of the Earth's mantle beneath major hotspots. *Nature*, *525*(7567), 95.

Gassmöller, R., Dannberg, J., Bredow, E., Steinberger, B., & Torsvik, T. H. (2016). Major influence of plume-ridge interaction, lithosphere thickness variations, and global mantle flow on hotspot volcanism—the example of Tristan. *Geochemistry, Geophysics, Geosystems*, *17*(4), 1454–1479.

Gibert, B., Seipold, U., Tommasi, A., & Mainprice, D. (2003). Thermal diffusivity of upper mantle rocks: Influence of temperature, pressure, and the deformation fabric. *Journal of Geophysical Research: Solid Earth*, *108*(B8).

Gourgaud, A., & Vincent, P. (2004). Petrology of two continental alkaline intraplate series at Emi Koussi volcano, Tibesti, Chad. *Journal of volcanology and geothermal research*, *129*(4), 261–290.

Griffiths, R., & Campbell, I. (1991). Interaction of mantle plume heads with the Earth's surface and onset of small-scale convection. *Journal of Geophysical Research: Solid Earth*, *96*(B11), 18295–18310.

Gülcher, A. J. P., Ballmer, M. D., & Tackley, P. J. (2021). Coupled dynamics and evolution of primordial and recycled heterogeneity in Earth's lower mantle. *Solid Earth*, *12*(9), 2087–2107.

Hart, S., Hauri, E., Oschmann, L., & Whitehead, J. (1992). Mantle plumes and entrainment: isotopic evidence. *Science*, *256*(5056), 517–520.

Herzberg, C., Asimow, P. D., Arndt, N., Niu, Y., Lesher, C., Fitton, J., ... Saunders, A. (2007). Temperatures in ambient mantle and plumes: Constraints from basalts, picrites, and komatiites. *Geochemistry, Geophysics, Geosystems*, *8*(2).

Ho, K.-S., Ge, W.-C., Chen, J.-C., You, C.-F., Yang, H.-J., & Zhang, Y.-L. (2013).

Late Cenozoic magmatic transitions in the central Great Xing'an Range, Northeast China: Geochemical and isotopic constraints on petrogenesis. *Chemical Geology*, *352*, 1–18.

Hoggard, M. J., Czarnota, K., Richards, F. D., Huston, D. L., Jaques, A. L., & Ghelichkhan, S. (2020). Global distribution of sediment-hosted metals controlled by craton edge stability. *Nature Geoscience*, *13*(7), 504–510.

Hoggard, M. J., Parnell-Turner, R., & White, N. (2020). Hotspots and mantle plumes revisited: Towards reconciling the mantle heat transfer discrepancy. *Earth and Planetary Science Letters*, *542*, 116317.

Holford, S., Schofield, N., MacDonald, J., Duddy, I., & Green, P. (2012). Seismic analysis of igneous systems in sedimentary basins and their impacts on hydrocarbon prospectivity: Examples from the southern Australian margin. *The APPEA Journal*, *52*(1), 229–252.

Ito, G., Lin, J., & Gable, C. W. (1996). Dynamics of mantle flow and melting at a ridge-centered hotspot: Iceland and the Mid-Atlantic Ridge. *Earth and Planetary Science Letters*, *144*(1-2), 53–74.

Jain, C., Rozel, A. B., Tackley, P. J., Sanan, P., & Gerya, T. V. (2019). Growing primordial continental crust self-consistently in global mantle convection models. *Gondwana Research*, *73*, 96–122.

Jaupart, C., & Mareschal, J. (2005). Production from heat flow data. *The Crust*, *3*, 65–84.

Jellinek, A. M., & Manga, M. (2004). Links between long-lived hot spots, mantle plumes, D", and plate tectonics. *Reviews of Geophysics*, *42*(3).

Johnson, R. W., Johnson, R. W., Knutson, J., & Taylor, S. R. (1989). *Intraplate volcanism: in eastern Australia and New Zealand*. Cambridge University Press.

Jones, I., Ubide, T., Crossingham, T., Wilding, B., & Verdel, C. (2020). Evidence of a common source component for east Australian Cenozoic mafic magmatism. *Lithos*, *354*, 105254.

Jones, T., Davies, D. R., Campbell, I., Iaffaldano, G., Yaxley, G., Kramer, S. C., & Wilson, C. (2017). The concurrent emergence and causes of double volcanic hotspot tracks on the Pacific plate. *Nature*, *545*(7655), 472.

Jones, T., Davies, D. R., Campbell, I., Wilson, C., & Kramer, S. C. (2016). Do mantle plumes preserve the heterogeneous structure of their deep-mantle source? *Earth and Planetary Science Letters*, *434*, 10–17.

Kaislaniemi, L., & van Hunen, J. (2014). Dynamics of lithospheric thinning and mantle melting by edge-driven convection: Application to Moroccan Atlas mountains. *Geochemistry, Geophysics, Geosystems*, *15*(8), 3175–3189.

Katsura, T., Yoneda, A., Yamazaki, D., Yoshino, T., & Ito, E. (2010). Adiabatic temperature profile in the mantle. *Physics of the Earth and Planetary Interiors*, *183*(1-2), 212–218.

Katz, R. F., Spiegelman, M., & Langmuir, C. H. (2003). A new parameterization of hydrous mantle melting. *Geochemistry, Geophysics, Geosystems*, *4*(9).

Keller, T., Katz, R. F., & Hirschmann, M. M. (2017). Volatiles beneath mid-ocean ridges: Deep melting, channelised transport, focusing, and metasomatism. *Earth and Planetary Science Letters*, *464*, 55–68.

Kennett, B., & Davies, D. (2020). Intra-plate volcanism in North Queensland and eastern new Guinea: A cryptic mantle plume? *Gondwana Research*, *79*, 209–216.

King, S. D. (2007). Hotspots and edge-driven convection. *Geology*, *35*(3), 223–226.

King, S. D., & Adam, C. (2014). Hotspot swells revisited. *Physics of the Earth and Planetary Interiors*, *235*, 66–83.

King, S. D., & Anderson, D. L. (1998). Edge-driven convection. *Earth and Planetary Science Letters*, *160*(3-4), 289–296.

King, S. D., & Ritsema, J. (2000). African hot spot volcanism: small-scale convection in the upper mantle beneath cratons. *Science*, *290*(5494), 1137–1140.

Klöcking, M., White, N., Maclennan, J., McKenzie, D., & Fitton, J. (2018). Quantitative relationships between basalt geochemistry, shear wave velocity, and asthenospheric temperature beneath western North America. *Geochemistry, Geophysics, Geosystems*, *19*(9), 3376–3404.

Koptev, A., Burov, E., Calais, E., Leroy, S., Gerya, T., Guillou-Frottier, L., & Cloetingh, S. (2016). Contrasted continental rifting via plume-craton interaction: Applications to Central East African Rift. *Geoscience Frontiers*, *7*(2), 221–236.

Koptev, A., Calais, E., Burov, E., Leroy, S., & Gerya, T. (2015). Dual continental rift systems generated by plume–lithosphere interaction. *Nature Geoscience*, *8*(5), 388.

Kramer, S. C., Greaves, T., Funke, S. W., Wilson, C., Avdis, A., Davies, R., ... Ham, D. A. (2021, August). *Fluidityproject/fluidity: Zenodo release.* Zenodo. Retrieved from `https://doi.org/10.5281/zenodo.5221157` doi: 10.5281/zenodo.5221157

Kramer, S. C., Wilson, C. R., & Davies, D. R. (2012). An implicit free surface algorithm for geodynamical simulations. *Physics of the Earth and Planetary Interiors*, *194*, 25–37.

Lebedev, S., Schaeffer, A. J., Fullea, J., & Pease, V. (2018). Seismic tomography of the Arctic region: Inferences for the thermal structure and evolution of the lithosphere. *Geological Society, London, Special Publications*, *460*(1), 419–440.

Le Gall, B., Nonnotte, P., Rolet, J., Benoit, M., Guillou, H., Mousseau-Nonnotte, M., ... Déverchère, J. (2008). Rift propagation at craton margin.: Distribution of faulting and volcanism in the North Tanzanian Divergence (East Africa) during Neogene times. *Tectonophysics*, *448*(1-4), 1–19.

Lei, W., Ruan, Y., Bozdağ, E., Peter, D., Lefebvre, M., Komatitsch, D., ... Pugmire, D. (2020). Global adjoint tomography—model GLAD-M25. *Geophysical Journal International*, *223*(1), 1–21.

Maia, T. M., dos Santos, A. C., Rocha-Júnior, E. R. V., de Morisson Valeriano, C., Mendes, J. C., Jeck, I. K., ... Mohriak, W. U. (2021). First petrologic data for Vitória Seamount, Vitória-Trindade Ridge, South Atlantic: a contribution to the Trindade mantle plume evolution. *Journal of South American Earth Sciences*, *109*, 103304.

Mana, S., Furman, T., Turrin, B. D., Feigenson, M. D., & Swisher, C. C. (2015). Magmatic activity across the East African North Tanzanian divergence zone. *Journal of the Geological Society*, *172*(3), 368–389.

Manglik, A., & Christensen, U. (2006). Effect of lithospheric root on decompression melting in plume–lithosphere interaction models. *Geophysical Journal International*, *164*(1), 259–270.

Marty, B., Upton, B. G., & Ellam, R. M. (1998). Helium isotopes in early Tertiary basalts, northeast Greenland: Evidence for 58 Ma plume activity in the North Atlantic–Iceland volcanic province. *Geology*, *26*(5), 407–410.

Mathews, C. (2021). *Methods for tracking material properties within an unstructured, adaptive mesh computational modelling framework, with application to simulating the development of seismic anisotropy at spreading centres and transform faults* (Unpublished doctoral dissertation). Research School of Earth Sciences, ANU Colleges of Science, The Australian National University.

McKenzie, D. (1984). The generation and compaction of partially molten rock. *Journal of Petrology*, *25*(3), 713–765.

McNab, F., Ball, P., Hoggard, M., & White, N. (2018). Neogene uplift and magmatism of Anatolia: Insights from drainage analysis and basaltic geochemistry. *Geochemistry, Geophysics, Geosystems*, *19*(1), 175–213.

Meeuws, F. J., Holford, S. P., Foden, J. D., & Schofield, N. (2016). Distribution, chronology and causes of Cretaceous–Cenozoic magmatism along the magma-poor rifted southern Australian margin: Links between mantle melting and basin formation. *Marine and Petroleum Geology*, *73*, 271–298.

Meyer, R., Van Wijk, J., & Gernigon, L. (2007). The North Atlantic Igneous Province: A review of models for its formation. *Special Papers-Geological Society of America*, *430*, 525.

Missenard, Y., & Cadoux, A. (2012). Can Moroccan Atlas lithospheric thinning and volcanism be induced by edge-driven convection? *Terra Nova*, *24*(1), 27–33.

Morgan, W. J. (1971). Convection plumes in the lower mantle. *Nature*, *230*(5288), 42.

Nikogosian, I., Gartner, A. B., Van Bergen, M., Mason, P., & Van Hinsbergen, D. J. (2018). Mantle sources of recent Anatolian intraplate magmatism: A regional plume or local tectonic origin? *Tectonics*, *37*(12), 4535–4566.

Niu, Y. (2021). Lithosphere thickness controls the extent of mantle melting, depth of melt extraction and basalt compositions in all tectonic settings on Earth–a review and new perspectives. *Earth-Science Reviews*, 103614.

Nyblade, A. A., & Sleep, N. H. (2003). Long lasting epeirogenic uplift from mantle plumes and the origin of the Southern African Plateau. *Geochemistry, Geophysics, Geosystems*, *4*(12).

Özdemir, Y., & Güleç, N. (2014). Geological and geochemical evolution of the Quaternary Süphan Stratovolcano, Eastern Anatolia, Turkey: evidence for the lithosphere–asthenosphere interaction in post-collisional volcanism. *Journal of Petrology*, *55*(1), 37–62.

Permenter, J. L., & Oppenheimer, C. (2007). Volcanoes of the Tibesti massif (Chad, northern Africa). *Bulletin of volcanology*, *69*(6), 609–626.

Pollack, H. N., & Chapman, D. S. (1977). On the regional variation of heat flow, geotherms, and lithospheric thickness. *Tectonophysics*, *38*(3-4), 279–296.

Putirka, K. (2008). Excess temperatures at ocean islands: Implications for mantle layering and convection. *Geology*, *36*(4), 283–286.

Putirka, K. (2016). Rates and styles of planetary cooling on Earth, Moon, Mars, and Vesta, using new models for oxygen fugacity, ferric-ferrous ratios, olivine-liquid Fe-Mg exchange, and mantle potential temperature. *American Mineralogist*, *101*(4), 819–840.

Rawlinson, N., Davies, D. R., & Pilia, S. (2017). The mechanisms underpinning Cenozoic intraplate volcanism in eastern Australia: Insights from seismic tomography and geodynamic modeling. *Geophysical Research Letters*, *44*(19), 9681–9690.

Ribe, N., & Christensen, U. (1999). The dynamical origin of Hawaiian volcanism. *Earth and Planetary Science Letters*, *171*(4), 517–531.

Ritsema, J., Deuss, a. A., Van Heijst, H., & Woodhouse, J. (2011). S40RTS: a degree-40 shear-velocity model for the mantle from new Rayleigh wave dispersion, teleseismic traveltime and normal-mode splitting function measurements. *Geophysical Journal International*, *184*(3), 1223–1236.

Sarafian, E., Gaetani, G. A., Hauri, E. H., & Sarafian, A. R. (2017). Experimental constraints on the damp peridotite solidus and oceanic mantle potential temperature. *Science*, *355*(6328), 942–945.

Sengör, A., & Burke, K. (1978). Relative timing of rifting and volcanism on Earth and its tectonic implications. *Geophysical Research Letters*, *5*(6), 419–421.

Shorttle, O., Maclennan, J., & Lambart, S. (2014). Quantifying lithological variability in the mantle. *Earth and Planetary Science Letters*, *395*, 24–40.

Sleep, N., Ebinger, C., & Kendall, J.-M. (2002). Deflection of mantle plume material by cratonic keels. *Geological Society, London, Special Publications*, *199*(1), 135–150.

Smith, R. B., Jordan, M., Steinberger, B., Puskas, C. M., Farrell, J., Waite, G. P., … O'Connell, R. (2009). Geodynamics of the Yellowstone hotspot and mantle plume: Seismic and GPS imaging, kinematics, and mantle flow. *Journal of Volcanology and Geothermal Research*, *188*(1-3), 26–56.

Steinberger, B. (2000). Plumes in a convecting mantle: Models and observations for individual hotspots. *Journal of Geophysical Research: Solid Earth*, *105*(B5), 11127–11152.

Steinberger, B., Bredow, E., Lebedev, S., Schaeffer, A., & Torsvik, T. H. (2019). Widespread volcanism in the Greenland–North Atlantic region explained by the Iceland plume. *Nature Geoscience*, *12*(1), 61–68.

Stracke, A., Hofmann, A. W., & Hart, S. R. (2005). FOZO, HIMU, and the rest of the mantle zoo. *Geochemistry, Geophysics, Geosystems*, *6*(5).

Tang, Y.-J., Zhang, H.-F., & Ying, J.-F. (2006). Asthenosphere–lithospheric mantle interaction in an extensional regime: implication from the geochemistry of Cenozoic basalts from Taihang Mountains, North China Craton. *Chemical Geology*, *233*(3-4), 309–327.

Tatsumi, Y., Hamilton, D., & Nesbitt, R. (1986). Chemical characteristics of fluid phase released from a subducted lithosphere and origin of arc magmas: evidence from high-pressure experiments and natural rocks. *Journal of Volcanology and Geothermal Research*, *29*(1-4), 293–309.

Turcotte, D., & Oxburgh, E. R. (1978). Intra-plate volcanism. *Philosophical Transactions of the Royal Society of London. Series A, Mathematical and Physical Sciences*, *288*(1355), 561–579.

van den Hove, J. C., Van Otterloo, J., Betts, P. G., Ailleres, L., & Cas, R. A. (2017). Controls on volcanism at intraplate basaltic volcanic fields. *Earth and Planetary Science Letters*, *459*, 36–47.

Wellman, P., & McDougall, I. (1974). Cainozoic igneous activity in eastern Australia. *Tectonophysics*, *23*(1-2), 49–65.

White, W. M., McBirney, A. R., & Duncan, R. A. (1993). Petrology and geochemistry of the Galápagos Islands: Portrait of a pathological mantle plume. *Journal of Geophysical Research: Solid Earth*, *98*(B11), 19533–19563.

Wilson, C. (2009). *Modelling multiple-material flows on adaptive unstructured meshes* (Unpublished doctoral dissertation). Imperial College London.

Wolfe, C. J., Bjarnason, I. T., VanDecar, J. C., & Solomon, S. C. (1997). Seismic structure of the Iceland mantle plume. *Nature*, *385*(6613), 245–247.

Ye, Y., Schwering, R. A., & Smyth, J. R. (2009). Effects of hydration on thermal expansion of forsterite, wadsleyite, and ringwoodite at ambient pressure. *American Mineralogist*, *94*(7), 899–904.

Zhang, R., Wu, Q., Sun, L., He, J., & Gao, Z. (2014). Crustal and lithospheric structure of Northeast China from S-wave receiver functions. *Earth and Planetary Science Letters*, *401*, 196–205.

Supporting Information for 'Continental Magmatism: The Surface Manifestation Of Dynamic Interactions Between Cratonic Lithosphere, Mantle Plumes And Edge-Driven Convection'

DOI: 10.1002/

Thomas Duvernay[1], D. Rhodri Davies[1], Christopher R. Mathews[1], Angus H. Gibson[1], Stephan C. Kramer[2]

[1]Research School of Earth Sciences, The Australian National University, Canberra, ACT, Australia

[2]Department of Earth Science and Engineering, Imperial College London, London, UK

Contents of this file

1. Figures S1 to S3

Corresponding author: Thomas Duvernay, Research School of Earth Sciences, The Australian National University, 142 Mills Rd, Acton ACT 0200, Australia. (thomas.duvernay@anu.edu.au)

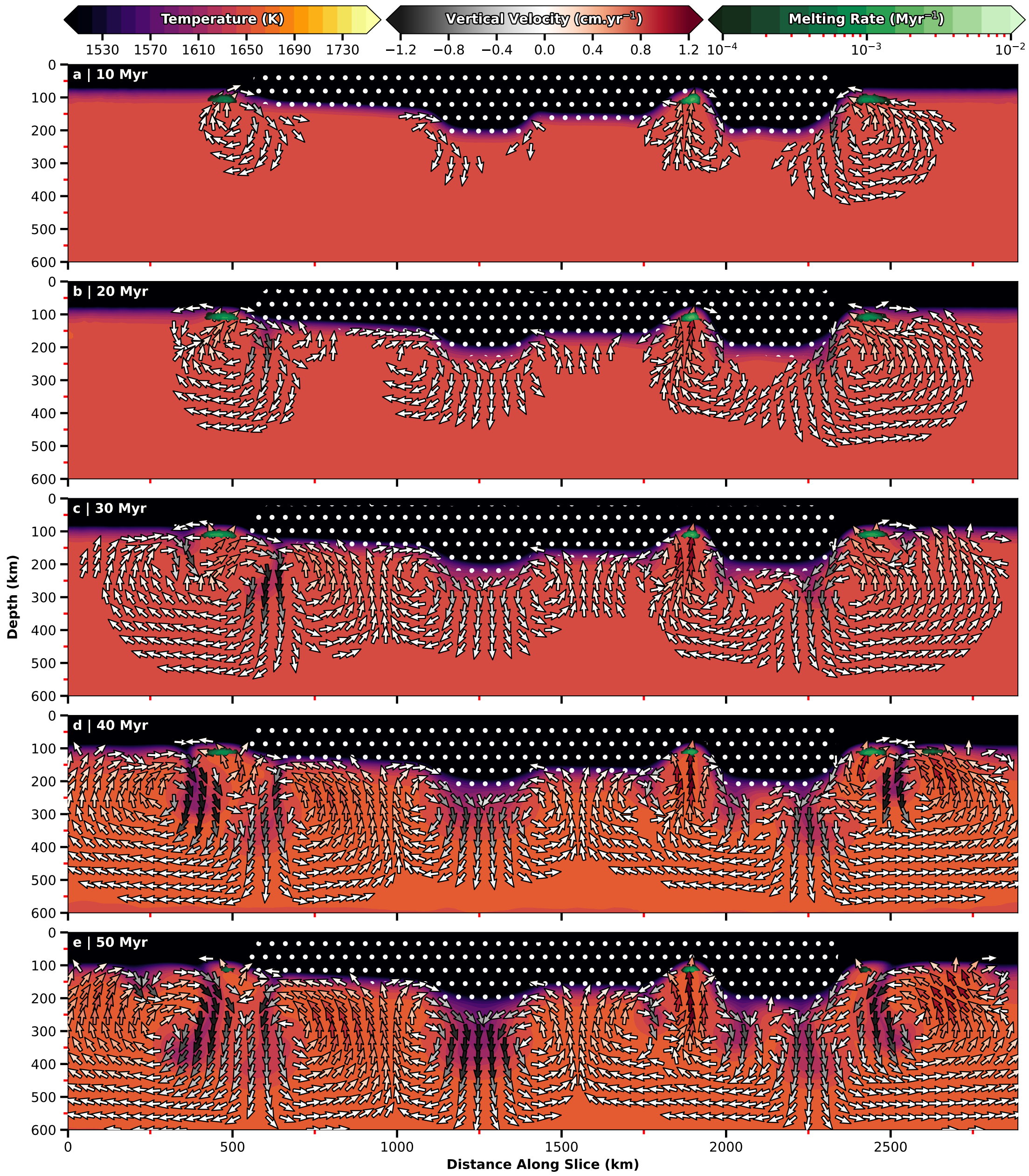

Figure S1. Instability development beneath and adjacent to the *Complex* continental geometry along a chosen vertical cross-section (refer to Figure 2b for the location of the cross-section). Background colours represent the temperature field, with superimposed green regions depicting areas of active melting according to their intensity. Arrow glyphs illustrate the velocity field projected onto the pictured cross-section. Glyphs are drawn where the magnitude of the projected field is greater than 0.5 mm yr^{-1} and are coloured by the intensity of the vertical velocity component. White circles highlight the location of continental material (crust excluded).

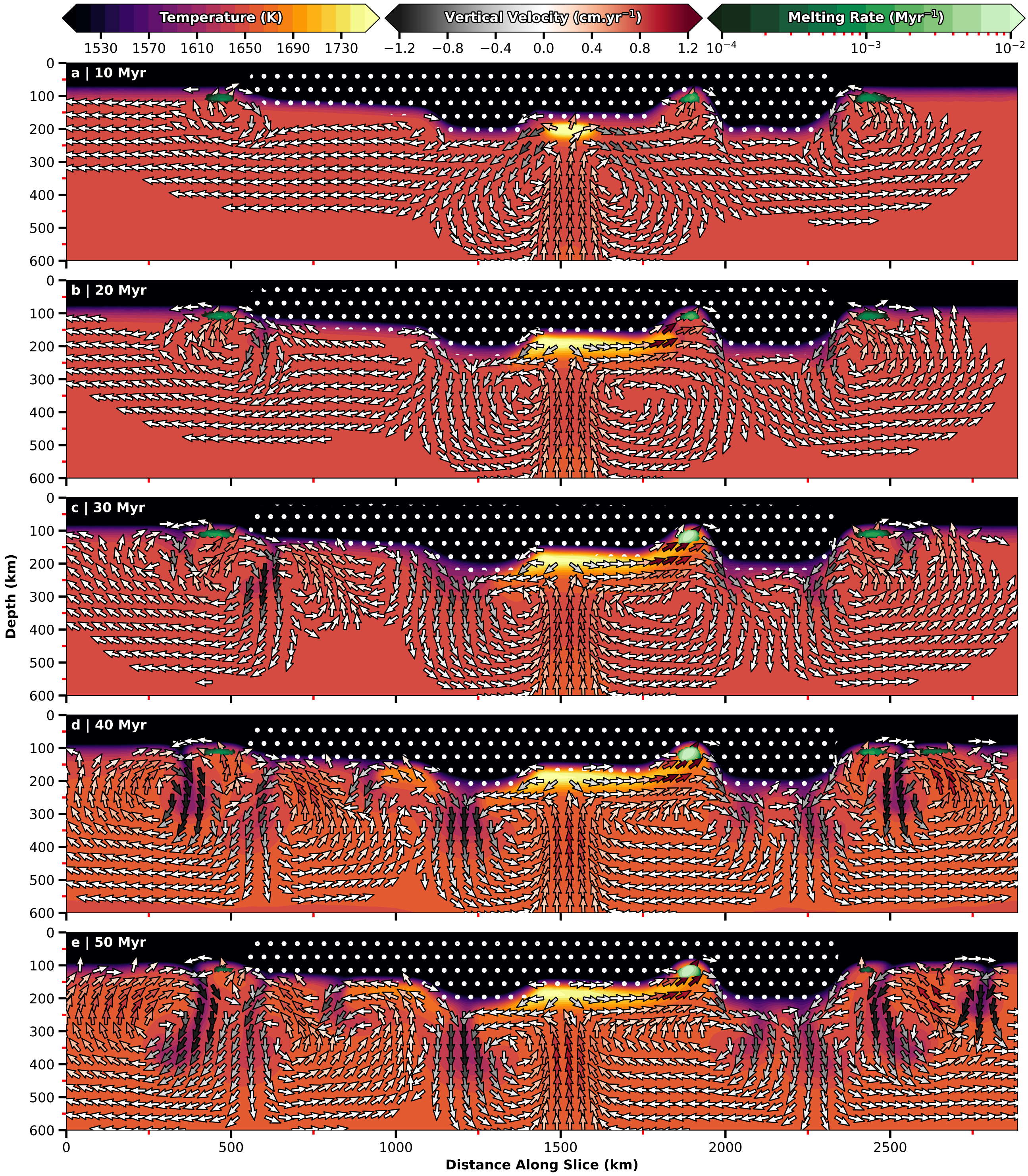

Figure S2. Instability development beneath and adjacent to the continental lithosphere of case *Complex_Cont_Centre* as the plume ascends through the upper mantle. Chosen cross-section and graphical illustration similar to Figure S1.

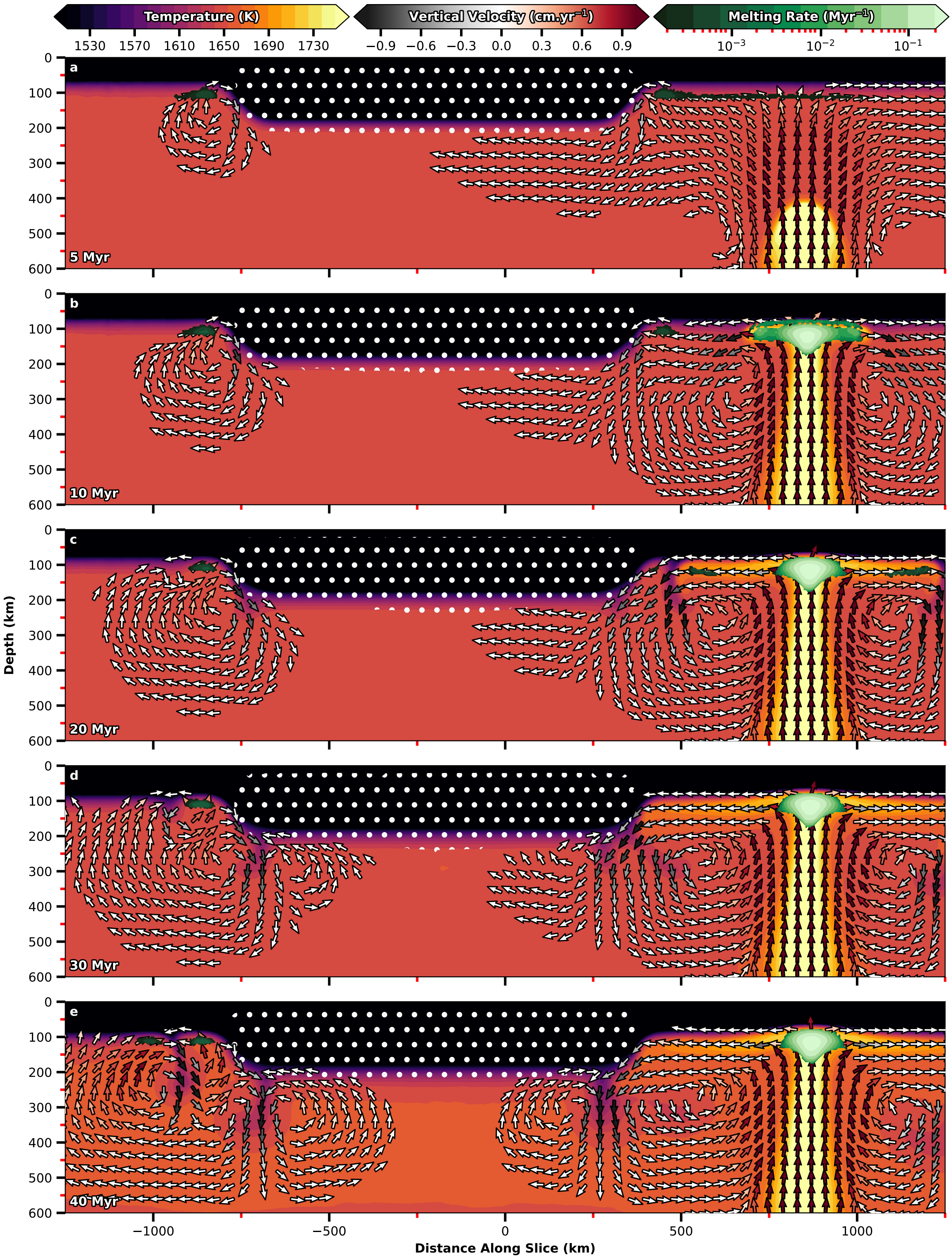

Figure S3. Instability development beneath and adjacent to the continental lithosphere of case *U400_Ocean_Offshore* as the plume ascends through the upper mantle. Displayed cross-section is located at $y = 2000\,\mathrm{km}$. Graphical illustration similar to Figure S1.